MEASUREMENT OF FORCES WITHIN THE FLEXOR DIGITORUM SUPERFICIALIS DURING FLEXION OF THE PROXIMAL INTERPHALANGEAL JOINT

Thesis submitted in accordance with the requirements of the University of Liverpool for the degree of

Doctor of Medicine

by

Gerard Francis Lambe

May 2009

ABSTRACT

This thesis is a study of the Flexor Digitorum Superficialis tendon and its action on the proximal Interphalangeal Joint (PIPJ) in the human hand. Previous work has demonstrated that the PIPJ does not flex as a simple hinge rather there is a small but significant degree of rotation towards a common point in the palm. The FDS inserts on to the sides of the middle phalanx via two slips analogous to a pair of reins. These are known as the radial and ulnar terminal tendons. The hypothesis that this rotation is due to the action of the FDS tendon producing differential loading through these terminal tendons is explored.

The author hopes that a precise understanding of the distribution of forces acting at the PIPJ during flexion will aid in the development of prostheses to replace the joint.

In order to investigate the hypothesis of differential loading in the terminal tendons different methodologies for sensitive tendon strain measurement were developed and investigated. Fresh frozen human cadaveric hand specimens were used for all experiments. 3 different methods were adopted.

First, small angle X-ray diffraction (SAXS) was used to measure the strain at the fibrillar level in tendon samples. This was successful in quantifying fibrillar strain over the linear phase of the stress/strain curve but could not be applied to the terminal tendons. This was due to an alteration in the structure of the terminal tendons which made acquisition of diffraction patterns difficult in this region

Secondly, image analysis of Magnetic Resonance Scans of the tendons during loading was investigated examining change in texture and then tendon outline. During these experiments, a technique of maximising the tendon images, known as 'Magic Angle imaging' was utilised. This methodology was not ultimately successful due to limitations in the resolution of the scanner and sensitivity of the computer analysis algorithms.

Finally, a method of full field strain measurement using video image analysis was utilised. The results from the index and ring fingers of five cadaveric hands during cyclical loading in a tensiometer were recorded. These results demonstrated that the loading in the radial and ulnar terminal tendons was directly proportional to the dimensions of the slips and therefore asymmetric. The author concludes that the FDS does drive the motion of the PIPJ through differential loading in the terminal tendons and this is proportional to the differential in the width of these tendons.

The development of the experimental methodology through the course of this work raised interesting results. The utilisation of magic angle imaging to obtain clear pictures of tendon anatomy in the hand was refined and published in The British Journal of Hand Surgery. This technique has great potential for the investigation of closed injuries in the hand. The algorithms developed for analysis of the MR images would be suitable for use in areas with larger tendon volumes and could be employed in the investigation of other joints.

The author anticipates that a better understanding of the dynamic forces acting on the PIPJ will aid in the development of prostheses to replace the joint with a particular emphasis on improving lifespan before revisional surgery is required.

CONTENTS

LIST OF FIGURES

Number *Page*

ACKNOWLEDGMENTS

The author wishes to thank the Department of Human Anatomy and Cell Biology at Liverpool University, Royal Preston Hospital Medical Imaging Dept, North Western Medical Physics, Daresbury Laboratories, Dr C Hall, Mr Paul McArthur, Dr G Coutts, Dr C Coutinho, Dr Peter Dangerfield, Dr N Chockalingam and A Rahmatalla, Oxford Brookes Image analysis Department, Prof. W. Clocksin.

This work was supported by grants from the British Society for Surgery of the Hand, the Royal College of Surgeons of England and the Research Directorate Royal Preston Hospital.

A huge thank you to my parents, wife and children Zoe and Rosanna. Thank you for your love, understanding, caring, support and inspiration.

Chapter 1

1 Introduction

The purpose of this thesis is to gain an understanding of the distribution of forces acting at the PIPJ through the FDS tendon. To achieve this it has been necessary to develop and test different methodologies of strain measurement in tendon.

None of the present methodologies for the measurement of tendon strain were suitable for the task due to either being not sufficiently sensitive or too bulky. The author therefore developed new methodologies for the measurement of strain in small slips of the tendon insertion. Subsequent chapters will describe these developments and the experimental findings in more detail.

The aims were therefore to:

1. Develop a sensitive and accurate reproducible method for the quantification of strain in small regions of tendon.
2. To investigate the pattern of loading in the terminal tendons of the FDS.

The motivation for this investigation came from previous work demonstrating that the PIPJ did not move as a hinge but exhibited a more complex motion with a small, but significant degree of rotation. Small rotational movement at such joints can be a cause of failure in arthroplasty reconstruction of the joint and therefore a clear understanding of what is driving the motion is important information in designing new prostheses for the joint.

The thesis will take the following structure:

First, previous work done on the function of the FDS tendon and hypotheses regarding the reasons for the complex structure of the FDS at the PIPJ will be discussed. The author will also discuss McArthur's work [51] which demonstrated torsional motion of the PIPJ.

Subsequent chapters will describe the different experimental approaches adopted to develop a sensitive strain measurement method and results which provided insight into the anatomy and structure of the FDS.

Chapter 1 describes the use of X-Ray diffraction techniques to measure the change in intermolecular distances as the tendon was loaded and the limitations of this method with respect to the measurement of strain close to the insertion of the FDS.

Chapter 2 discusses the use of image analysis of MRI scans using different computer algorithms first employing the changes in texture of specimens and then the change in outline as the tendons were loaded in a special testing jig. The limitations of this method and the success of the new computer algorithm will be presented and discussed.

Finally a method employing the use of a conventional tensiometer together with a validated, method of video analysis based on texture to define discrete regions of strain is described. These experiments yielded results showing that the tendon strain was directly proportional to the width of the tendons and therefore showed that there is differential loading at the PIPJ demonstrating an active driver of the torsional motion.

The significance of these findings from the three experiments is discussed in the next chapter and then further work is described together with the author's conclusions.

The author has used fresh frozen human cadaveric hands for all of the experiments and the literature regarding the effect of freezing on tensile testing of such specimens will be discussed. The relevant literature review is placed before each of the three chapters in order to present the relevant articles next to their experiments and aid the reader in interpreting the results.

The following section provides a brief overview of the relevant hand and tendon anatomy pertinent to interpreting the work in this thesis.

1.1 Anatomy

The hand is an intricate linkage system with muscles that work synergistically to produce complex tasks ranging from power grip to fine and delicate motion. The hand has been described as a 'functional puppet' [50] with neurological impulses arising from

the motor cortex of the brain that are coordinated and sent as signals for graded contraction or relaxation of a specific set of muscles. This action is modified by feedback from multiple sources including the eye, sensory end organs muscle and proprioceptors. The biomechanics of the hand have been studied in depth to understand normal function, as well as pathophysiology when joints start to deform under the influence of arthritic disease processes. A detailed understanding of the forces acting at each joint aids understanding of the normal function of the hand.

The hand is controlled by muscles and tendons that are grouped into either extrinsic or intrinsic depending on whether the muscle bellies originate in the forearm or hand respectively. The interaction of these muscle groups through the linked joints of the digits allow for a wide range of function.

1.1.1 Osteology

Each finger consists of four bones, a metacarpal and three phalanges. The phalanges are termed proximal, middle and distal. The thumb differs in that it has only two phalanges. The joints of the fingers from proximal to distal are called the metacarpophalangeal joint (MCPJ), proximal interphalangeal joint (PIPJ) and distal interphalangeal joint (DIPJ).

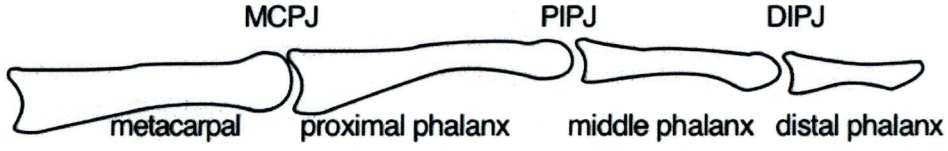

Figure 1 Articulations in the finger

All of these joints are prone to injury and degenerative arthritic change. The PIPJ is particularly important to the normal function of the hand and has been considered as " the epicentre of hand surgery as nowhere in the human frame are anatomy and function

so interrelated" [9]. The PIPJ is said to account for up to 85% of range of motion in the hand during the action of grasping an object. It is thefore not difficult to see how dysfunction of the PIPJ could lead to significant reduction in overall hand function.

1.1.2 PIPJ Anatomy

The PIPJ is the articulation between the distal end of the proximal phalanx and the proximal end of the middle phalanx and has been described as a hinge joint because it primarily exhibits motion in only one plane, flexion and extension. The ligaments and supporting structures around the joint allow little abduction, adduction or extension. This is due to the box like configuration of ligaments and capsule that surround the joint. Let us look first at the bony anatomy. The proximal aspect of the joint consists of two condyles separated by an intercondylar groove. It has been noted by Ash et al [2] and Kuczynski [45] in studies of the PIPJ proximal condyles that they are asymmetrical. In the index and middle fingers the ulnar condyle projects further forward than the radial. The opposite is true for the ring and little fingers with the radial condyle projecting further forward in these digits.

The ligaments supporting the joint medially are known as the true and accessory collateral ligaments. The accessory collateral ligament is more dorsally located and narrow. It runs obliquely from a prominent ridge on the side of the proximal phalanx head to the side of the base of the middle phalanx. The true collateral ligament is a broad fan shaped structure that takes some of its origin from the lower aspect of the ridge that the accessory collateral ligament arises from then it broadens out to insert on to the base of the middle phalanx and on to the volar plate.

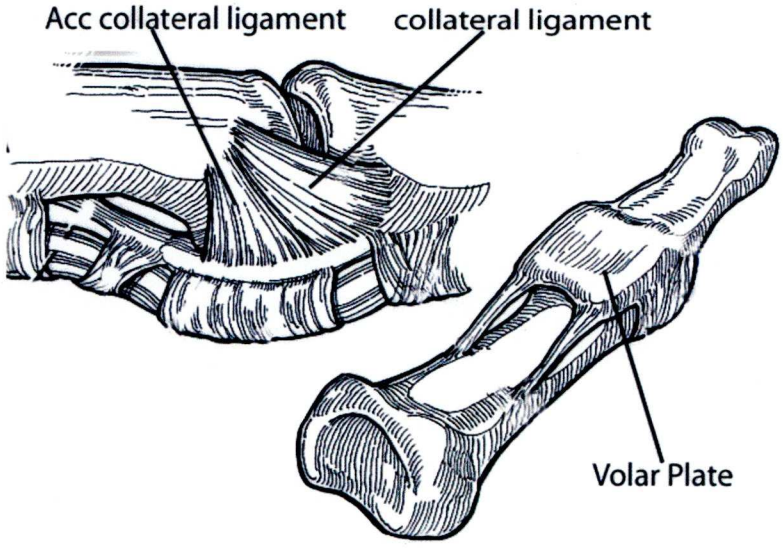

Figure 2 Collateral ligaments and volar plate of PIPJ

(Source: Green's Operative Hand Surgery 5th Ed)

The volar plate is a fibrocartilaginous ligament on the palmar aspect of the joint which acts to resist hyperextension at the joint. It is tough and fibrous proximally but membranous and loose distally. It is continuous with part of the flexor sheath. The volar plate proximally is shaped like a swallow's tail. This allows passage of a vessel to the joint through the gap between the two tails. The roof of the capsule is formed by the extensor expansion.

1.1.3 Intrinsic and Extrinsic Flexors

1.1.3.1 Intrinsics

The flexion of the phalanges into the palm requires the action of both the extrinsic long flexors, FDP and FDS modified and enhanced by the action of the intrinsic muscles, the lumbricals and interossei. The lumbricals arise from the tendon of the FDP in the palm and insert on to the extensor tendons over the dorsum of the PIPJ. The interossei arise

from the shafts of the metacarpals and insert on to the base of the proximal phalanx and into the extensor tendon over the MCPJ. In order to simplify the experiments and calculations the actions of the intrinsic musculature has not been examined in the present study.

1.1.3.2 Extrinsics

The flexor digitorum profundus (FDP) and the flexor digitorum superficialis (FDS) are the extrinsic flexors as their muscle bellies arise in the forearm. Both of these tendons are able to flex the PIPJ but the FDP is a secondary flexor of the joint as its insertion is past the DIPJ and it therefore flexes all joints of the finger at once. Only the FDS is able to cause independent flexion of the joint. Both tendons have a secondary action on the MCPJ and the wrist. The anatomy of the FDS is complex close to the insertion as the tendon weaves around the FDP. The relationship between the anatomy and function of the FDS has been investigated by a number of different authors. These papers will be discussed later in this chapter.

1.1.4 FDP Anatomy

The FDP also arises from a broad origin on the forearm it forms four tendons that also pass through the carpal tunnel and then on to the flexor sheaths of the individual digits. Throughout their course the tendons of the FDP lie deep to the tendons of FDS. The FDS tendon therefore has to pass around the FDP tendon to reach its insertion on to the middle phalanx and it achieves this through a unique and intricate anatomical arrangement. The tendons of FDS split and spiral around the FDP then meet again on the underside of the tendon were they form what is known anatomically as a decussation. Some fibres continue on the same side while some fibres cross over. This forms the chiasma of Camper and the crossed and uncrossed fibres form a radial (RTT) and ulnar (UTT) terminal tendon which insert on to the sides of the middle phalanx.

1.1.5 FDS Anatomy

The FDS muscle belly originates in the forearm from two bony attachments along an oblique line. Between these bony attachments is a fibrous arch. The first attachment is the common flexor origin, located on the medial aspect of the elbow, the medial epicondyle. There is also a small attachment to the ulna at this point. The larger area

from which muscle fibres arise is a roughened surface on the anterior aspect of the radius known as the anterior oblique line. From this muscle belly arise four tendons to the index, middle, ring and little fingers. The tendons commence just proximal to the wrist. The tendons to the middle and ring fingers lie superficial to the tendons to the index and little. They pass under a fibrous arch known as the flexor retinaculum which bounds a narrow bony space formed by the carpal bones, the carpal tunnel. The tendons then enter the palm where they are covered by a thin membranous layer termed the synovial sheath. This sheath helps to lubricate and nourish the tendons. They then pass into a narrow fibrous tunnel called the fibrous flexor sheath. This tunnel starts at the level of the metacarpal necks and continues to the distal phalanx. It is composed of a set of pulleys known as annular and cruciate depending on their pattern of fibres. The purpose of this sheath is to hold the tendons close to the bones maximising mechanical efficiency by preventing bow stringing of the tendons across the joint during flexion.

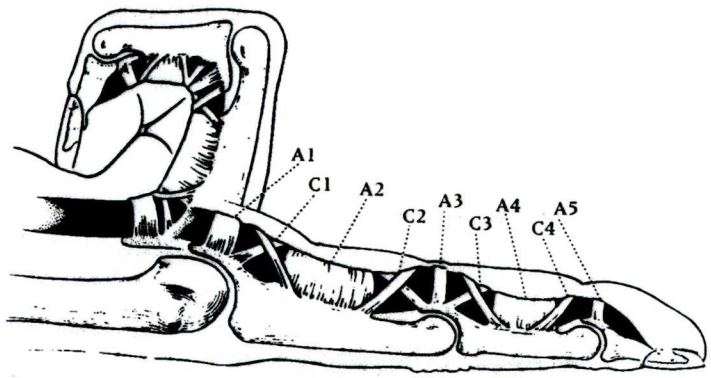

Figure 3 The fibrous flexor sheath

(Source: Green's Operative Hand Surgery 5th Ed)

The FDS has to split to pass around the FDP tendon to reach its insertion on to the middle phalanx, just beneath the A4 pulley. The tendon starts to divide into separate slips just distal to the MCPJ. The two slips spiral around the FDP tendon. Some fibres continue straight on to their insertion but others cross to the other side of the joint, this is known as a decussation and forms an area called the chiasma of Camper. The mixture

of crossed and uncrossed fibres then forms the radial and ulnar terminal tendons, which insert on to the sides of the middle phalanx.

1.1.6 CHIASMA ANATOMY

Shrewsbury [71] looked at the variation in anatomy of the FDS around the chiasma in a cadaveric study. The dimensions of the component strands of the chiasma in a dissection of 23 hands was recorded together with a nomenclature for the different strands that constitute the chiasma, as shown in the figure below.

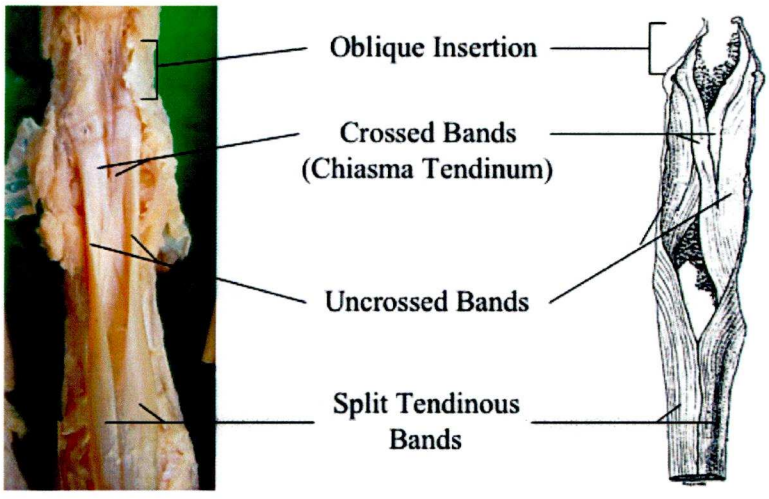

Figure 4 Nomenclature of the FDS strands

M. M. Shrewsbury, A. B. Tucker, **36**, 40 (1975).

The criss-crossing of fibres to form the chiasma can be seen in the diagram on the right and in the prosected specimen on the left. The purpose of this intricate arrangement has been investigated by a number of different authors.

1.1.6.1 Review of Previous work on FDS

Shrewsbury [71] and Stack [74] both argued that the function of the chiasma is to allow the FDP and FDS to pass the axis of flexion of the PIPJ at the same distance from the joint,

thus equalling the moment arms and hence the excursion of the tendons. Stack (1962) also suggested that the chiasma may act to resist hyperextension at the PIPJ acting to reinforce the volar plate.

Walbeehm and McGrouther [82] noted that the split tendinous bands of the FDS moved together during flexion of the joint and suggested that this created a gripping effect, similar to a Chinese finger trap, on the body of the FDP tendon. They argued that the chiasma acts to push the FDP tendon against the distal edge of the A2 pulley. Using electron microscopy they observed a roughness to the under surface of this part of the pulley and reasoned that the purpose of the chiasma may be to decrease the work of flexion by increasing friction between the FDP and the A2 pulley.

Shrewsbury [71] investigated the FDS function by constructing a model of the PIPJ and the component strands of the FDS. By creating tension in different groups of strands and observing the motion of the model joint, he drew a number of conclusions.
Firstly, that the joint could not be flexed by tensioning only the uncrossed fibres in one terminal tendon. This instead produced lateral deviation or abduction at the joint, even when all fibres in one terminal tendon were tensioned it resulted in a coronal deviation of the joint. Shrewsbury and Tucker concluded that the crossed fibres assisted the alignment of the flexion forces by rotating the joint surfaces.

These suggestions as to the function of the FDS chiasma and structure may be, in part, correct but if we return to Shrewsbury and Tucker's anatomical study we see that not all aspects of the anatomy of the FDS have been fully explained.
Shrewsbury and Kuczynski [70] demonstrated a consistent difference in the width of the radial (RTT) and ulnar terminal tendons (UTT). This data is summarised in table 1.

Table 1 Width of the FDS Terminal Tendons

In (mm)	*Index*	*Middle*	*Ring*	*Little*
UTT	3	3	3	2.5
RTT	3.5	3.5	2.5	2

It can be seen from the table that the radial fingers consistently have a wider radial terminal tendon whereas for the ulnar digits this trend is reversed. Shrewsbury and Kuczynski [70] argued that this might lead to differential loading of the PIPJ. Although the differences in the dimensions of the terminal tendons are relatively small they state that parallel collagen fibrils are able to transmit tensile forces of 15 to 30 kgs/mm^2.
This finding agrees with Shrewsbury and Tucker's previous work [71] looking at tensioning different strands of the chiasma in a model.

1.1 PIPJ Motion

As mentioned earlier in this chapter evidence for differential loading in the terminal tendons comes from a detailed investigation of PIPJ biomechanics by McArthur [51].
McArthur examined the plane of motion of the PIPJ using a method of T-shaped metal markers fixed to the phalanges of cadaveric fingers and plain radiographs. The plane of motion of the PIPJ in all the digits was investigated. In order to eliminate cumulative errors when calculating the joint motion the MCPJ and DIPJ joints were fixed in flexion. McArthur concluded that the PIPJ undergoes a complex arc of motion with 3-5 degrees of abduction/adduction and pronation/supination taking place as the joint flexes. The radial digits, index and middle, were found to follow a similar arc of pronation while the ulnar digits were reported to move in the opposite manner i.e. supinating.

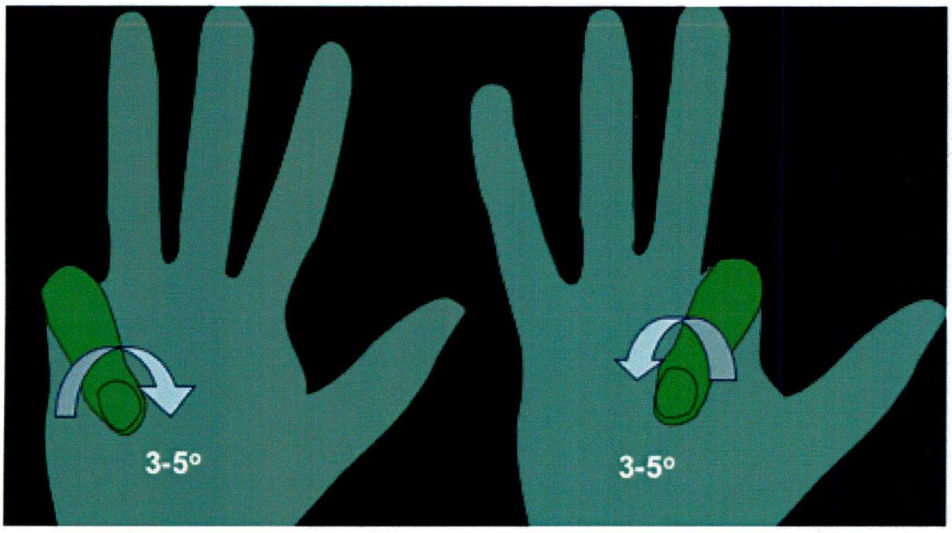

Figure 5 Rotation of Radial and Ulnar Digits with PIPJ flexion

This observed motion is summarised in the diagram above. McArthur speculated that the FDS may be responsible for actively driving this motion.

1.1.1 Condyles and PIPJ motion

The FDS is not the only factor that may be responsible for the observed motion. The bony anatomy of the articular surfaces of the PIPJ is not symmetrical as described earlier. This therefore could be a passive cause for the motion of the PIPJ. A way of testing this would be to alter the joint surfaces so that they were symmetrical and then examine the motion of the joint.

Uchiyama et al[77] examined the kinematics of the PIPJ after resurfacing the joint with a metal-polyethylene prosthetic replacement (Avanta prosthesis, San Diego, CA). This was a symmetric bi-condylar implant and therefore eliminated the asymmetry of the bony anatomy. The digits were tested under ideal conditions using a magnetic Isotrak system (Polhemus Navigational Systems, Colchester, VT). Uchiyama et al found that the kinematics of the PIP joint after replacement were similar to that of the normal joint. The maximum angular displacement was 5 degrees for lateral deviation and 9 degrees

for rotation during the passive flexion and extension of the joint. This implies there may be another factor driving the PIPJ motion.

The work of McArthur [51] and Shrewsbury and Kuczynski [70] suggest that the complex pattern of fibres in the FDS will lead to the contraction of the muscle producing a complex pull at the PIPJ that may drive the rotational motion of the joint. This is especially true when one considers that during flexion of the joint the angle of insertion of the terminal tendon increases and the ability to produce an angular motion of the joint is thus increased.

The pattern of fibres that form the chiasma and the asymmetry of the terminal tendons suggest that the chiasma may produce a number of vectors at the PIPJ and be responsible for driving the motion of the joint. The proposed vectors are illustrated in the figure below.

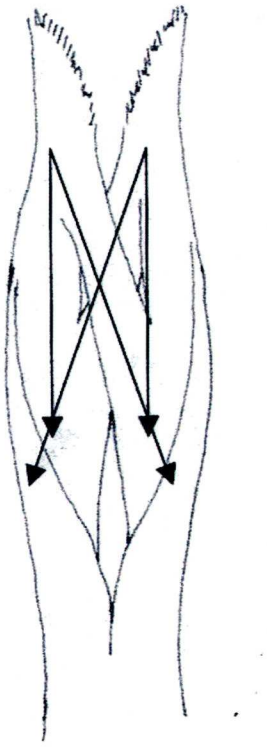

Figure 6 Vectors acting at the PIPJ

If we imagine the path of one collagen fibre from the bottom right of the image above it will spiral around the side of the FDP to rest on the under surface of this tendon. It may then take one of two directions either continuing straight on the same side of the digit or crossing to the opposite side to contribute to the opposite terminal tendon. These two paths will lead to different vectors of pull when this fibre is tensioned as indicated by the arrows in Figure 6.

1.1.2 Importance of rotation of the PIPJ

The degree of rotation observed by McArthur [51] and Uchiyama et al [77] is small amounting to a maximum of 5 degrees. This is potentially significant though when one is considering the effect of this motion on an implant reconstruction of the joint. Over the many hundreds of thousands of cycles of flexion and extension a relatively small degree of rotation can lead to premature failure of a prosthesis if it has not been accounted for in the original design. This was one cause for early failure of knee prostheses when the knee was considered to move as a simple hinge. It was only when subsequent designs accounted for the sliding and rotation of the femoral condyles that knee arthroplasty became successful in the long term [78].

1.2 Methods Of Strain Measurement

To determine if it is due to differential loading of the FDS terminal tendons that the PIPJ rotates during flexion it will be necessary to measure the forces in the terminal tendons. The standard methods for measuring forces and load in tendons are to load specimens in a tensiometer under controlled conditions. The rate of loading and the change in unit length of the tendon can all be accurately recorded using such an experimental set up. The needs of this investigation though preclude the use of this as the only method of investigation. To determine the loading in the two separate limbs of the FDS terminal tendons presents a challenge.

Loading specimens in a tensiometer will only provide data for the whole tendon and not any information on the difference in the radial and ulnar terminal tendons. Ideally the measurements should be conducted under conditions similar to those found in vivo and with the FDP intact if at all possible as this may alter the biomechanics during loading.

One commonly used method of measuring load in a discrete region of a tendon is through the application of strain gauges. These are small devices that are fixed to the specimen at two separate points. A linear increase in voltage is produced as the distance between the two points changes during loading [43]. The use of such gauges would be very difficult in the present investigation though as they are firstly too large to apply to such a small region of tendon and secondly they will risk damage to the tendon slips, which could give rise to errors. Thirdly it will be impossible to apply such gauges and leave the overlying FDP and sheath intact.

In order to record the strain and hence the force in such a small region of tendon under ideal conditions a different method of strain measurement is required. Ideally, this will be a non-contact method and one that allows overlying structures to remain intact but will be sufficiently sensitive to determine any real difference in loading between the two terminal tendons. In subsequent chapters, the different methodologies explored and developed will be discussed.

1.2.1 Relationship between force and strain

To determine the forces acting on each of the terminal tendons and therefore any differential we will measure strain. The following is a brief introduction to basic biomechanical concepts.

Strain is defined in the change in unit length of a sample while it is being loaded, i.e. the percentage increase in length of a sample for a given load. It can be expressed as a percentage but has no units.

$$\text{Strain} = \Delta L/L$$

Stress is defined as force per unit area and this is related to the cross sectional area of a sample.

$$\text{Stress}=F/A$$

Stress is expressed as Newtons per metre squared Nm^{-2}.

Stress and strain are related by the equation for Young's modulus (E)

$$E = \text{Stress}/\text{Strain}$$

Young's modulus (E) is a measure of the stiffness of a material. It has the same units as Stress i.e. Nm^{-2}. If we consider the equation for Young's modulus (E).

$$E = (F/A) / (\Delta L/L)$$

If we rearrange the equation

$$F = E \times A \times (\Delta L/L)$$

Therefore we can see that Force is directly proportional to the cross-sectional area and strain of the tendon. It follows then that in the following experiments if the strain measured in both terminal tendons is the same the force can be stated as being proportional to the width of each of the terminal tendons.

1.3 Effects of Freezing on Tensile Properties of Tendon

Fresh frozen human cadaveric hands from donors, with no previous history of hand disease or arthritis, which had been harvested within 4 hours post mortem, were used for all experiments described hereafter. Specimens were imported from the Anatomic Gift Foundation, Maryland, U.S.A. Full ethical approval for the use of specimens was obtained from the Preston and Chorley Local Research and Ethics Committee. The Home Office and H.M Inspector for Anatomy were informed prior to the importation of specimens. Specimens were stored at –80 degrees Celsius in a non frost-forming freezer within the Pathology Department of Royal Preston Hospital. All specimens were defrosted at room temperature for 4 hours prior to use. All specimens were tested immediately after they were thawed completely in order to minimise the effects of repeated freezing and thawing.

A number of authors have looked at whether freezing tendons and their method of storage affects their properties in tensile tests. Smith et al [72] tested porcine toe extensor tendons after subjecting them to various different conditions used for storage. They reported that there was little difference in the values obtained from fresh samples and those which had been frozen between one and five times prior to testing.

Clavert et al [16] looked at the effect of freezing and thawing on the properties of the biceps brachii tendon. The investigators harvested pairs of tendons from human cadavers. One side was frozen then tested and the other was tested immediately. They reported a reduction in the Young's modulus and ultimate breaking force in the frozen and thawed specimens. Leitschuh et al [47] also reported a reduction in these properties, after freezing and thawing, when testing the extensor digitorum longus muscle tendon complex in rabbits.

As the principal objective of this research is to determine if there is differential loading in the terminal tendons, any change in properties of the tendon due to freezing will affect both slips equally. The potential to detect any differential loading in the terminal tendons should therefore not be altered as both slips will be affected equally by the freezing and defrosting process. However the absolute values for the results may differ from the reality in-vivo as a result of potential reduction in Young's Modulus.

1.4 Summary

In this chapter the central aims of the thesis have been presented, namely to develop a method for accurate strain measurement in small regions of the FDS tendon and then use this method to quantify the pattern of loading across the PIPJ. The relevant hand anatomy has been reviewed discussing the flexor muscles and the structure of the PIPJ. The unusual arrangement of the flexor tendons around the joint and proposed purposes of this arrangement have been reflected on. Suggestions in the literature included to minimise the work of gripping, to align flexion forces, equalise moment arms and to cause rotation of the joint surfaces. McArthur's work [51] showed a rotation of the PIPJ during flexion, the pattern of rotation matching the variation in both the bony anatomy

of the condyles and the terminal tendons of the FDS. Uchiyama et al 's study, however, indicated that the bony anatomy may not be the cause of the rotation as it was unchanged when the condyles were symmetrically reconstructed. Therefore the author wishes to investigate the FDS as a potential driver of the motion of the joint.

To determine forces acting at the joint it is necessary to measure the strain in the terminal tendons since the author could not find a suitable method in the literature for the purposes of the study it is proposed to develop and test methods for measuring strain in the terminal tendons and then apply them to the FDS. The general biomechanical principles involved have been presented. Fresh frozen human cadaveric hand specimens have been used for all tests. The effect of freezing on results has been reviewed but as this study is primarily comparative between the two slips in the tendon it is felt that the effects should be insignificant.

The next chapter will present the motivations, principles and results of experiments investigating small angle X-Ray diffraction (SAXS) as a potentially sensitive method of strain measurement.

Chapter 2

2 Small Angle X-ray Diffraction Study

2.1 Introduction

The following chapter details the experiments performed at Daresbury Synchrotron Laboratory. The purpose of the experiments was to determine if SAXS could be used as a method for accurately quantifying strain in human flexor tendons (HFT).

SAXS has been used by a number of previous authors [28, 52, 64] to look at the molecular events during tendon loading. The author wished to investigate the potential of this technique because it was a non-contact technique dependent on intermolecular distances to calculate strain. It therefore has the potential to be a very sensitive methodology. Prior to describing the experiments conducted the author would like to present a brief review of the principles of x-ray diffraction and small angle x-ray scattering followed by a description of the molecular structure of collagen and tendon. This will aid the reader in interpreting the results of the experiments in this chapter.

2.2 X-Rays

X-ray diffraction has been used for many years to investigate the atomic structure of materials and relies upon the ordered crystalline nature of solid materials, which deflect incident X-ray beams at a predictable angle described by Bragg's Law [10].

$$2d\sin q = n\,l$$

Using this equation it is possible to examine the angle between x-ray diffraction peaks to determine the distance between atoms or molecules in a sample.

X-rays are electromagnetic radiation with typical photon energies in the range of 100 eV - 100 keV. For diffraction applications, only short wavelength X-rays in the range of

a few Angstroms (1 Angstrom = 0.1 nanometres) are used. Because the wavelength of x-rays is similar to the size of atoms, they are ideal for probing the structural arrangement of atoms and molecules. The X-rays can penetrate deep into the material to discern information about the structure [83].

They are produced generally by either x-ray tubes or synchrotron radiation. In an x-ray tube, which is the primary x-ray source used in laboratory x-ray instruments, they are generated when a focused electron beam accelerated across a high voltage field bombards a stationary or rotating solid target. As electrons collide with atoms in the target and slow down, a continuous spectrum of X-rays are emitted. The high-energy electrons also eject inner shell electrons in atoms through the ionisation process. When a free electron fills the shell, an x-ray photon with energy characteristic of the target material is emitted [83]. Common targets used in x-ray tubes include copper and molybdenum. The energy E of an x-ray photon and its wavelength is related by the equation

$$\mathbf{E = hc/l}$$

where h is Planck's constant and c the speed of light.

2.2.1 Principles of x-ray diffraction analysis

The regularity and order that is the crystalline structure of solids is what gives rise to diffraction peaks. The diagram below shows a simplified scheme of what occurs during a diffraction experiment.

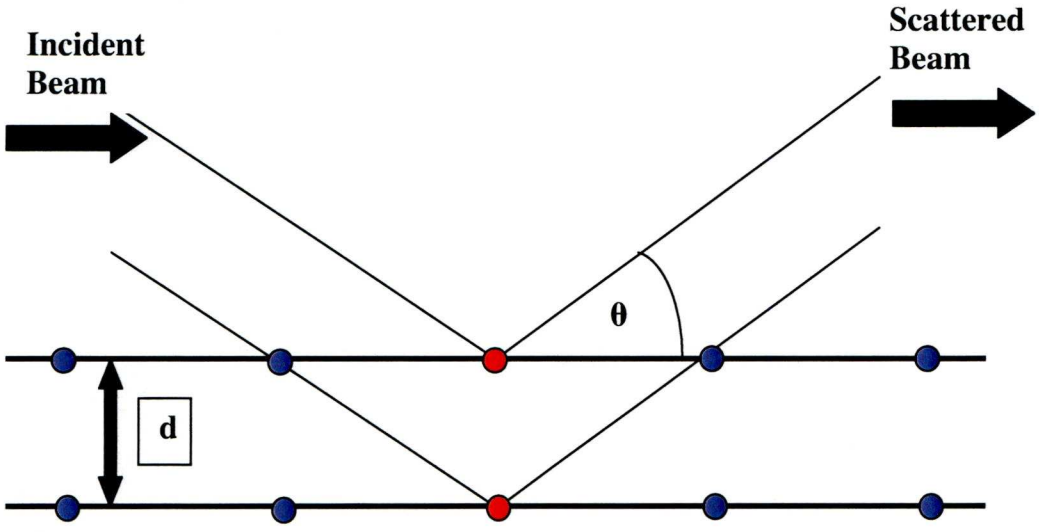

Figure 7 Simplified x-ray diffraction diagram

The circles represent atoms or molecules in a sample and the layers are known as lattice planes. D is the intermolecular distance. If we consider two x-ray photons incident upon a sample, the x-rays may be deflected back as shown in the diagram. The beams will interact with each other as they travel away from the sample and toward the detector. If the beams are in phase then they will mutually reinforce one another and if they are out of phase then they will cancel each other out. The regular structure of the solid provides a number of sharp and clear diffraction peaks, which are specific to the material being investigated.

The most important law in interpreting these diffraction patterns was derived by the English physicists Sir W.H. Bragg and his son Sir W.L. Bragg in 1913 [10] to explain why the cleavage faces of crystals appear to reflect x-ray beams at certain angles of incidence.

Bragg's law is stated as:

$$2d\sin\theta = n\lambda$$

In the equation, λ is the wavelength of the x-ray, θ the scattering angle, and n an integer representing the order of the diffraction peak.

Bragg's Law is one of most important laws used for interpreting x-ray diffraction data. Bragg's Law is clear from looking at the diagram below.

2.2.2 *Derivation of Bragg's Law*

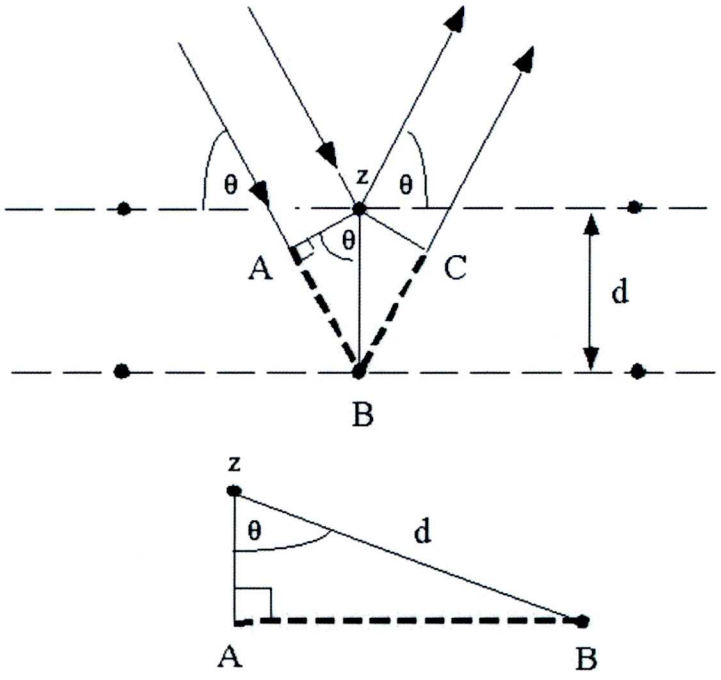

Figure 8 Derivation of Bragg's Law

.

The two incident beams are in phase with each other until the first beam hits the top layer atom or molecule. The second beam has to travel extra distance before it hits the next layer of atoms and is deflected. The extra distance (2D) must be an integral multiple of the wavelength in order for the two beams to remain in phase, reinforce each other, and hence give rise to a diffraction peak.

2.2.3 *SAXS*

SAXS is a modification of routine diffraction imaging that uses much smaller angles of incidence and very high-energy x-ray beams. This allows biological materials to be examined as they consist of macro-molecules. The small angles used require large distances between the sample and the detector in order to resolve the diffraction peaks

and analyse them. X-ray difraction allows a resolution for imaging down to 100 micrometers but with the use of SAXS a resolution of 1micrometer can be achieved. The intensity of the beam required for SAXS requires a bright synchrotron source.

2.2.4 Principles of Synchrotron radiation

A Synchrotron (or synchro-cyclotron) is a circular accelerator ring. It is composed of two main elements, a section that accelerate the particles within the ring (electromagnetic resonant cavity) and dipole magnets that bend the particles to keep them circulating as a beam around the ring. Charged particles as they are accelerated around the ring emit a small amount of energy in the form of synchrotron radiation. As particles increase in energy the strength of the magnetic field that is used to steer them must be changed with each turn to keep the particles moving in the same ring. A synchrotron provides a source of very high energy x-rays and this reduces the exposure times required to collect diffraction patterns. It will be seen later in the discussion on the effects of loading tendon that exposure times are critical in order to reduce difficulties during data analysis due to the effect known as creep. The molecular basis for this phenomenon is described later in the chapter.

2.3 Tendon Structure

The stress/strain plot of tendon can be understood by examining its molecular structure. Tendon is composed predominantly of Type 1 collagen, which is twisted into a left hand triple helix formation. The collagen molecules are approximately 280nm in length with a typical diameter of 1.5nm. The pitch of the left-handed helix is in the order of 0.95nm. The difference between left and right-handed helices is described as follows. With the line of sight along the helix's axis, if a clockwise screwing motion moves the helix away from the observer, then it is called a right-handed helix; if towards the observer then it is a left-handed helix

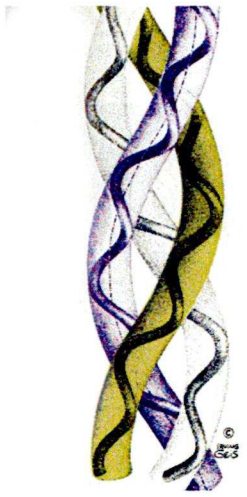

Figure 9 The Collagen Triple Helix

(Source: Voet - Biochemistry - © 1990, John Wiley & Sons.)

Figure 9 demonstrates the triple helix of collagen demonstrating how the left-handed polypeptide helices are twisted together to form a right-handed superhelical structure.

It was noted in early x-ray diffraction studies that there was a characteristic spacing of electron densities along the length of tendon i.e. the molecules were arranged such that there were areas of gap and overlap. One out of every 5 of the molecules is not present in these gap zones. This periodicity is known as the D-period and has a typical value of 67nm in tendon.

In 1962 Hodge and Petruska proposed a model based on a quarter staggered arrangement of collagen molecules which explained these x-ray findings [40]. This model is illustrated in Figure 10.

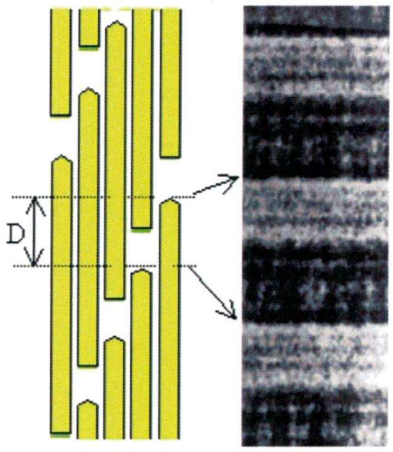

Figure 10 The D-period of Collagen

The image on the left is a diagrammatic representation of the molecular arrangement and the image on the right, a transmission electron micrograph of a negatively stained collagen fibril. The collagen molecules are bound together end to end and then assembled to form fibrils. The fibrils are embedded in a viscoelastic proteoglycan matrix. The fibrils form fibres, fascicles and then tendon as shown in Figure 11.

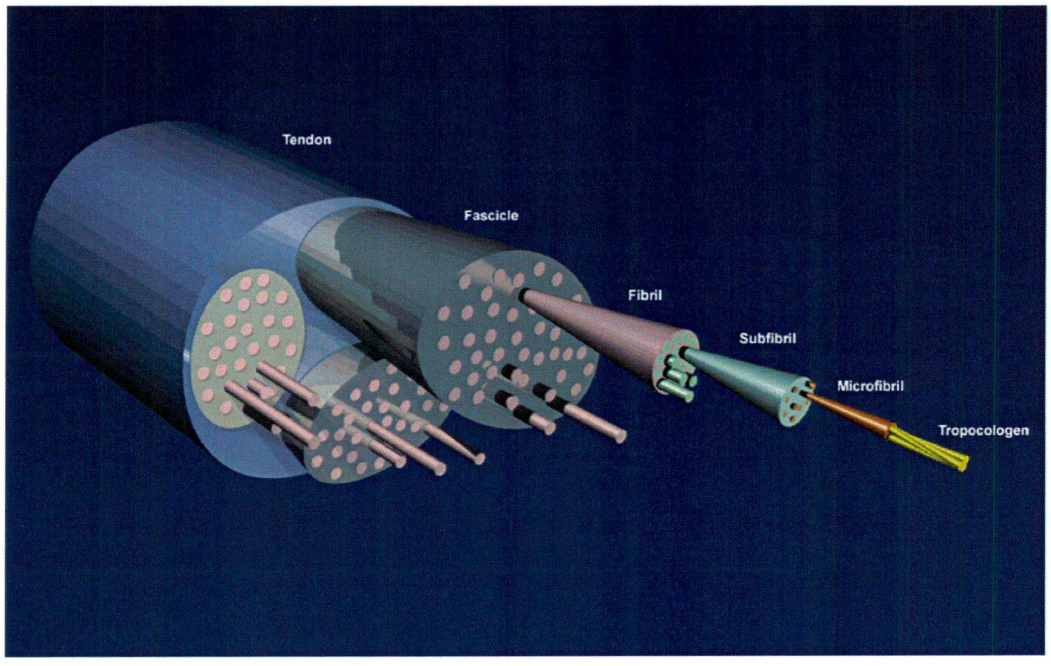

Figure 11 The hierarchical structure of tendon

The complex pattern of the stress/strain curve is due to the differing responses of the collagen molecule, fibrils and the proteoglycan matrix between the fibrils. The collagen molecule and proteoglycan matrix both demonstrate a time-dependent, viscoelastic, response to loading but the fibrils show a less complex response.

2.4 Relationship Between Strain And Molecular Events

The toe phase of the curve corresponds to the removal of a macroscopic kink in the tendon, which can be observed under the light microscope [21, 31, 79, 80].

The heel phase has been investigated by Misof et al[52]. Misof et al looked at samples of rat tail tendon (RTT) and examined the change in lateral ordering of molecules when the tendon was strained. They noted a decrease in the lateral disorder of the collagen molecules in this phase of the stress/strain curve and proposed a model based on 'thermally activated kinks' in the collagen molecules, which are removed when the tendon is strained. The heel phase may also be accounted for by the redistribution of water as the tendon is loaded. Helmer et al[37] looked at the pattern of water distribution in tendon during loading using NMR maps of proton density and found that there was movement of water from the centre of the tendon to the periphery. There is no doubt that tendon hydration is crucial as specimens which are allowed to dry out show markedly different results when loaded [35].

For the purposes of the experiments that follow in the next chapter it is the strain in the fibrils that is the most important component. This can be shown to be a constant fraction of the overall strain in the tendon at the linear part of the stress/strain curve and therefore a potential way of measuring small strain differentials.

The fibrillar strain can be measured by examining changes in molecular staggering represented by changes in the value of the D-period. This change in the D-period occurs via a number of different mechanisms, which have been elucidated by previous investigators looking at small angle x-ray scattering data from tendon samples. Common sources of collagen for these investigations include rat tail tendon (RTT) and bovine achilles tendon (BAT) and less commonly samples of human flexor tendons

(HFT). The molecular events that occur when tendon is strained and their time course have been investigated in order to understand the stress/strain curve of tendon.

Mosler et al[53] looked at samples of HFT and RTT and described three different mechanisms responsible for the change in the D-period.
These were:

1. Stretching of the collagen triple helices
2. An increase in the gap region between the molecules
3. A sliding of the molecules over each other

The sequence of these changes was described by Folkhard et al [26] and later by Sasaki et al [66]. It was found that the stretching of the collagen triple-helices was the first event. This accounts for only 0.8% of the observed change in the D-period.

The next two mechanisms, that is, gap region increase and molecular sliding occur together. Mosler et al[53] demonstrated this in a study of HFT and RTT samples. Their results did not fit with a model in which only the molecules were stretched, as this would have changed the D-period by a factor of 6%, rather then the measured change of only 2%. The data showed that an increase in the gap region alone could not explain the change in the diffraction spectra, as it showed that the overlap region had also become shorter. This could only occur if there was a sliding of the molecules over each other.
Sasaki et al [66] argue that this must be the case too, because if the two mechanisms of gap region increase and molecular sliding did not act in concert there would be an observed tilt in the D-period and this does not fit with their experimental data.
As it is possible to measure changes in the D-period using SAXS, is it possible to use this as an indirect but sensitive measurement of tendon strain to detect differential loading in the FDS terminal tendons? In order for this to be possible an understanding of how the change in the D-period relates to overall strain in the tendon is needed.

2.5 Relationship Between D- Period And Tendon Strain

Mosler et al [53] demonstrated that there was a 1.8% change in the D-period compared with a 5% change in the elongation of the specimen as a whole. They observed a change in the D-period from 67nm up to 68.3 nm and recorded that it returned to its original value at conclusion of the experiment when the load was removed. Fratzl et al [28] reported that in the linear region of the stress/strain curve the D-period increased by approximately 40% of the applied strain. In the toe and heel phase of the curve there was no change in the value of the D-period as can be seen in the graph below indicating that at these stages there is no strain in the fibrils. Note that the D period does not start to change until the heel region of the curve.

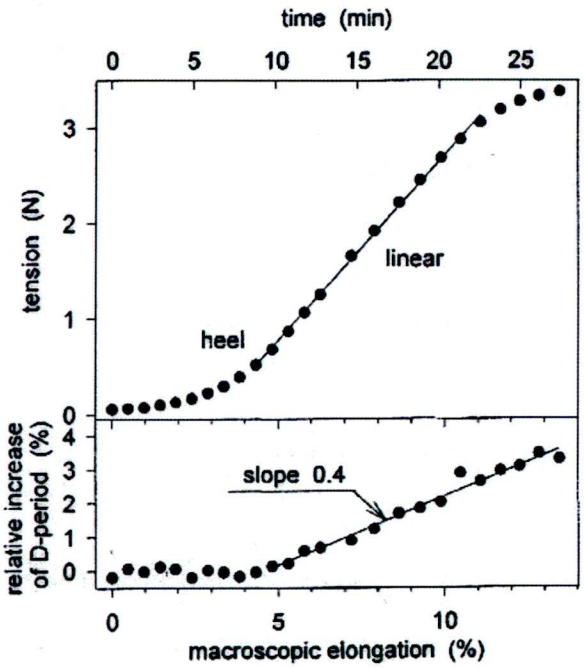

Figure 12 Change in the D-period with loading for a rat tail specimen.

Graph from P. Fratzl *et al.*, *Journal of Structural Biology* **122**, 119 (1998)

Sasaki and Odajima [64] noted that the steep region of the force/strain curve for the force/strain curve for the collagen fibril was linear and the slope was almost equal to that of the linear region of the tendon force/strain curve in their experiments on bovine achilles tendon (BAT). These results indicate that the strain induced by an applied tensile force at the linear region of the stress/strain curve is attributable to strain that occurs in the fibrils.

So, if the change in D-period of the FDS samples can be demonstrated to be linear then it would provide a sensitive measure of the strain in the fibrils and hence the strain in the linear region of the stress/strain curve for the tendon, thus allowing any small differences in strain to be detected over this phase of loading.

The fibrils are embedded within a proteoglycan matrix and Fratzl and Bordas [27] later argued that that tendon must be considered as a composite.

The diagram below demonstrates the relationship between D period, fibrils and matrix.

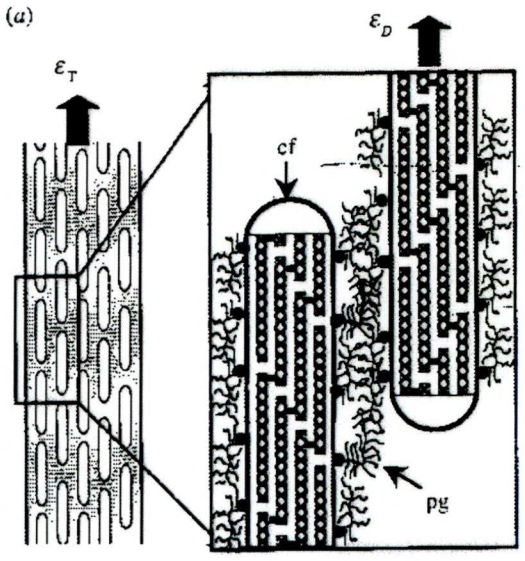

Figure 13 Fibrils embedded in PG matrix

Source: P. Fratzl, J. Bordas, *Synchrotron Radiation News* **15**, 18 (2002)

On the left a fibre is represented composed of multiple fibrils embedded in PG matrix. On the right detail showing fibrils composed of collagen molecules

The total strain in a tendon is:

Fibrillar strain + strain in the proteoglycan (PG) matrix.

and

Strain in the PG matrix = strain between neighbouring collagen fibrils.

Strain in the fibrils = molecular strain + shear between neighbouring molecules.

Therefore:

Tendon strain > Fibril Strain > molecular strain.

However, in order to maximise experimental sensitivity the viscoelastic elements of the tendon response must be understood and accounted for.

2.5.1 Molecular Creep

Sasaki and Odajima [65] investigated the stress/strain response of the individual collagen molecules in tendon to calculate the Young's modulus for a collagen molecule. They demonstrated a linear stress/strain relationship for the molecule and, importantly, a viscoelastic response.

The experiments by Sasaki and Odajima[62] on Bovine Achilles Tendon and the method were based on changes in the wide-angle x-ray scattering (WAXS) pattern which represents the distance between neighbouring amino acids in the molecular structure. They built on work that was done by Cowan et al [18]. These authors were unable to calculate a modulus due to a lack of information about the arrangement of collagen molecules in the fibril at that time.

Sasaki and Odajima [66] argue that this viscoelasticy was due to exchange of water molecules between 'helix stabilising' intramolecular bonds. The Young's modulus of a collagen molecule as recorded as 2.9 GPa, three times greater than their calculated Young's modulus of a fibril.

2.5.2 Proteoglycan Matrix and Creep

The majority of viscoelastic behaviour is due to the proteoglycan matrix in which the collagen fibrils are embedded [58]. This substance results in the creep phenomenon and is also responsible for the strain rate dependent changes in the mechanical properties of tendons.

Creep is the gradual elongation of a tendon when a load is maintained. Upon loading there is an initial elongation of a specimen but, if the load is maintained, there is a slower gradual lengthening of the specimen and this is known as creep [58].

The proteoglycan matrix (PG) has been investigated in rat tail tendon (RTT) and has been found to play a crucial role in its properties. Mosler et al [53] performed time resolved experiments showing that the molecular sliding process continued when the tension was maintained despite no change in the D-period indicating a viscous element to collagen at the molecular level. Fratzl et al [28] also concluded that interfibrillar gliding was mediated by a highly viscous substance containing proteoglycans and water.

Puxkandl et al [58] investigated the PG matrix. They were interested in the effect of the applied strain rate on the rate of change in the D-period as well as overall tendon strain. SAXS data from RTT in normal and cross-link deficient rats were compared and Puxkandl and colleagues concluded that the extension of the collagen fibrils inside the tendon was always considerably less than the overall strain in the tendon. They also found that for normal collagen the PG matrix becomes stiffer at higher strain rates leading to a smaller increase in the D-period at high strain rates. The cross-link deficient collagen had a greatly reduced fracture stress emphasising the importance of the PG matrix in the stability and load bearing capacity of tendon.

Puxkandl et al [58] described a model of collagen based on the fibril extension and the shear stress in the 'glass-like' PG matrix. The importance of the PG matrix for the stability of collagen was confirmed earlier by Davison who had taken the opposite approach to the problem by stabilising the bonds in the PG matrix of RTT samples [19]. This was achieved by reducing the amino acid bonds in a solution of sodium

borohydride. Davison demonstrated a significant increase in the resistance of the collagen fibrils to fracture stress following this treatment.

It can be seen therefore that the time dependent nature of the stress-strain response in tendon is attributable to the collagen molecule response and the PG matrix. In order to obtain accurate results for strain differential in the terminal tendons the rate of application of strain must be consistent and the method for measuring the strain in the fibrils must be able to employ a technique that uses short exposure periods to allow for the confounding effect of the gradual change in the D-period due to viscoelastic responses.

Therefore by keeping exposure times limited the initial change in loading the tendon can be measured without any interference from the viscoelastic changes that occur during creep, making data interpretation less complicated. This reduction in exposure times is easily accomplished if a high energy source such as Synchrotron is used.

2.6 Summary

To summarise, tendon is a complex structure of collagen molecules assembled from microfibril and fibrils which are embedded in a viscoelastic proteoglycan matrix. During loading a typical 3-phase response is seen known as the toe, heel and linear phases. For the purpose of these experiments in this chapter the most important phase is the linear phase of the curve. At this phase of the curve the fibrils and matrix between them bear the load.

The strain in the fibrils can be measured by looking at the change in the repeating gap and overlap pattern of collagen molecules within a fibril known as the D-Period. This stagger changes under loading as the molecules slide over one another. However with prolonged application of load the phenomenon known as creep causes a slow gradual increase in length of the specimen. This is due to the viscoelastic properties of the proteoglycan matrix between the fibrils. It is therefore important to limit the exposure times in order to simplify data interpretation by using a bright synchrotron source.

2.7 Experiment 1- Tendon Diffraction

The first experiment was designed to test if diffraction patterns could be reliably collected from the human flexor tendon samples from the cadaveric specimens and to investigate change in the D-period with applied load. If a linear change in the D-period could be demonstrated for the FDS terminal tendons then this could potentially be used as a sensitive measure of strain over the linear phase of the stress/strain curve. The method would then be applied to each of the terminal tendons in turn in order to determine the loading characteristics.

2.7.1 Experimental set up

An experimental set up that would allow loading of tendon samples under carefully controlled conditions was required as small changes in temperature or humidity have the potential to alter the SAXS pattern independent of any loading [35].

2.7.2 Method

The experimental apparatus is described below

The beamline used for the experiments was the station 2.1 in Daresbury, the medical beamline.

A chamber was constructed that would allow precise positioning and loading of the tendon samples under temperature and humidity control.

The goals in constructing the chamber were to allow:

1. Controlled loading of specimens
2. Measurement of the applied load during the exposure.
3. Control of temperature and humidity
4. Registration of diffraction patterns
5. Precise positioning of specimens in the beam

A clamp that could fit within the limited space of the experimental apparatus and prevent slipping of the specimen over the range of loads applied was required. Furthermore accurate positioning of the beam on the specimen needed to be achieved in

order to analyse the terminal tendons in turn. This was done through mounting the chamber on a rig that could be translated along X and Y axes.

The experimental chamber was fashioned from steel and glass insulated with polystyrene.

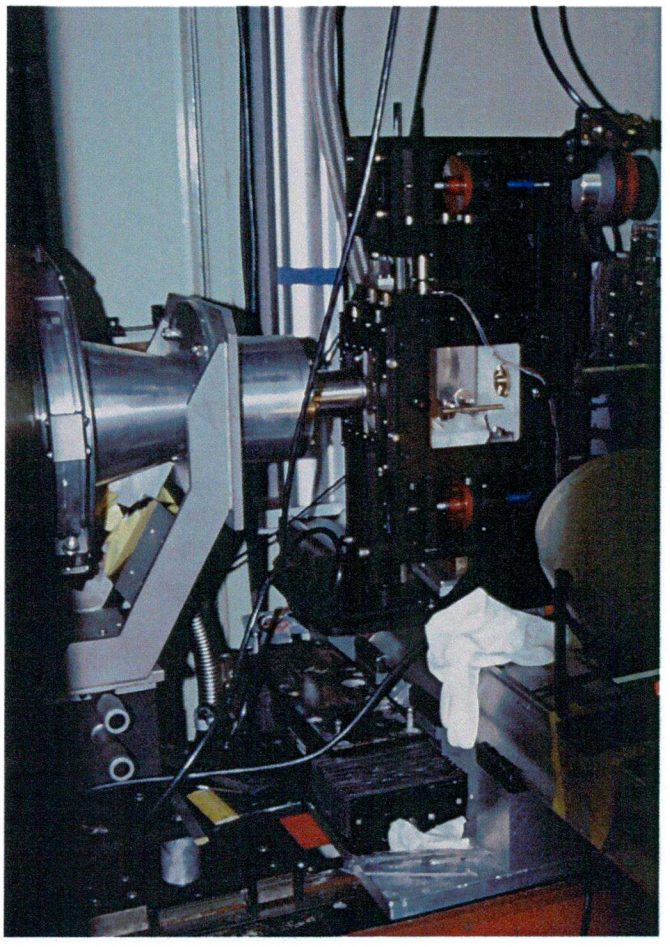

Figure 14 The experimental chamber mounted on the beamline

Small holes in the top and bottom of the chamber allowed the passage of loading rods to which clamps were attached. The clamps used were made from brass lined with sandpaper after the method of Sasaki et al [66]. These authors had successfully used a similar technique to measure the change in D-period of bovine achilles tendon samples.

The clamps were sufficiently strong to prevent specimen slippage within the range of loads that were to be applied for the experiments. It was not possible to use any bulky method of clamping the tendons due to limitation of space within the experimental chamber. Any slipping of the specimen would have been readily apparent from a change in the SAXS reflections during an exposure.

The upper and lower clamps could be moved apart at the same time and rate via step motors so that the region of the specimen being imaged by the beam would be the same throughout an experimental run.

A load cell with a range from 0-1000N was used to measure the applied load. The upper clamp was hinged and therefore pressed against the cell as the load was increased. The load cell output was read via a voltmeter. A calibration curve was plotted for the load cell prior to starting the experiment by loading the upper clamp with a series of weights of known mass. 4 bolts were used to seal the side of the chamber and 100% humidified air was pumped in throughout experiments and circulated by a small fan in the chamber. Humidity was measured via a sensor. Two small windows were cut in the chamber and covered with MICA to allow free passage of the beam across the chamber. MICA has very little effect on the X-ray beam and therefore allowed the chamber to be sealed without interfering with collection of the diffraction data. The chamber was set on a stage that could be moved in X and Y directions in small increments from the safety of the experimental hutch.

For these pilot experiments the author wished to use samples of other flexor tendons from the cadavers in order that the set up could be refined prior to testing on the FDS tendons. The tendons chosen were flexor carpi ulnaris (FCU) and palmaris longus (PL).

The FCU and PL are similar to the FDS in that they form part of the flexor musculature in the forearm. The PL is a vestigial tendon that is not present in all people. It is a somewhat smaller and flatter tendon than FDS but this made it a good choice for initial testing of the experimental arrangement. The reduced dimensions of the tendon allowed decreased beam strength and exposure time thus minimising the effect of creep.

The FCU is one of the two primary wrist flexors and is therefore a larger and thicker tendon than both the PL and FDS. Correspondingly the loads needed to be greater to observe the same magnitude of change in the D Period as the PL. If a reliable linear change in the D–Period could be measured in both samples then it would serve as a good indication that the FDS terminal tendons could be examined using this experimental set up.

The fresh frozen human cadaveric forearm specimens were thawed at room temperature overnight before being dissected. Specimens of palmaris longus PL and FCU were harvested on the morning of the experiment. Specimens were wrapped in saline soaked swabs and sealed in specimen pots until mounted in the experimental rig.

Data was collected up to the 9th order reflection and analysed as described in the next section. The change in intensity of the 9th order was used to calculate the change in the D-period and plotted against applied load.

2.7.3 Data collection method

Data were collected on the small angle x-ray scatter (SAXS) station 2.1 on the Synchrotron Radiation Source at the Daresbury Laboratory. The optics on station 2.1 starts with a Ge <111> bent triangular crystal positioned 8 m from the dipole magnet tangent point. This monochromator is capable of accepting up to 15 milliradians of horizontal radiation. It is approximately 300 mm long and is clamped with its base facing the source. Bending of the crystal tip is provided by a ceramic eccentric roller driven by a vacuum stepper motor in order to focus the beam horizontally at different positions. For these experiments the beam was focussed on the face of the x-ray detector. The crystal has an asymmetric Fankuchen cut of 11.6° resulting in a beam compression of ~11 times. Following the monochromator is a mirror which is necessary for focussing the beam vertically. This is an uncoated fused quartz mirror 75 cm long and lies 9.25 m from the dipole magnet tangent point. The mirror is mounted so as to reflect the beam uphill. In order to vertically focus the beam anywhere along the optic bench inside the experiment hutch the mirror can be bent to a radius anywhere between 891 mm and 2427 mm. Four pairs of defining slits are positioned after the monochromator in order to collimate the beam in the vertical and horizontal planes. The slits are used to define the beam size at the sample position. Each set of slits comprises

of two vertical and two horizontal jaws which can be moved independently. Set 1 (slits 1 & 2) is installed between the monochromator and the mirror. Following the mirror are a further set of slits (slits 3 & 4) which are incorporated into the end of the mirror vessel. Slits 5 & 6 are 30 cm from the wall which separates the experimental hutch from the optics area. The last set of slits (slits 7 & 8) are mounted within the experimental hutch at a distance of approx. 50 cm from the sample position. The sample to detector distance (known as the camera length) can be set from 2.0 metres to 9.3 metres on this station depending on the scatter angle range required in the data. For the purpose of these experiments the camera length was set to either 4.3 metres or 6.25 metres. The wavelength of the X-raybeam on station 2.1 is fixed at 1.54 angstroms (8.0 keV). At the sample position the dimensions of the beam were defined to be 1.0 mm by 0.5 mm by the system of slits. X-rays scattered from the sample were recorded using a Daresbury built 2-D Area detector. This is a delay line readout multi-wire proportional counter. The detector is filled with Argon / Xenon / CO2 counter gas and it is capable of recording $1x10^6$ X-rays per second over an area of 200 mm by 200 mm.

The detector is made of pixels and each pixel consists of one gas filled chamber. When an x-ray photon hits the chamber it interacts with molecules of gas inside it producing positive and negative ions. A voltage is applied across the chamber so that these ions will accelerate towards the anode and cathode at such a rate that they produce secondary ionisations. These newly created ions will again produce more ions as they move across the chamber causing an avalanche of ions and up to 10^6 amplification of signal.

The accumulating x-ray scatter pattern is displayed in real time using a large colour monitor in the control room of the station. At the end of collection time the pattern is recorded to disk using a standard non-crystalline diffraction file format BSL.

2.7.4 Data reduction and analysis

The reduction of the data started by correcting for the non-linearities and inefficiencies in the detector. The inefficiencies are due to a 5% variation in response between pixels in the detector and from a grid pattern secondary to the fine anode wires used in the gas chambers. To account for these variations a white field illumination from a radioactive source is obtained. This uniform illumination image must be normalised to 1.0 based on the response from the pixel with the most signal. This image can then be subtracted

from the raw SAXS images so that small variations in the SAXS pattern are not swamped by the noise from the detector response.

A calibration image is made during the initial stages of the experiment using a prepared length of rat tail tendon. The tendon is almost pure collagen type 1 with a reliable D spacing of 67 nm when wet. This image is used to accurately determine the camera length and hence scatter angle for all the data collected during that run. A correction for the intensity of the beam is then made. The strength of the x-ray source on the synchrotron is directly related to the electron current in the acceleratory. This was recorded at the time of taking the data and subsequently used to normalise the intensity of the scatter from the sample. An alternative was to measure the beam after being transmitted through the sample using either an ion chamber, or a photodiode. This correction also accounts for any small variation in the x-ray attenuation of the sample at different strains or positions.

Once normalised and calibrated the images are transformed to polar coordinates. One coordinate is the azimuthal angle ϕ around the centre of scatter i.e. the direct beam. The other is the magnitude of the scattering vector **q,** which is related to the radial distance to the scatter centre. The magnitude of q is $4\pi/\sin(\theta)$ where θ is the scatter angle with respect to the direct beam.

For highly oriented fibre data such as collected from the tendon it is useful to reduce the 2-D data to 1-D using a sector integration of the 2-D image. This process produces a graph of intensity against q integrated over a range of ϕ. The graph shows the peaks, referred to as 'reflections', due to the D spaced electron density fluctuations in the tendon collagen under examination. In order to detect small changes in these reflections the background and peaks are fitted using the Data Analysis and Visualisation Environment (DAVE) suite from the NIST centre for neutron research .In most cases a linear background under a Gaussian peak fits sufficiently well to parameterise the reflections. A better fit could be made with the following function added to a linear background:

$$y = a + \frac{4bn}{(1+n^2)} \text{ Where } n = e^{\frac{-(x-c)}{d}}$$

In most cases the simpler background plus Gaussian was used to find the centre and width of the reflections.

2.8 Results

2.8.1 Change in D-period

The graphs below plot the change in D period from flexor carpi ulnaris and the change in the position of the 9th order reflection for the palmaris longus tendon for loads from 0 to 14 N and 0 to 40N respectively. A change in the D-period from 66.75nm to a maximum of 67.08nm is demonstrated.

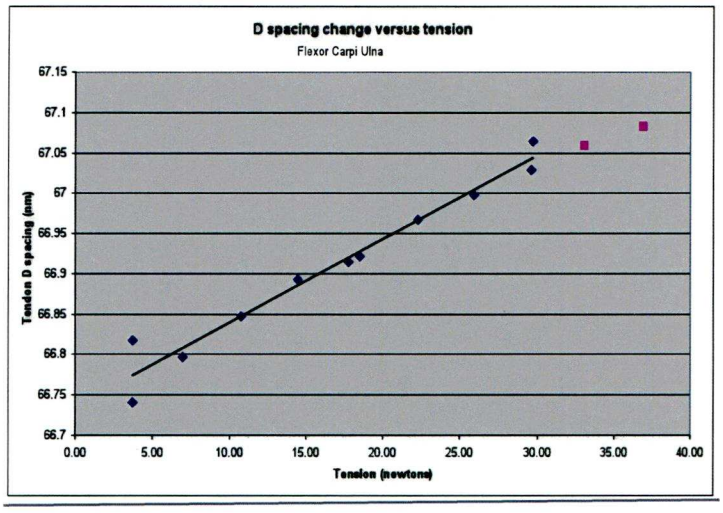

Collagen D spacing change as a function of tension, measured using the 9th order.

(Colours represent different experimental runs but same specimens.)

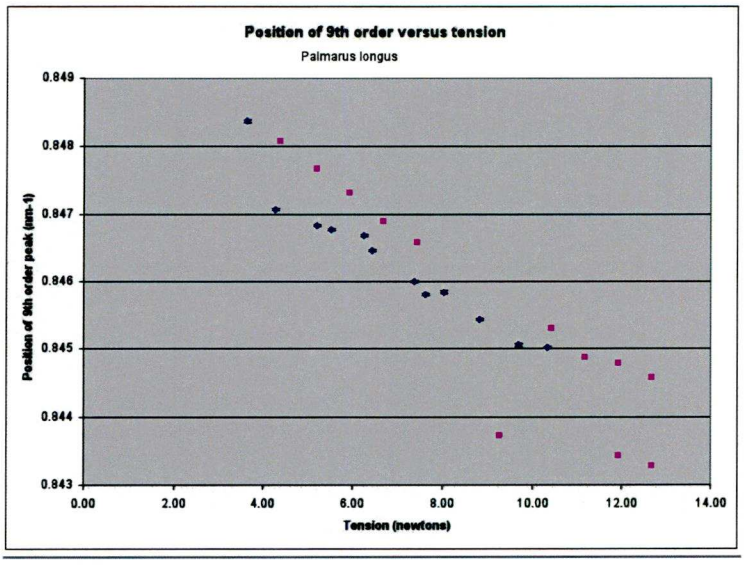

There is a linear relationship between change in the D-period and applied load for the FCU and PL tendons for the range of loads examined.

Following the success of the pilot experiments testing the experimental set up and showing that it was possible to measure the fibrillar strain through the change in the D-Period the author progressed to testing on the FDS terminal tendons.The goal was to reproduce the results from the previous experiment in the terminal tendons of the FDS allowing the change in the D-period to therefore be used to determine the strain in the terminal tendons. This could then be used as a sensitive measure of any difference in loading between the radial and ulnar terminal tendons

2.9 Anatomical Dissection

As the terminal tendons overlie the PIPJ and the proximal portion of the middle phalanx with only a short length before the tendons insert on to the bone the author wished to determine if the tendons could be examined without disturbing the joint surface.

To do this with the experimental apparatus it would be necessary to remove any interposing bone as this would produce its own diffraction pattern. Therefore, a window through which the x-ray beam could pass without interacting with bone, was required. Any bone between the beam and detector would give rise to an additional complex diffraction pattern. This would be difficult to subtract from the diffraction pattern of the tendon. As the change observed in the diffraction pattern in the first experiments was relatively small it was important to gain the highest quality data from the tendon rather than trying to subtract from the pattern or apply any filtering.

The author needed to determine if was possible to create such a window in the base of the middle phalanx while maintaining the articular surface of the joint. To answer this question an anatomical dissection of embalmed specimens was undertaken in the Anatomy Department at the University of Liverpool.

Cadaveric hand specimens, supplied by Liverpool University, were dissected in the department of to determine if it would be possible to fashion such a hole and still maintain the attachment of the terminal tendons. It was important that this could be done without any compromise the distal PIPJ joint surface.

A Brunner [11] incision, a volar zig-zag style of incision, was used to expose the tendon sheath which was then opened to expose both flexor tendons. The Flexor Digitorum Profundus was transected proximally at the level of the distal palmer crease and then pulled through the FDS to allow inspection of the chiasma. The same procedure was performed with the FDS transecting it proximally so it could be retracted to expose the volar plate of the PIPJ.

The volar pate was excised to allow assessment of the distance between the beginning of the FDS insertion and the distal joint surface of the PIPJ i.e. the base of the middle phalanx. An image from the dissection is shown below demonstrating the length of bone between the joint margin and the FDS insertion. The left hand side of the image is the distal portion of the finger.

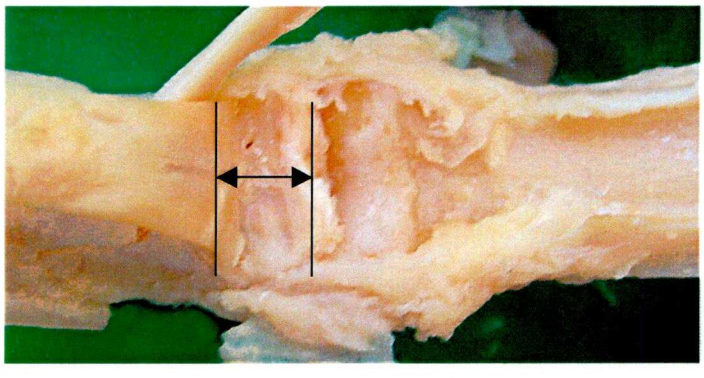

Figure 15 Space between insertion and articular surface

It was determined that it would be possible to fashion a hole through this portion of bone without breaching either the joint surface or detaching the FDS from the middle phalanx. A specimen with such a hole fashioned is shown in Figure 16

Figure 16 Hole for passage of SAXS beam

Following the dissection study that demonstrated that it was possible to image the terminal tendons through a hole in the base of the middle phalanx without disturbing the insertion or joint margin a second experiment was designed.

2.10 Experiment 2 – FDS Diffraction

A hole was fashioned in the base of the middle phalanx of the finger for this experiment using a small drill in the position determined by the dissection study. Great care was taken that the insertion and joint surfaces were not disturbed.

The experimental set up for examining the FDS terminal tendons was as follows. The middle phalanx was clamped in the upper clamp and the FDS tendon was clamped in the lower clamp. The two terminal tendons were examined through this window in the bone in turn, by translating the stage.

A diffraction pattern was first collected from the proximal part of the FDS tendon to obtain a baseline reading of the diffraction pattern.

The margins of the bone window were then mapped out prior to imaging the terminal tendons. This was performed by raising the tendon away from the bone window and directing the beam through it. The values needed to translate the stage to the margin of the hole were noted. This ensured that any diffraction patterns collected were from the terminal tendons alone and not due to interference from the margins of the bone window.

2.10.1 FDS Tendon Strain Experiments

The diffraction pattern obtained from the terminal tendons was significantly different from the proximal tendon. The normal collagen reflections were superimposed on an amorphous background. Given that the margins of the bone window had been carefully mapped out and the angle of scatter was far too small for the diffracted beam to have hit the margin of the hole while traversing the length of the phalanx the author concludes that the structure of the tendon at this point was significantly different.

Figure 17 displays, the diffraction patterns obtained from the terminal tendons of the FDS, a region very close to the insertion of the tendon onto the bone. It can be seen by comparison with Figure 18 – a significant qualitative difference in the clarity of the

reflections. The pattern from the body of the tendon displays clear, sharp reflections whereas near the insertion this definition in the reflections is almost completely lost.

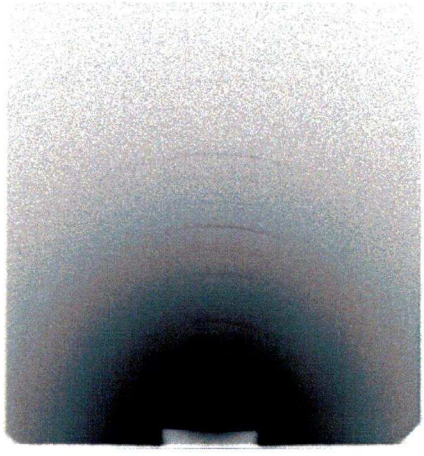

Figure 17 Diffraction pattern near to the insertion

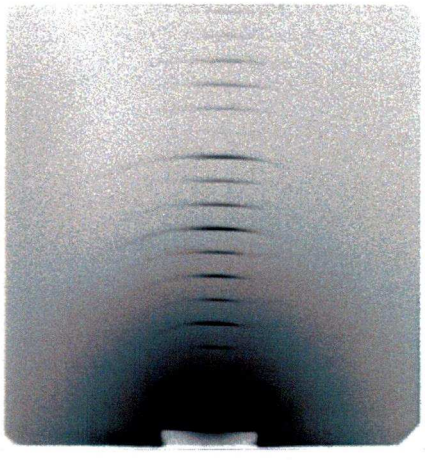

Figure 18 Diffraction Pattern from body of the FDS

2.10.2 Raster Scan

In order to determine where the change in composition of the tendon started a further experiment to map the diffraction patterns from the terminal tendons was devised. This procedure is known as a raster scan [(83)].

This allows the build up of a 2-dimensional map of the structure of the terminal tendons.

Figure 19 Shows the results of the raster scan from the terminal tendons of the FDS displaying the changing patterns as the tendon is examined from its insertion to more proximally towards the chiasma.

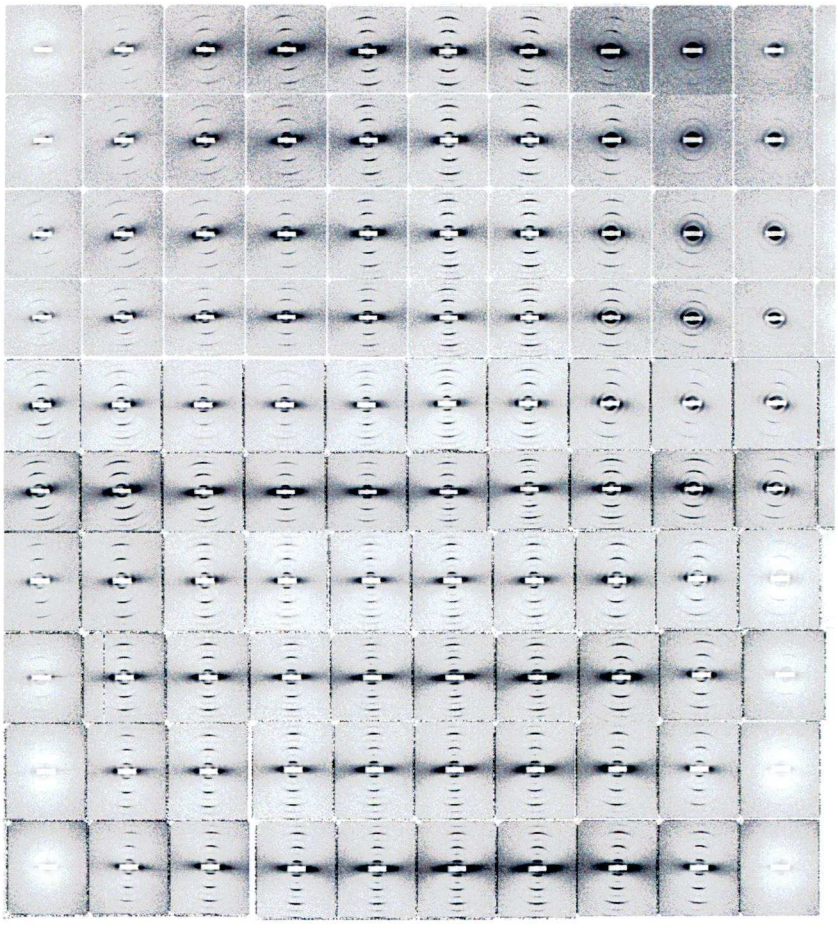

Figure 19 Raster scan of the FDS terminal tendons.

Lower half of the image is from the proximal tendon and the upper half is the insertion site. The orientation of the fibres within the tendon can be discerned from the changing angle of the diffraction pattern. An increase in the background scatter near the insertion (top) as compared with the chiasma (bottom) is demonstrated.

It can be seen that at the bottom portion of the map the diffraction patterns are clear and sharp but progressing towards the insertion the reflections are less clear and the background scatter is more pronounced. In the proximal part of the tendon the

diffraction peaks are represented as narrow arcs but towards the insertion it can be seen that the reflections appear as rings, an indication of increasingly random orientation of the collagen fibres in this part of the terminal tendons.

2.11 Discussion

The diffraction experiments initially yielded promising results. The ability to register very subtle changes in the diffraction pattern from the proximal tendon body and the demonstration of a linear change with loading demonstrated the feasibility of quantifying strain at the fibrillar level. This would have provided an extremely sensitive method for investigating any potential difference in strain between the terminal tendons.

The surprise from the investigation was that the composition of the terminal tendons was significantly different along the length of the whole terminal tendon. Hirsch [39] investigating the enthesis found that the zone of transition from tendon to bone varies from only a micron to a millimetre long in an adult. Infants have slightly longer transition zones but all specimens used in these experiments were from adults. It is therefore unusual to find such markedly different diffraction patterns much further away from the insertion. What was different about this region of the terminal tendons as compared with the main body of the tendon?

A review of other studies regarding the transition from tendon to insertion found that there are a number of described changes in this region. Historically Sharpey [69] was one of the first to examine the enthesis in detail. He described collagen fibres passing directly from tendon and into the substance of the bone. These were termed "Sharpey's fibres" but there existence was questioned in later work by Dolgo [22] who stated that what Sharpey described may have been collagen fibres drawn out as he pulled sections of the lamellae apart. Dolgo's description of the enthesis was more complete. He described four distinct zones in a study of cat patella tendon. The zones were tendon, fibrocartilage, mineralised fibrocartilage and lastly bone. Could it be possible that the

transition zone in the terminal tendons is much longer? The changes observed in the raster scan started 3-4 mm away from the insertion though and it is difficult to imagine that the tendon would exhibit fibrocartilaginous differentiation at such a distance greater than previously described.

Were there any other changes in this region that may account for the change in diffraction pattern? The raster scanning demonstrated that the collagen was less ordered in the terminal tendons and this agrees with the findings of Thomopoulos et al [75] who demonstrated less ordered collagen fibres on what he termed, the bony side of the insertion but this again would be expected to be much further down the terminal tendons than the region examined in this study. Thomopoulos et al also found that the expression of collagen types was different on the bone side of the insertion. Types II, IX and X are present on the bone side but not on the tendinous side. It may be that these collagen types are present in the more proximal parts of the terminal tendons and this plus the less ordered arrangement of fibres may be what is disrupting the diffraction data.

A further change in this region of the enthesis is the expression of proteoglycans Aggregan is the main chondroitin sulphate of cartilage Wagget et al [81] demonstrated its presence in the fibrocartilaginous zone of the insertion but not in the mid substance of Achilles tendons. Decorin and biglycan are the usual proteoglycans associated with tendon but they differ greatly in terms of size aggregan is 320Kd compared with 40Kd for decorin and biglycan. A more proximal expression of aggregan could also result in a more complex background diffraction pattern.

Further study on the terminal tendons would be required to answer these questions as to whether the types of collagen, proteoglycans or cartilaginous differentiation are causing the change in the diffraction pattern but the author wished to pursue the development of a methodology to investigate strain in the terminal tendons and therefore no further histological investigations were performed on the specimens to examine collagen or proteoglycan expression.

2.12 Summary

To summarise, the SAXS experiments demonstrated that fibrillar strain could be measured with the experimental set up in human flexor tendons by registering a change in the D-Period. The method was not applicable to the terminal tendons due to a significant difference in their structure compared with the body of the tendon. Therefore a different approach was sought, one that would not be affected by such differences in composition and preferably a method that would allow soft tissues to be left intact.

In the next chapter a method using different algorithms for analysis of magnetic resonance images of the cadaveric specimens is presented.

Chapter 3

3 MRI

3.1 Introduction

Following the x-ray diffraction experiments in the preceding chapter the author sought a different approach to the research question. A report in the literature [6] detailed a methodology for strain quantification in tendon using analysis of MR images. The author perceived that this would have a number of benefits over the x-ray diffraction method in that soft tissues and the FDP tendon could be left intact. This would therefore reproduce the in vivo conditions more accurately. The passage of the FDS around the FDP body would no doubt have a significant effect on the vector of pull of the terminal tendons.

The question was if the method would be applicable to the FDS as the volume of tissue was much smaller than that described by Bey et al, and if a suitably sensitive algorithm could be devised to detect the change in the images. The first task was to determine if detailed images of the tendon could be acquired that would allow the application of any suitable image analysis methodology. This required exploiting an unusual property of tendon when imaged using MR, known as the magic angle phenomenon.

Following successful acquisition of suitable images, different approaches to the problem of the analysis were investigated using first a texture or optical flow analysis and then secondly an approach based on the change in outline of the tendon.

First a review of the principles involved in the imaging and analysis is presented.

3.2 Principles Of Magnetic Resonance Imaging

The following is a brief synopsis of MR imaging physics.

3.2.1 Hydrogen

All nuclei that have an uneven number of protons and neutrons have a small magnetic moment. In clinical MRI the nucleus that is exploited is Hydrogen, as it is a relatively abundant element within the human body and its solitary proton induces a large magnetic moment.

3.2.2 Precession

An important component of the magnetic moments of the individual hydrogen nuclei is that they are not static but are said to precess. This has been compared to the motion of a spinning top and means that the magnetic moment describes a vector, that graphically represented, resembles a cone.

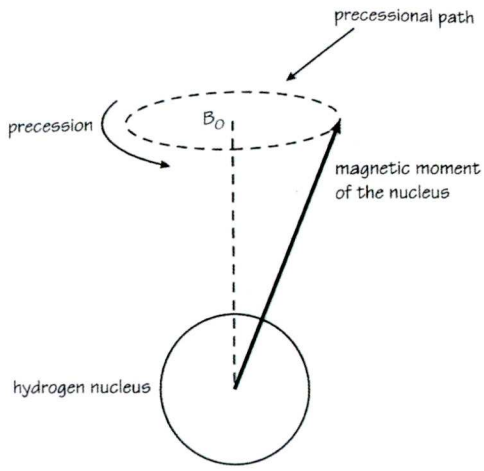

Figure 20 Precession of a Hydrogen Nucleus.

3.2.3 NMV and MR Signal

The magnetic moments of hydrogen nuclei when placed in a strong external magnetic field can adopt one of two states. Either they can align their magnetic moments with the field, known as parallel or low energy, or they can align themselves against the field, known as anti parallel or high energy. The stronger the external field applied then the more nuclei will align themselves with the field as the energy needed to adopt the anti-

parallel state increases. This results in a patient placed in such a field having a net magnetisation vector (NMV).

The NMV can be modified to produce a signal by using radiofrequency pulses. If a radiofrequency (RF) pulse is applied at the same, resonant, frequency as the hydrogen nuclei are precessing then two things occur.

1. Energy Absorption
2. Phase Coherence

3.2.4 Energy Absorption

Nuclei absorb energy from the RF pulse so more of them are able to align their magnetic moments anti-parallel to the main external magnetic field B^0. If just enough energy is transferred then the number of protons aligned parallel and anti-parallel to the field will be equal. This will result in the NMV flipping into the transverse plane.

3.2.5 Phase Coherence

The RF pulse also causes the magnetic moments to move into phase with each other. The NMV is therefore in the transverse plane and precessing around the patient.

3.2.6 Signal Generation

If a receiver coil is placed next to the patient in the transverse plane then the NMV will induce a voltage in the coil. This is the MR signal.

Once the RF pulse is removed, the signal will begin to decrease. This is termed free induction decay (FID).

3.2.7 Relaxation Processes

Two separate processes result in decay of the MR signal.

Following removal of the RF pulse, nuclei will move from the high energy to the low energy state, shifting their magnetic moments to align with the field again by losing energy in a process known as spin lattice energy transfer. This will cause the NMV to shift from the transverse plane and back in line with B^0.This is known as T1 recovery.

There is also a loss of precessional coherence as the RF pulse is removed through two mechanisms.

The first is known as T2* decay and is due to local inhomogenities in the field strength. This results in adjacent nuclei either precessing slightly faster or slower than their neighbours depending on whether they are in a region of increased or decreased field strength relative to B^0.

T2 decay is due to interaction between the magnetic fields of adjacent nuclei (spin-spin relaxation). The structure of tendon limits the motion of water molecules and this facilitates exchange of energy between nuclei leading to a rapid T2 decay.

Manipulation of these processes are used to produce contrast in the MR image, as different tissues will be subject to these relaxation processes at different rates.

3.2.8 Fourier Transform

The MR signal is a complex waveform that contains all of the image data. It must be decoded to extract the data. In order to decompose it into its constituent frequencies, which can then be used to construct an image a mathematical process known as a fast fourier transform (FFT) is used.

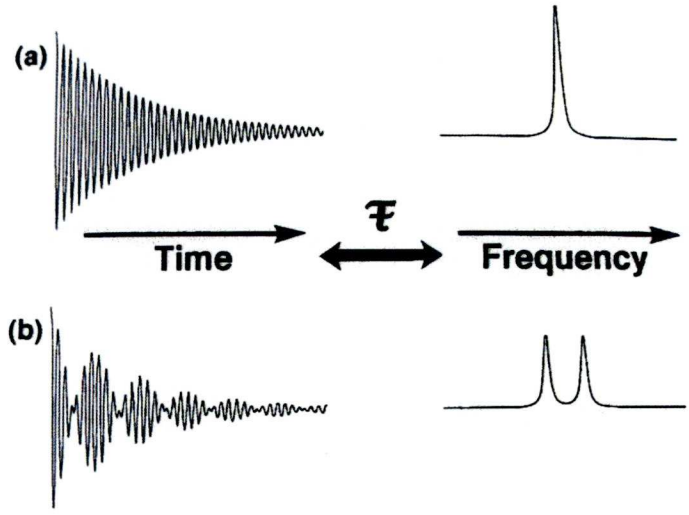

This process is able to tease out the component frequencies from the FID signal.

3.2.9 Problems in imaging tendon

Tendon has a short T2 relaxation time making it difficult to visualise on routine MR scans. The effect of this is that the tendon appears as a signal void. To combat this, very short echo times (TE) are used on the scanner in an attempt to detect signal prior to decay but in practice the echo times are outside the range of clinical scanners. However, an alternative is to find a way of increasing the T2 decay time so that it falls within the range that can be detected by the scanner. This can be achieved by exploiting the magic angle effect.

3.3 Magic angle imaging

In tissues in which water motion is unrestricted, T2 decay is minimised and rotation of a specimen in the main magnetic field (B^0) has no effect on signal generation. The magic angle effect relies on the highly ordered structure of tendon, which limits the motion of the water molecules associated with the collagen and leads to the change in properties depending on the angle the tendon makes with B^0. The following section describes the physics behind the effect in greater detail.

This effect was first noted during solid nuclear magnetic resonance spectroscopy. This was the first use of what is known as magic angle spinning to increase the signal from samples with a rapid T2 decay curve [56].

Berendsen [5] was the first to publish data on the magic angle effect in collagen samples and described the expression:

$$3\cos^2\theta - 1$$

as the function predicting the degree of interaction between nuclei at a given angle, theta to the main magnetic field B^0. This equation returns a value of zero at the 'magic angle' of 54.7 degrees. Erickson et al [24] later looked at the physics governing the interaction between the water molecules in collagen and explained the effect in more detail. They reasoned that protons in the MR scanner act as small magnets or dipoles. This magnetic interaction can be modelled as the interaction between two current loops as the same laws of physics apply.

3.3.1 Water compartments

Following Berendsen's work, Hazlewood et al [36] and Cooke and Wien [17] argued that within tendons water existed in two different conditions from an NMR perspective. Following analysis of the T2 decay curve they described compartments in which water was either free or bound depending on its ability to exchange energy. The bound water is that which is loosely associated with collagen, forming a hydration layer that is relatively limited in motion while free water has no such limitation and is therefore able to readily exchange energy enhancing T2 decay. Fullerton et al [29] while investigating whether the magic angle effect would have implications for clinical imaging, stated that only one of these compartments composing 70% of the water in the samples was responsible for the increased signal change.

Krasnosselskaia et al [44] investigated the decay curve further to gain a clearer understanding of the relative proportions of the two water compartments. Proportions were calculated by looking at the dimensions of dry samples of collagen. It was hypothesised that the bound water was aligned along the long axis of the collagen molecules in the hydration layer and the free proportion of the water sat in gap regions at the end of the collagen molecules. Krasnosselskaia and colleagues argued that the gap regions were connected, and could thus form channels through which the water could move from one state to the other. The ratio of the two water components was calculated as 5.2 to 1. This is close to the six-fold increase in the MR signal at the magic angle. This description of these channels fits with the staggered arrangement of collagen molecules which giver rise to the D-period as described in the X-ray diffraction chapter. It also agreed with earlier work by Fung [30] who reported that the two water compartments were not static but rather rapid exchange of molecules could occur between the two.

Fullerton et al [29] and Erickson et al [23] found that the effect was very sensitive to any change in the angle, 15 degrees difference being almost sufficient to lose the increase in signal. Erickson and his co-workers looked more closely, at the clinical implications of the effect by examining the position of the arm when scanning subjects and the effect on

the signal level from the extensor tendons. A significant increase in signal at the magic angle was demonstrated although the effect was not as apparent in the flexors due to their undulating course as compared with the extensors. It was found that with routine patient positioning and scan settings the magic angle effect was significant in some tendons and the authors cautioned against interpreting high signal as always being indicative of tendon pathology. Other investigators have also warned about the effect causing tendon imaging artefact in the shoulder [76] knee [57] and foot [73].

Therefore, the magic angle effect was primarily treated as an artefact in clinical MR imaging for some time. However, Bydder [14] described utilising the phenomenon to obtain high-resolution images of tendon. Bydder's paper primarily looked at the back and the Achilles tendon but also presented one image of a finger in sagittal section demonstrating the flexor tendon anatomy.

So, it is clear that the application of the effect to image tendon has been little exploited and primarily the effect has been seen as a potential pitfall when imaging as it can lead to misinterpretation of areas of brightness in a tendon as representing pathology when actually it is due to the orientation in the main field. Certainly, with respect to imaging in the hand, the technique has not been investigated for it may be a very sensitive method of non-invasive soft tissue imaging. The question was whether high resolution images of the cadaveric hands could be achieved and if they could then be analysed to equate strain in the tendon. In the next section a brief review of the development of image analysis to equate strain is presented.

3.4 Image Analysis

The development of image analysis technique for strain quantification started very simply with the use of video and markers fixed to specimens. One of the earliest papers was by Hoffman and Grigg [41]. They described a relatively low-resolution method of image analysis for quantifying soft tissue strain. Experiments were performed on the posterior capsule of feline knee joints. A system of five markers and still frame capture

utilising a video camera was employed and the images were processed using a finite element model. The algorithm and equations used to track the markers and calculate the resultant strain were also published.

A number of investigators subsequently refined the method and improve resolution. Derwin et al [1] attempted to validate a video capture system for the measurement of strain in a sample of rabbit Achilles tendons. The tendon was marked with a number of horizontal lines, using tissue stain, and then filmed while under test. A combination of manual input and a computerised analysis of the marks was used. The position of the marks was entered into the software and then a threshold value was set to register the changes in their position. Accuracy of 0.05% strain at 3.52% strain in the sample was reported using this method. Derwin et al noted the sensitivity of the system to out of plane motions and the need for high-grade optics due to imperfections in the lens of the cameras giving rise to apparent strain.

Following these simple methods of image analysis, more complex and detailed methods evolved based on tracking the motion of either naturally occurring or applied patterns on the surface of samples. The goal being to improve sensitivity so that areas of high strain could be picked up.

Bey et al [3] compared the results of using a marker-based system and a texture analysis algorithm for quantifying strain in contact radiographs of trabecular bone. A low-resolution marker system was tracked as the bone was loaded using a similar methodology of image capture to Hoffman and Grigg [41]. The results were then compared to those obtained using the texture analysis. The texture analysis relied on using the random pattern of the trabecular bone as a 'ready-made'marker system.

Each image was divided into a grid system. Inside each square was a region of the trabecular pattern, unique in its appearance so that the computer algorithm could identify it in subsequent deformed images. The computer looked for a 'best fit' because following deformation under load there would not be an exact match. The algorithm calculated a percentage match for each region and then referenced the new position of the grid point based on the highest probability fit.

In an attempt to validate the texture-based method, peak strains using both methods were compared. They found that the peak strains were higher using the texture-based method although a qualitative assessment of the strain pattern showed a high degree of similarity between the two techniques. It was concluded that it was not possible to validate the method to any higher degree of certainty.

3.4.1 MRI Texture correlation

Bey et al [4] were the first researchers to report the application of image correlation methods to MR images for quantifying tendon strain. Discrete regions of strain within the supraspinatus tendon of human cadaveric specimens were examined. The specimens were mounted on an MR compatible rig and loaded in order to measure the strain in three different regions of the supraspinatus tendon. Using this approach, strains up to 12% were successfully recorded. The ability to image the tendons using the MR in detail by exploiting the magic angle effect and the use of image analysis technology to compute a strain tensor made it an ideal method for investigation of the FDS. The ability to reconstruct images in any plane and three-dimensions was also valuable as it suggested that strain could be measured in different planes.

As it was non-invasive it would allow the soft tissues to remain intact; skin, pulleys and the flexor digitorum profundus could be kept in situ. This was clearly important if conditions were to be maintained, as they are in vivo. The FDS exerts a lateral compressive force on the FDP, as shown by Walbeehm and McGrouther [82]. Therefore, if the FDP were removed it could alter the vector of pull of the FDS as it courses around the body of the FDP.

The author therefore wanted to determine what level of anatomical detail could be resolved by employing magic angle imaging to the cadaveric specimens. Then if images that were suitable for analysis could be captured computer algorithms for analysis of these images were to be developed. The first approach to the analysis was to use the method as described by Bey et al [7] analysing the texture of the images. The following section describes the experiments conducted.

3.5 Methods

3.5.1 Scanner Specification

The MRI scanner used for all experiments was a 1.5 Tesla Siemens symphony. A 4 cm diameter receiver coil was used for signal collection.

3.5.2 Magic Angle Imaging Experiments.

The first experiment was to determine if high quality images of the FDS tendon could be obtained using the scanner available to the author and exploiting the magic angle phenomenon. Different scan parameters were to be tested to determine the settings that would result in the best image for the texture analysis.

One specimen was imaged, first orientated along the line of the main magnetic field B0. The scanner settings were as follows:

Conventional T1-weighted images were acquired with TE 24ms, TR 400ms, NSA 2, FOV 92mm with 512 matrix giving an in-plane resolution of 0.18mm with a 1mm slice thickness. Scan time was approximately 9 minutes for each sequence.

3.5.2.1 Results imaging experiments-Gradient echo and SE images

An example of the image obtained is shown below

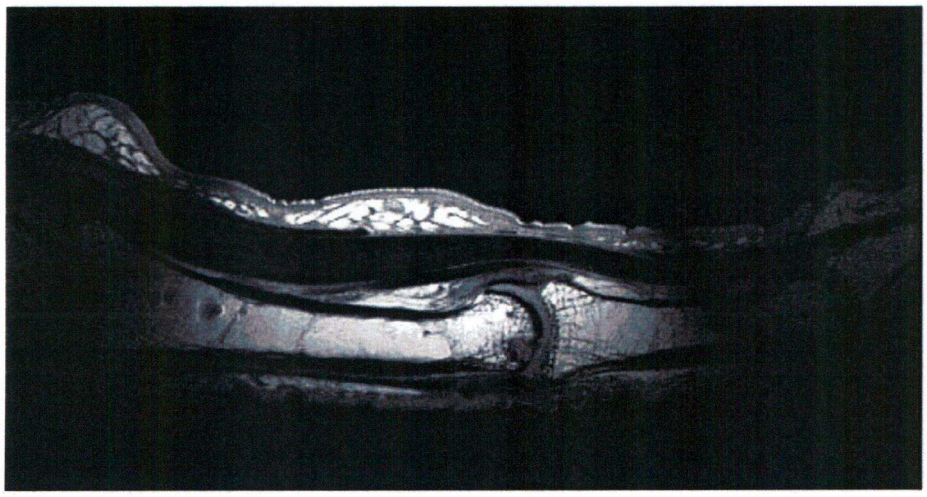

Figure 21 Finger orientated along magnetic field.

This image demonstrates the rapid T2 relaxation of tendon that results in no perceivable structural detail being detected, the tendon appears as a 'signal void'.

A second scan was performed with the same settings on the scanner but this time re-orientating the hand so that the finger being imaged was at the magic angle, 55 degrees to the main magnetic field.

A sample from this sequence is shown below.

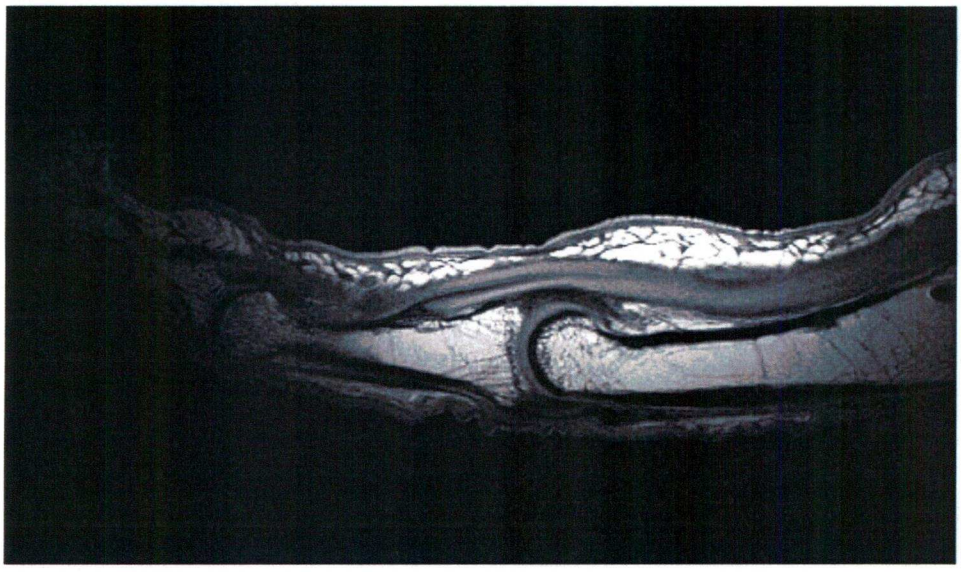

Figure 22 Finger orientated at 'magic angle'

The magic angle effect is apparent with a significant increase in signal from the tendon. The boundary between the FDS and FDP tendons is visualised as they course over the condyles of the PIPJ. In the slice shown in Figure 22 the insertion of the radial terminal tendon of the FDS is demonstrated in sagittal section.

The proposed method for measuring strain was based on the texture i.e. inhomogenities in the appearance of the tissue. Therefore, different scan sequences were run to determine which settings were best for visualising any variation in the appearance of the tendon substance.

A gradient echo sequence provided the greatest level of contrast in the internal structure of the tendon. A sample from this experimental run is shown in the figure below.

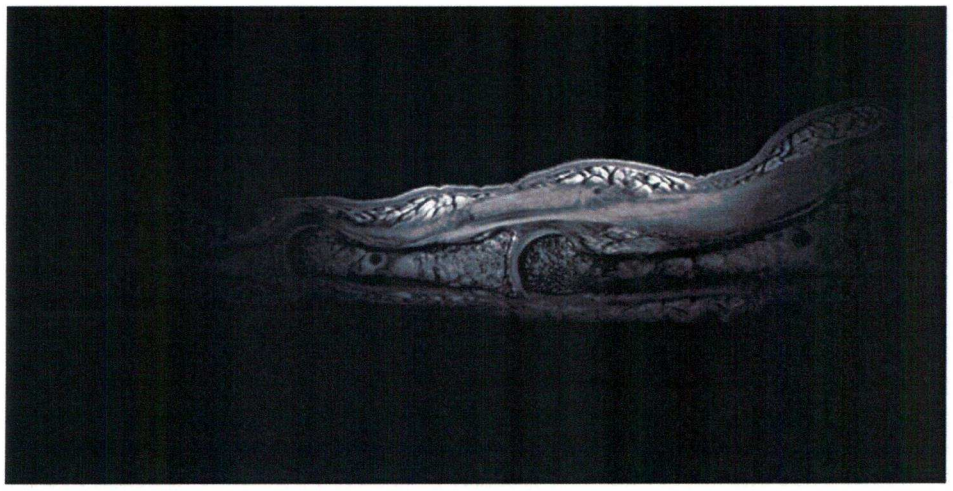

Figure 23 gradient echo sequence

The use of magic angle imaging in the hand had not been explored in any detail in the literature that the author could find and so further images were obtained in order to determine if the technique could be applied in clinical practice to investigate closed injuries of the hand. Below are a sample of images showing the pulley system in cross section and the volar plate as well as images of the FDS during flexion of the PIPJ.

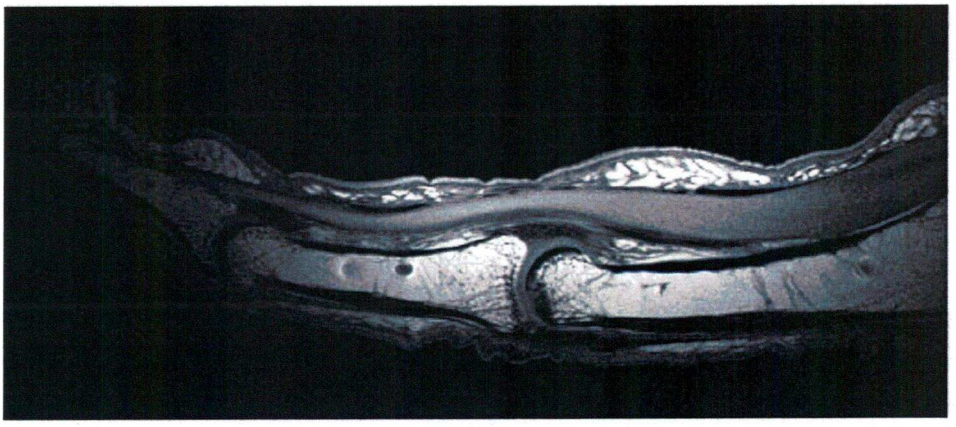

Figure 24 Pulley system in longitudinal-section

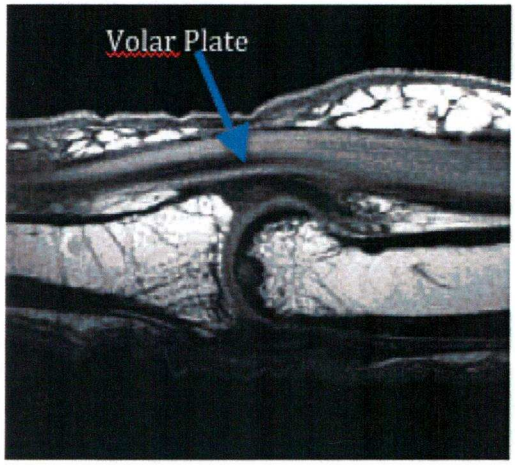

Figure 25 Volar Plate

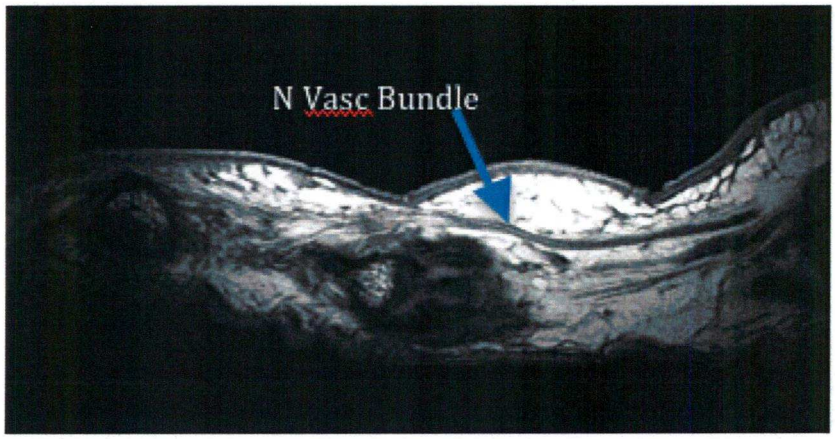

Figure 26 Neurovascular Bundle

These experiments confirmed the feasibility of imaging the FDS terminal tendons using the magic angle effect to gain images of sufficient clarity to attempt the use of a texture-based algorithm to measure strain in the loaded FDS tendon.

3.6 Texture Correlation

Having determined that it was possible to achieve satisfactory images of the FDS and the terminal tendons by exploiting the magic angle effect the author proceeded to trialling analysis of the tendon images using a texture analysis routine.

A programme was written in interface description language (IDL) based on the algorithms by Hoffman [41] to track movement of discrete regions of the tendon from one image to the next.

A resected specimen comprising the tendon of FDS from the forearm was used to trial the software. This was chosen because although the load required to produce a given strain would be higher for a specimen of greater dimensions than the FDS the advantage was a larger volume of tissue and therefore a greater number of pixels in the image. This would therefore allow the analysis to be less sensitive in the initial experiments and subsequently the algorithm could be refined for analysis of the FDS.

3.7 Pilot Study

The section of the proximal part of the FDS tendon was resected from the same cadaveric specimen as used for the initial imaging trial, Hand 1. A Modified Kessler number 5 Ethibond suture was passed through the tendon at each end. One end of the suture was tied to a post on the experimental rig (described later). The other end was used to load the tendon to 49 Newtons and the load maintained by clamping the suture taut in the rig. The tendon was covered with a saline soaked swab to prevent it from drying out during the scan time.

Coronal and sagittal slices were acquired with the load applied and then with the suture clamp released. The image pairs were then analysed with the correlation software. Matching points based on the correlation function were plotted and connected to display displacement vectors.

The pattern of displacement was assessed qualitatively. The displacement pattern was compatible with what would be expected for the pattern of loading in a tendon sample with greater displacement at the left hand side of the image, which is the direction of loading. A sample image from the analysis showing the displacement vectors is shown

below. The lines on the image represent the movement of points from the loaded and unloaded image pairs.

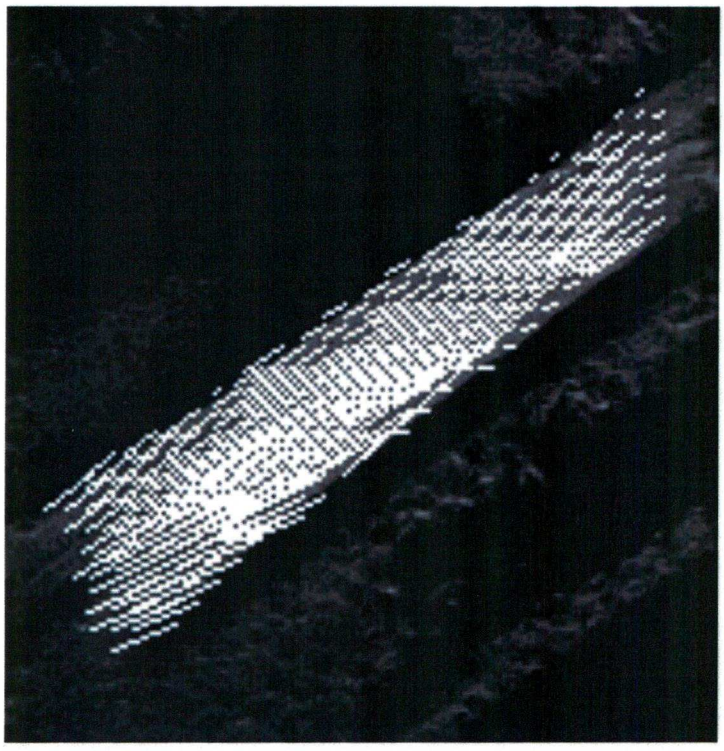

Figure 27 Strain analysis on resected portion of the proximal FDS.

3.8 Equipment Constructed For Experiments

The next experiment was designed to reproduce the plot of the displacement vectors in the terminal tendons of the FDS.

In order to load the tendons and maintain the load during the duration of the scan it was necessary to construct an experimental rig.

The purpose of the rig was firstly, to hold the specimens in the scanner at the magic angle so that optimal signal could be achieved from the tendon. Secondly, it was to maintain the specimen in the same position while the tendon was loaded. This was in order that any change in the appearance of the tendon in a given slice was attributable only to the applied load changing the strain and not specimen movement resulting in a different slice appearance. This would result in a false reading of apparent strain.

Materials that were MRI compatible were used throughout construction of the rig. A high-density polyethylene was used as it provided sufficient strength to accommodate the loads involved in the experiments and it was easy to work with.

The experimental rig consisted of a base plate from which 4 screws protruded to slot in to a high density foam base. The foam base was designed to slot into the scanner in the same position each time and the holes in the base were positioned so that the hand would be orientated at the magic angle for each scan.

The proximal part of the rig was designed to maintain tension on the suture through the FDS tendon after the load was removed and the specimen placed in the scanner. This was achieved by passing the suture through a hole drilled in a block of plastic at the end of the rig. A screw was tightened to clamp the suture at the loaded tension. A small marker was applied to the suture and read off a millimetre scale affixed to the base of the rig in order that it could be confirmed that the load was maintained throughout the experiment. A typical run would last approximately 8-9 minutes depending upon the scan parameters used.

A section of the rig was designed to hold the wrist of the specimen while the tendon was loaded. This consisted of two plates grooved on their inner surfaces that were able to slide laterally and then be screwed in position. This was bolstered by two plates at the back of the clamps that the cut ends of the radius and ulna would abut on as the tendon was loaded. This prevented proximal migration of the specimen as it was loaded.

The distal part of the rig was designed to hold the finger in position while under load and to hold the receiver coil over the area being imaged. The first version used a post with an adjustable arm that pressed on the pulp of the digit being loaded. This was improved upon in later experiments as the DIPJ of the digit would tend to become hyperextended as the load was increased altered the position of the finger. This changed the slice of tissue being visualised between loaded and unloaded images.

The post was therefore adapted to hold the receiver coil by using a compressible U shaped piece that could be inserted in the ring of the receiver coil and then angled over the palmar surface of the PIPJ.

In order to hold the finger in place under the relatively high loads used in the experiments holes were drilled through the proximal and middle phalanges and then through the base plate of the rig. Cable ties were then passed through the phalanges then through the base of the rig. This provided a strong grip on the digit and a hold on tissue that was least likely to deform under load i.e. the bones. It also ensured that there was no compressive force exerted over the flexor sheath that may have altered the force and strain distribution.

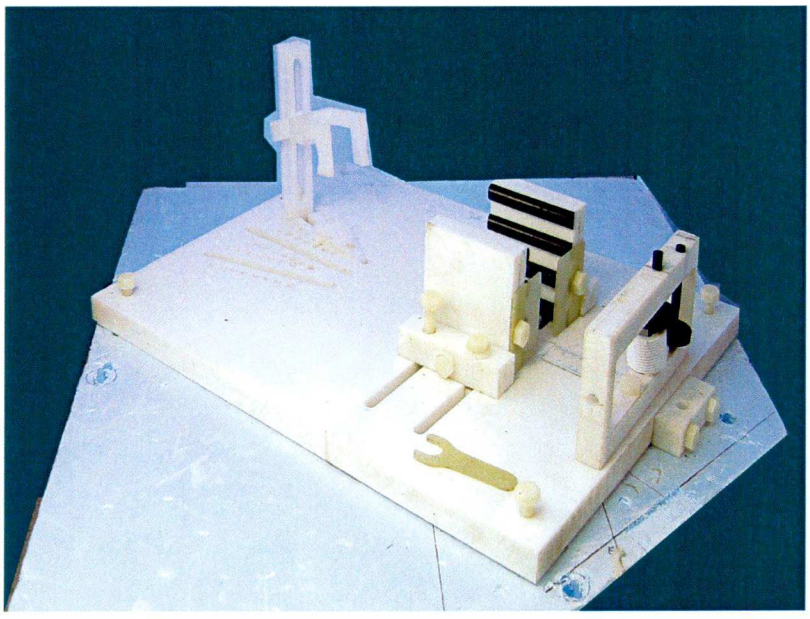

Figure 28 Experimental MRI Jig showing clamps and loading apparatus

3.9 Texture Algorithm Experiment

The cadaveric specimens were prepared for testing by transecting the specimen at the proximal wrist crease. The FDS tendons to all of the digits were identified and dissected

free. A No. 3 Ethibond ™ suture was passed through the end of each FDS using a modified Bunnell technique [12].

Hand 1 specimen was used for the trial of the texture algorithm. Pairs of images were acquired of the FDS terminal tendons of the middle finger using the following scan settings:

1mm thick slices in the sagittal plane with 0.18 mm in plane resolution.

Following scout scans, slice-positioning sagittal sections were obtained. This meant that it was not necessary to run another scout sequence and reposition the slices ensuring that loaded and unloaded images were comparable in terms of image plane.

The tendon was loaded outside the scanner using a 50N weight and the load was maintained by using the tension screw, as described previously, to keep the suture taut until the end of the first imaging run. The specimen was then left in position in the scanner while the screw and therefore the load was released. A second sequence of images was then acquired.

Pairs of matching slice images were analysed using the IDL texture analysis algorithm.

Results

The texture algorithm was unable to detect any change in nodal points on the terminal tendons. It was not clear whether this was a failure on the part of the sensitivity of the algorithm or whether the terminal tendons were perhaps too stiff to be strained to any appreciable degree by this magnitude of load.

3.9.1 3D Sequences

In order to image the tendon in different planes and perhaps discern the motion of landmarks such as the chiasma, 3D sequences were performed so image reconstruction would allow a clearer view of the whole tendon. In these sequences the voxels were

isotropic i.e. equal-sided in three dimensions. This was necessary to allow 3D reconstruction without introducing significant artefacts. This facilitated reconstruction of the image in any plane and the ability to reconstitute coronal slices of the digit so that it was possible to see both terminal tendons within the same image plane.

The disadvantage of this was that the in-plane resolution of these scans was reduced to approximately half that of the spin-echo sequences and therefore less sensitive for distinguishing small differences in strain. A further disadvantage was that when reconstructing the image slices there was a degree of artefact introduced into the image during the reconstruction process.

Result

The texture correlation routine was still not able to detect any displacement between the loaded and unloaded image pairs.

3.10 Analysis Of Texture

To determine why the routine was unable to detect any change a collaboration with the authors of the original paper, Bey et al [7] was forged.

Images were sent to Dr Soslowsky who ran a texture correlation with the loaded/unloaded image pairs from the Hand 1 image sequence. The purpose was to determine if the images differed enough to allow a texture algorithm to accurately determine strain with any degree of confidence. Nodes were numbered so that their index increased moving down the column.

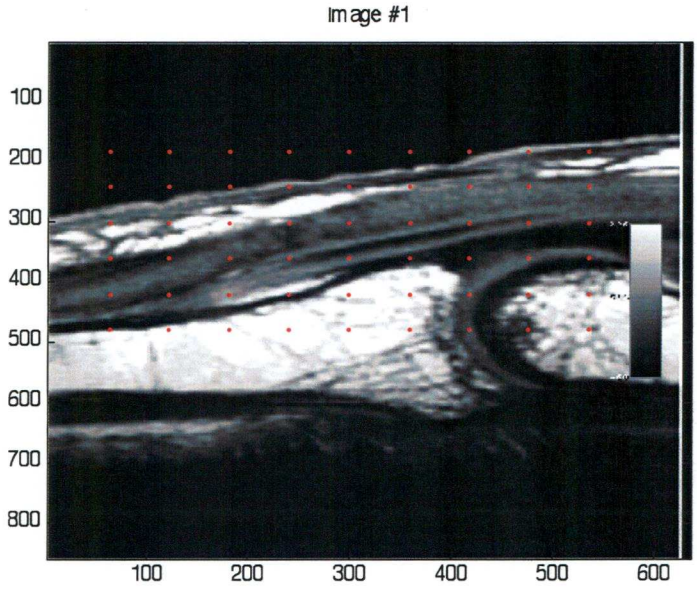

Fig 1: Unloaded image.

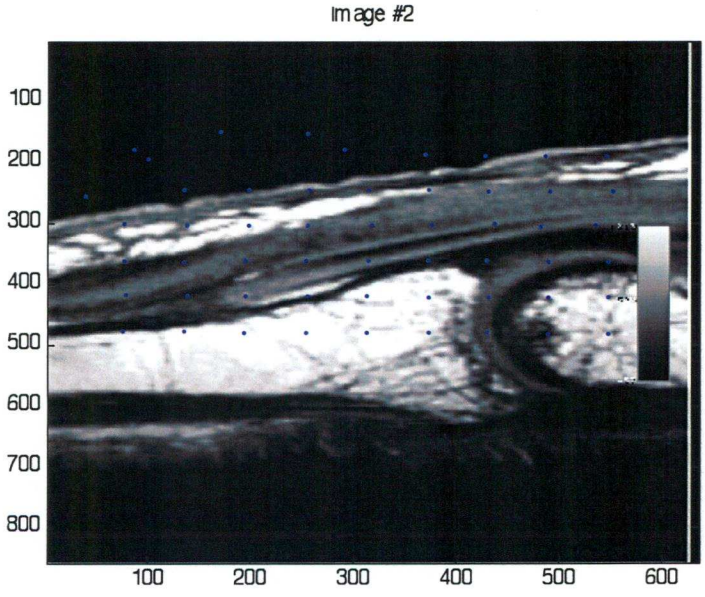

Fig 2: Loaded image.

Then nodes in the background were discarded because they skewed some elements that were near the edge of the tendon.

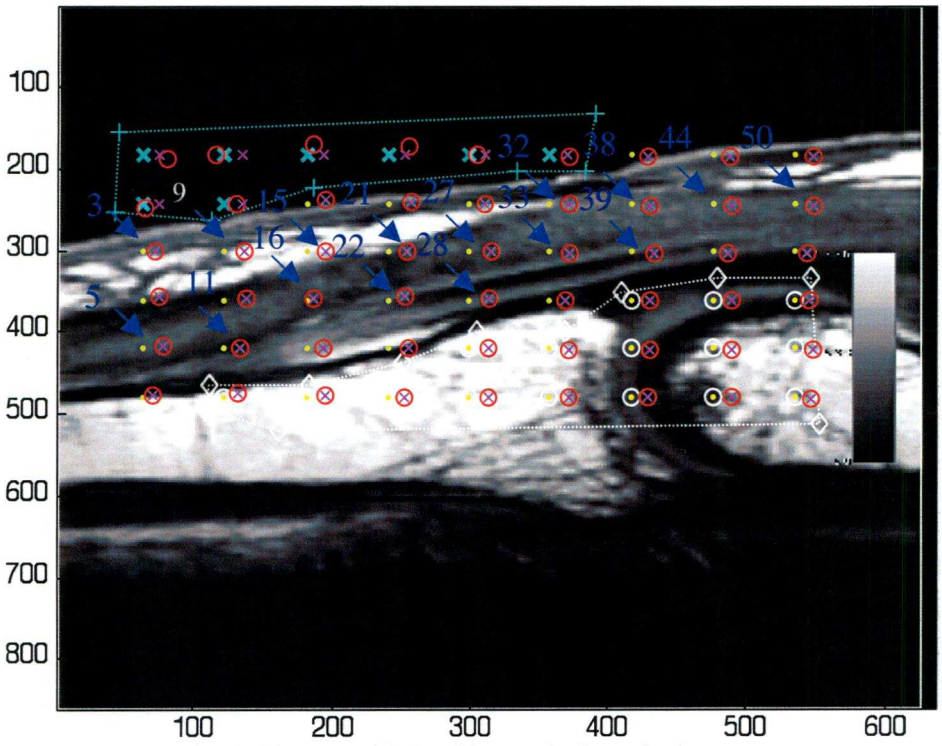

Fig 3: Unloaded image with "nothing nodes" masked out.

The correlation maps for selected nodes were mapped to determine if the image had enough texture that would be picked up by texture correlation. This was a map of the optimisation process to the correlation function. A global peak would indicate that the texture was varied enough and that there was an optimal solution to the correlation function. If there were no local peaks or no defined global peak- then there were many solutions (or points) that satisfied the similarity function- and it would not be possible to have confidence in the solution

A total of 54 nodes (including the "nothing nodes") remained. The nodes for which the correlation maps were plotted were marked.

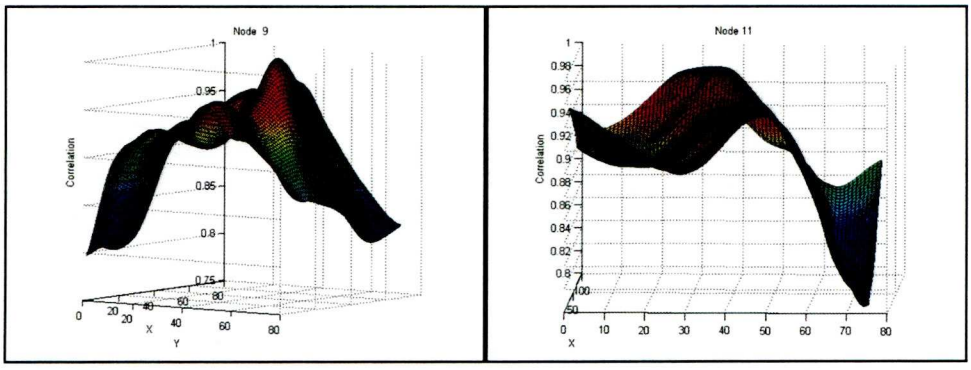
Node 9
Correlation
X
Y
Node 11
Correlation
X

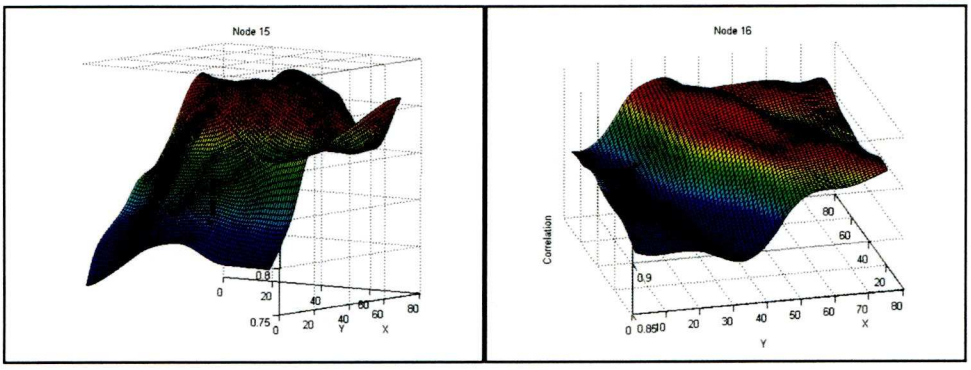
Node 15
Node 16
Correlation
X
Y

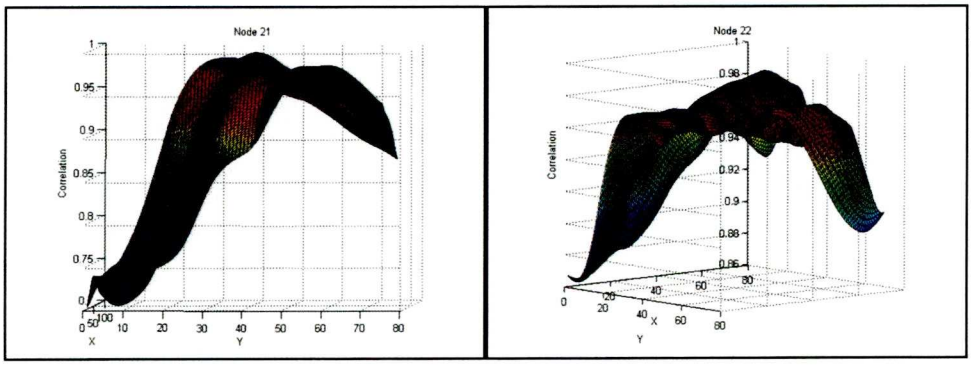
Node 21
Node 22
Correlation
X
Y

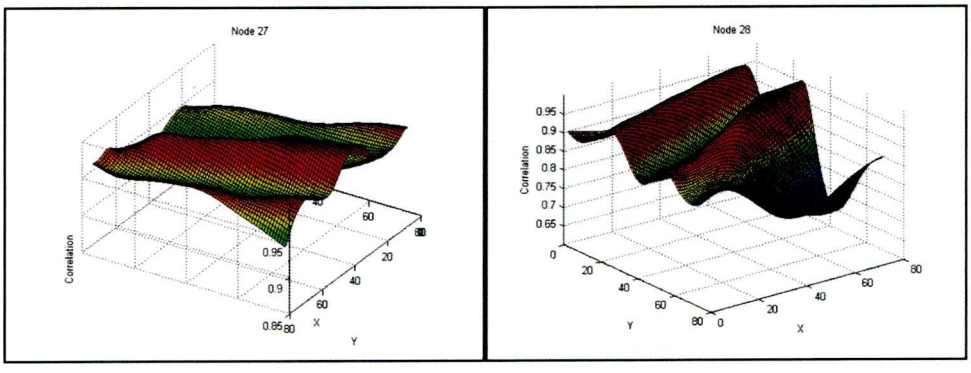
Node 27
Node 28
Correlation
X
Y

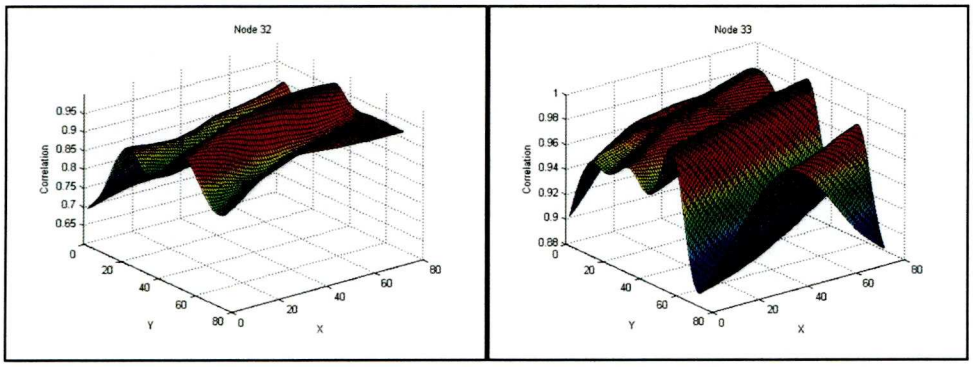
Node 32
Correlation
0.95
0.9
0.85
0.8
0.75
0.7
0.65
0
20
40
60
80
Y
X
Node 33
Correlation
1
0.98
0.96
0.94
0.92
0.9
0.88
Y
X

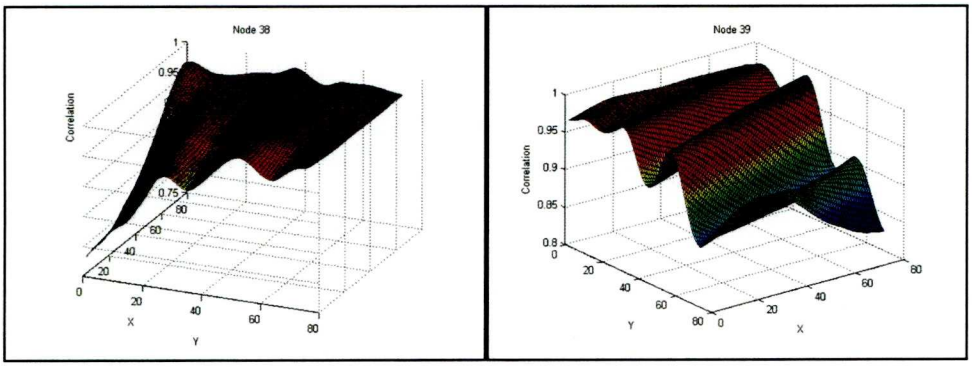
Node 38
Correlation
1
0.75
X
Y
Node 39
Correlation
1
0.95
0.9
0.85
0.8
Y
X

The correlation maps for the nodes examined did not display a peak which would indicate a solution to the correlation equation that could be treated with any level of confidence i.e. there were many possible solutions to the equation of equal probability due to the images not displaying enough variation in texture around the nodes.

3.11 Experimental Limitations

The data from the excised specimen used in the pilot study of the texture correlation routine was not suitable to compute the strain tensor as there were errors in the data that were not apparent from a qualitative point of view but became significant in the calculations to compute the strain. These errors were magnified by the conversion and this made the data unsuitable for any further analysis. The possibility of applying the technique to the terminal tendons, which represent only a very small volume of tissue within each image slice, was therefore not feasible.

It was thus decided to seek an alternative method of analysing the images. A collaboration was formed with Prof Clocksin in Oxford Brookes University. It was suggested that an alternative method of analysis may be to use the change in outline of the tendon.

3.12 Outline Analysis

The goal of this experiment was to perfect the protocol for collection of the images and to assess if the method was viable for the completion of the project. Hand 1 specimen was for the experiments. Pairs of loaded and unloaded images of the terminal tendons were acquired utilising the same scan settings as the initial imaging experiments. The gradient echo sequence was not used as it was not necessary to highlight texture rather it was the goal to delineate the boundary of the terminal tendons as clearly as possible. Scan settings were as follows

Conventional T1-weighted images were acquired with TE 24ms, TR 400ms, NSA 2, FOV 92mm with 512 matrix giving an in-plane resolution of 0.18mm with a 1mm slice thickness. Scan time was approximately 9 minutes for each sequence.

The specimen was mounted on the rig and the middle finger was bound down to the

base of the rig using the cable ties passed through the holes in the proximal and middle phalange so that the finger would not move as it was loaded. The wrist of the specimen was held by lateral compression from the grips and was prevented from migrating proximally when loaded by the plastic stops that were fitted to the wrist grips. The middle finger FDS was loaded by passing a No 5 Ethibond Kessler suture through the tendon and then loading it to 50N using a weight. The suture was clamped taut using the screw clamp and the weight was then removed. A check that the tension was maintained throughout the scan was made by fitting a mm scale to the rig and then affixing a marker to the suture. After the first loaded scan had been completed the tension on the suture was released while the specimen and the rig were still in the scanner. This was accomplished by backing the specimen out using the patient table to allow access to the rig. The table has a memory for the position it was in therefore it was possible to be certain that the position of the specimen was the same for the acquisition of the unloaded scan.

A number of different slice sequences were used in an attempt to find which would give the best results. Both sagittal and coronal sections were obtained. The sagittal sections were able to demonstrate the tendons clearly but because of the diverging directions of the tendons it was often the case that the tendon length would be spread over two of the slices which was not the ideal for the analysis of the boundary. The coronal sections were therefore also obtained in order to permit analysis of both of the terminal tendons together. The tendon however describes an undulating path as it traverses over the head of the PIPJ and so an initial scout had to be performed in the sagittal, coronal and axial planes in order to orientate the slice correctly. 3D sequences were also acquired to determine if it would be possible to use these to reconstruct an image of the tendon in any plane. The disadvantage of this was that the voxels in the image are isotropic to facilitate a 3D reconstruction and this reduced in plane resolution.

The two sequences, loaded and unloaded, were analysed to find the slices with the best images of the terminal tendons. Corresponding images in the loaded and unloaded sequences were used to plot the tendon boundary.

The author performed the plotting of the boundary in a Dicom image viewing software package called OsiriX (OsiriX Medical Imaging Software). This allowed the image to be viewed in the original DICOM format rather than losing information by converting it to JPEG, or other similar formats, and then plotting the outline in another image editing package. The boundaries were plotted and then exported as XML files which were converted to plain text files to be read into the boundary analysis software. The boundary analysis routine was written by Professor Clocksin in Java so that it could be run on Windows or Macintosh computers, both of which were used through the course of the project.

The boundary was represented by a 32-term Fourier expansion, with linear interpolation between fiducial points. The programme worked by finding the optimal correspondence between the two boundaries and then estimating the strain tensor. Finding optimal correspondences was not straightforward because the fiducial points did not relate to the same places on the tissue in both images. Therefore, a new method that "relaxed" one boundary onto the other to find optimal alignment loci on the boundary was used. Movies to show the tendon "morphing" between the loaded and unloaded forms were also developed.

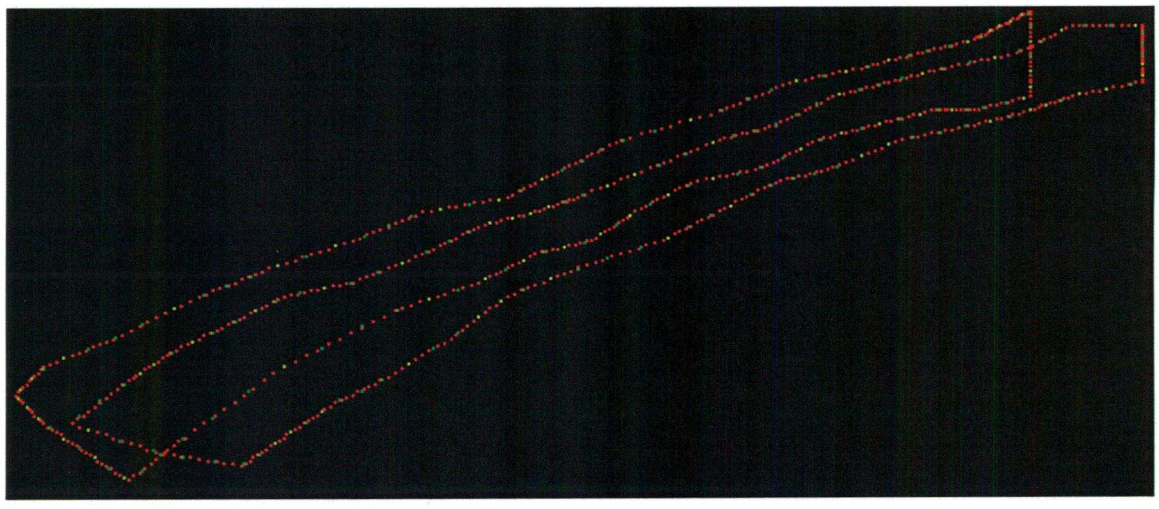

Figure 29 Boundary created by interpolation of the fiducial points.

During the pilot study the outline analysis routine was adjusted to format the display of the data in a way that was most easily interpreted. The first version of the routine represented the data as vectors within the tendon with magnitude and direction.

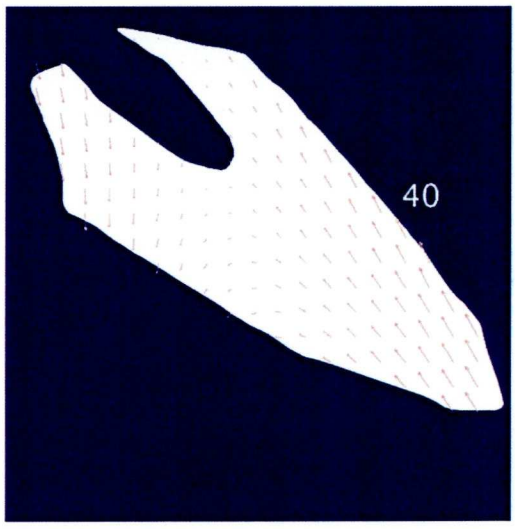

Figure 30 Vector representation of the deformation of the FDS.

This was not the most easily interpreted method though and a mesh model was adopted next.

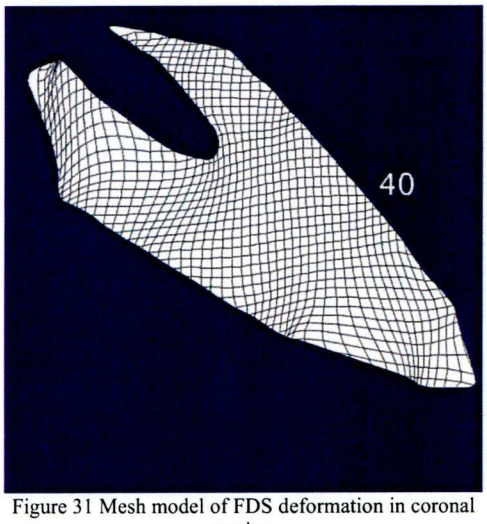

Figure 31 Mesh model of FDS deformation in coronal section

The routine was further adapted to display the degree of deformation of the mesh as a colour fill. This made it easier to see areas of high strain within the tendon at a glance.

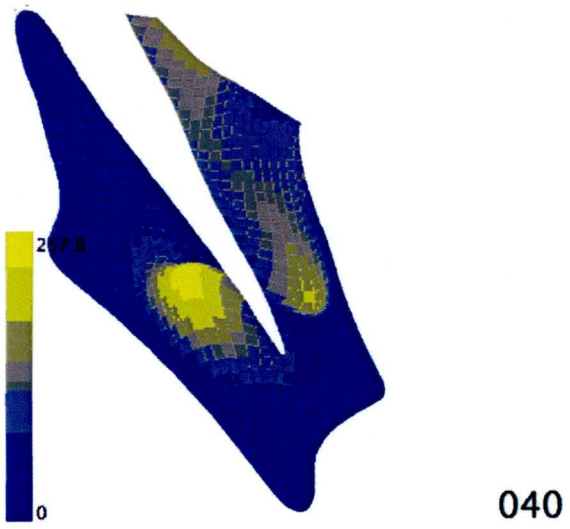

Figure 32 Updated colour scheme for the display of strain magnitude

The colour fill was settled on as the best method of representing the data graphically and was the method adopted for the remainder of the study.

The examples above are representations of the outline data from the coronal sections of the FDS when loaded to 50N and then unloaded. The method for outlining the tendon was not ideal, as it was not clear were the proximal boundary of the FDS was between loaded and unloaded images. It was also not clear if the tendon was moving in and out of the slice plane between images. This would have the effect of altering the outline of the tendon within the slice, giving rise to an apparent strain.

3.13 Problems

It became apparent as the experiments continued that there were a number of problems:

1. The boundary outline of the tendon was difficult to determine proximally as there were no anatomical landmarks.

2. The proximal boundary was the most sensitive one in the analysis in terms of the resultant strain seen.

3. Slice reproducibility was key as any change in position of specimen would give rise to an apparent strain in the terminal tendons and so it was necessary to eliminate as much movement as possible between loaded and unloaded sequences to reduce this error.

3.13.1 Rig modified

In an attempt to address these issues, the rig was modified to minimise motion between scans. The plates fitted to the ends of the wrist clamp stopped the specimen migrating proximally and the cable ties through the bone were used to stop any movement of the finger under test. The tendon still moved out of slice on the unloaded sequence and it was decided that this was probably because all load was being removed from the tendon allowing it to go slack. The protocol for the experiments was therefore changed so that instead of removing the load completely a small mass of 150g was left on the tendon thus preventing it from losing all tension and falling out of the imaging plane.

The initial outline analysis results showed that the proximal boundary was the most sensitive and therefore determining the accuracy of the border was crucial. The distal boundary was marked by the insertion. To increase the sensitivity of the analysis a method for marking the proximal boundary was sought.

3.14 Marker Experiments

It was also clear after the initial experiments with the loaded and unloaded sequences that the strains were close to the limits of the scanner resolution of 0.18mm. Therefore the limit of the tendon outline proximally was critical for an accurate result.

The marker was to provide an unambiguous reference for the proximal limit of the tendon; the distal limit was defined as the insertion on to the middle phalanx.
A section of tendon from the extensor carpi radialis longus (ECRL) was harvested from the forearm of the Hand 1 specimen after defrosting following the same protocol used for the Hand specimen. A suture was passed through each end of a section approximately 10 cm in length. A set up similar to that used in the previous experiment with the excised tendon was used. One suture was tied to a post on the experimental rig and the other end was loaded to 1.5N to remove any slack and provide a level plane for imaging. A swab soaked in 0.9% saline was wrapped around the tendon section both to keep it moist and to increase overall signal for the scan.

The first materials tested were surgical sutures.
Four different sizes of Ethilon suture were used, 3/0, 4/0, 5/0 and 6/0. The sutures were passed through the width of the tendon with a reverse cutting needle and tied in a loop over the top. This allowed sagittal sections of the tendon to show the suture 'end on' therefore producing a mark equal to the diameter of the suture material.

A second scan was performed with the sutures removed to assess if the needle track had marked the tendon.

3.14.1 Results

The sutures were visible on the sagittal scans but there was no clear distinction in the size of the marker, as would have been expected as the suture decreased in width.
The sagittal sequences with the suture removed displayed similar marks on the tendon as when the sutures were in-situ. It was concluded that the needle track was acting as a marker rather than the suture itself. The concern was that this hole would deform as the tendon was strained and would therefore not act as a reliable and robust marker.

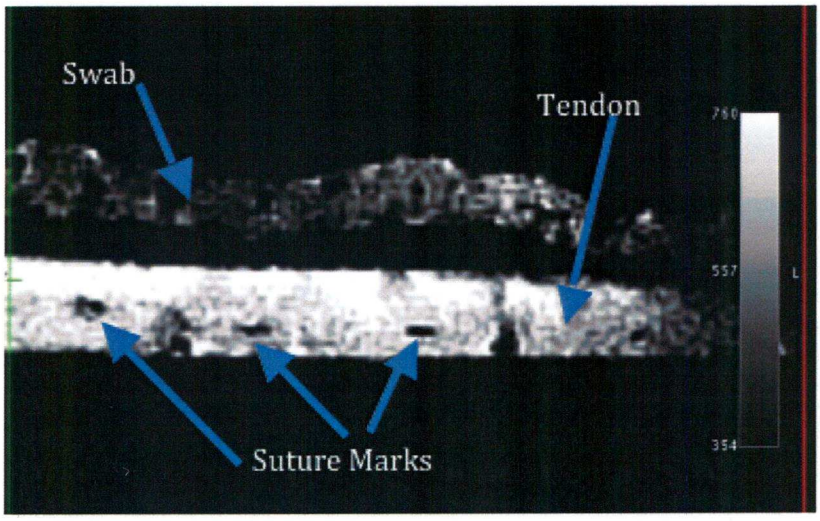

Figure 33 Sutures in-situ

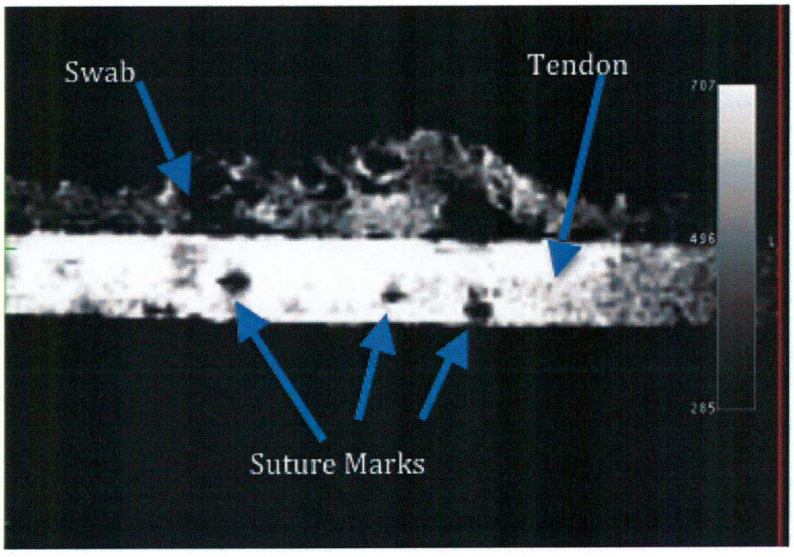

Figure 34 Sutures Removed

3.14.1.1 Oil Soaked Sutures

A second experiment seeking a more suitable marker sutures was performed. It was hypothesised that braided sutures soaked in oil would register as an area of high signal, a bright region against the tendon. Three different sutures were used Vicryl, Silk and Ethibond. All sutures were 3/0 in size. The sutures were soaked in olive oil first and

inserted in the same fashion as the previous experiment using the Ethilon sutures. The same section of ECRL tendon was used for this experiment. The sutures were removed after acquiring sagittal sections and the experiment repeated with fresh sutures of the same size and same materials but this time with the sutures soaked in animal lard. This was to assess which substance would bind to the suture most effectively and produce a higher signal.

A second run was performed using the Ethibond suture as this produced the highest signal on the initial scans. A larger suture material was used (No. 3) to determine if greater diameter suture would soak up more oil and therefore produce a higher signal.

3.14.2 Results

The first run with the sutures soaked in oil showed low signal. It did not provide sufficient contrast against the signal level from the tendon to be reliable as a marker.

The large No 3 Ethibond suture displayed the highest signal on the images but was again too close to the signal level from the tendon and too large to use as an accurate marker in a tendon of 3– 4 mm diameter.

It was concluded that the sutures were not a suitable option for a reliable marker but the use of contrast material as had provided the best results and so this method was adopted by using small cannulae filled with different materials.

3.14.3 Cannulae Experiments

Fine bore cannulae filled with a contrast agent were investigated. The volume of contrast in the cannulae was likely to be greater than that absorbed by the braided sutures. Two diameter of cannulae were used in this experiment 25 and 23 gauge.

One cannula of each size was filled with the following potential contrast agents:

- Lard
- KY Jelly (Johnson)
- KY Jelly (Johnson) and Magnevist Schering (Dimeglumine Gadopentate) Ratio 1:100
- KY Jelly (Johnson) and Magnevist Schering (Dimeglumine Gadopentate) Ratio 1:10

The same specimen of resected ECRL was used for these experiments. The cannulae were passed through the width of the tendon and sagittal and coronal sections acquired using the same scan settings as the suture experiments.

3.14.4 Results

The lard filled cannulae were visible but the signal level was again close to that from the tendon.

The KY Jelly was visible but indistinct.

The low concentration Gad was close to the signal level of the tendon and not suitable.

The high concentration Gad however was a clear dark, low signal, band against the tendon.

The 25 gauge filled with KY and the high concentration gad was chosen as the most suitable marker, as it was small and provided distinct contrast against the tendon.

With this marker in situ on the tendon it provided an unambiguous reference for the subsequent experiments. The next stage was then to try to determine if the scanner could detect any strain in the samples.

3.15 FDS and Marker Experiments

It was apparent that a baseline measure of the expected strain for a given load on the FDS was required to determine if scanner resolution or the sensitivity of the algorithm were the cause of the negative results in the earlier experiments.

Visualisation of the whole terminal tendon in one image slice was not always easily achieved. Also it was difficult to be certain that loaded and unloaded image slices were imaging precisely the same region of tissue. It was reasoned that it might be simpler from a methodological point of view to scan a tendon in the palm which would stay in the same plane when strained and was of greater dimensions, so that any change in the tendon was within the scanner resolution. The proximal portion of the FDS in the palm was selected as it was easily accessed and being the same tendon would provide information on the baseline stress/strain response for the specimen.

The goal of this experiment was to strain the tendon with two markers in situ to provide accurate limits of the tendon and use any change in position of these markers to determine the strain. This would then provide a starting point for the analysis of the terminal tendons.

3.15.1 Method

The palm was opened with a Brunner incision and two Markers, KY/ Gd 1:10 concentration 23G venflons, were inserted into the tendon 3 cm apart as this was within the limit of the field of view using the small receiver coil. Scans were then acquired using the previously described settings with 0.18mm in-plane resolution and loads of 49N and then 1.5N on the FDS.

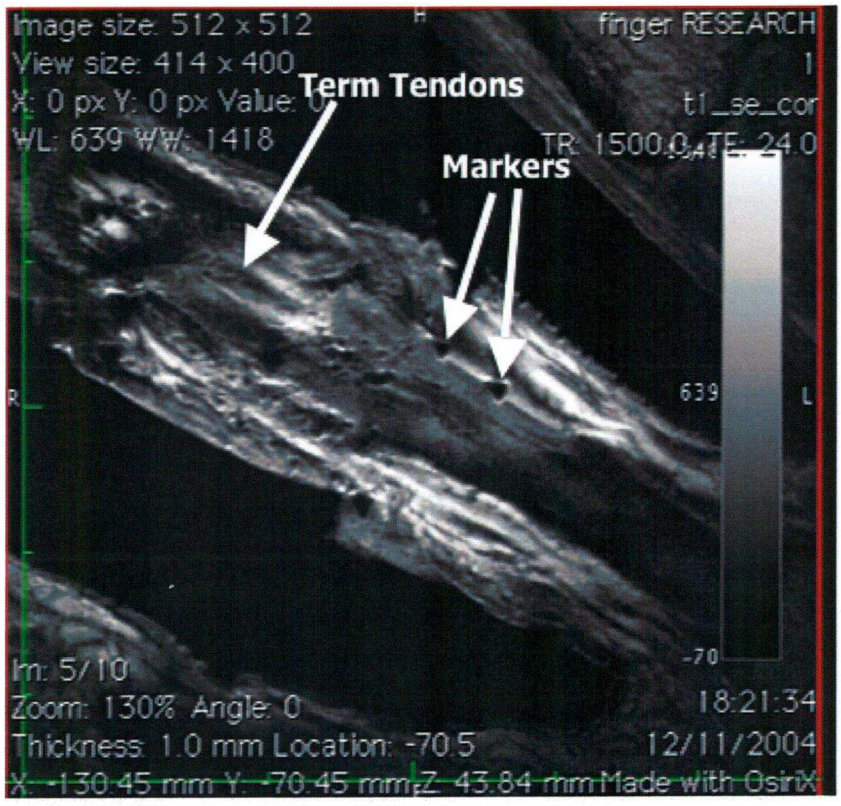

Figure 35 Coronal MRI markers in-situ

3.15.2 Result

There was no observable difference in the distance between the markers. Possible reasons for this negative result were hypothesised as:

1. The resolution of the scanner was not high enough to detect small changes that were present.
2. The load used in the experiments was not sufficient to produce a strain in the tendon.
3. The body of the FDS tendon was significantly broader in cross-section within the palm and therefore it would theoretically, require higher loads to produce a 1% strain than for the terminal tendons which had a smaller cross-sectional area.

It was crucial in order to maintain the accuracy of the analysis to be certain that the slices for one image sequence to the next of the same finger were reproducible. Any shift in position of the specimen, giving rise to a different slice of tissue would manifest itself as a change in the appearance of the tendon and would register as an apparent strain. However, it was still not possible to eliminate all movement in the specimen as it was loaded and unloaded. This was especially true if all load were removed. There was a need for a certain amount of tension to take up the initial slack in the tendon and tissues.

These different problems all led to the conclusion that the method would not be suitable for analysis of the FDS strains.

3.16 Conclusion

The purpose of the experiments described in this chapter was to study the anatomy of the FDS tendon and quantify strain in the terminal tendons utilising analysis of high resolution MR Images. The ability to acquire detailed images of the tendon required the use of what was previously considered an artefact, the magic angle effect. Specimens were orientated at the magic angle and this allowed very detailed images of the cadaveric fingers to be obtained.

The experiments yielded a positive result in plotting displacement vectors with the software that was written by the author and his co-investigator. The problem arose with the data not being reliable enough to compute a strain tensor, however, and so it was necessary to look at the possibility of a different approach to the analysis of the images. The difficulties with the methodology were in part due to the small dimensions of the area under investigation and the resolution of the scanner. It is possible that with the improvement in scanner technology this problem will be resolved in the future.
The outline analysis was a new technique and may have been successful if the volume of tissue being imaged was larger and the acquisition of reliable slices was more reliable but the nature of the anatomy made this very difficult and even with the addition of markers for the proximal limit of the tendon the analysis could not be relied upon.

The experiments presented in this chapter have succeeded in looking at the anatomy of the FDS and surrounding structures. Some very detailed images have been presented but the experiments did not mange to equate strain from the terminal tendon as the author had hoped.

A number of questions were raised by these experiments. The first being was there any strain in this region of the tendon with the range of loads that were being used and hence none detected by the texture analysis routine? A clearer understanding of the baseline values for the elastic response of the tendon was required.

The gold standard for determining these values is from tensiometer testing. The author therefore decided that the ideal of measuring strain with the soft tissues and FDP intact would have to be sacrificed in order to gain baseline data. The next section will describe tensiometer experiments performed in Stoke University Biomechanics Dept and the adoption of the texture analysis principle to successfully equate the strain in the terminal tendons.

Chapter 4

4 Tensiometer Study

4.1 Introduction

Following the MRI experiments it was decided to take a step back in order to gain baseline data on the response of the terminal tendons. This was to provide definitive data on the displacement expected for a given load. It was not clear in the MR experiments if there was a measurable strain at the loads used or if it was not detected due to low scanner resolution or low sensitivity of the analysis. The author determined that testing on the tensiometer would give unequivocal data regarding the response of the terminal tendons to loading.

It was proposed that the use of the texture analysis method not be discarded but applied to the testing of the specimens in the tensiometer in order to gain data on the strain in each terminal tendon. This was to be done after the method of a number of other authors [42, 59] who have reported using the technique in the engineering industry to quantify strain in materials. The principle is the same, mapping motion of regions on a specimen but by using an applied random pattern rather than natural variation in the specimen's appearance. The application of a fine and high contrast pattern facilitates improved sensitivity of the analysis.

Testing in this way raises a number of different issues and these are reviewed in the next section. The following areas are addressed.

- Appropriate clamps to use for tendon testing.
- Variations in testing protocols and the potential outcome on results.

- Previous work on texture analysis of biological tissues.
- A comparison of grip-to-grip v surface marking results.

4.2 Clamps

Biological tissues such as tendon have properties that make them more technically demanding for tensile testing. The ability to hold the sample firmly without any slipping of the specimen is crucial. If a specimen is not held correctly it will result in the load not being transmitted to all parts of the tissue or it may snap at the meeting of the clamp tendon junction due to the clamp causing a stress raiser.

4.2.1 Ideal properties of a clamp

A tendon clamp must hold a compressible moist aqueous tissue sample firmly, so that it will not slip during testing. It must also be able to transfer the applied load to all of the tendon fibres in order to avoid shearing between fibres close to the surface of the clamp and those in the centre of the specimen under test.

Ideally, a clamp that is able to fulfil these criteria would result in mid-substance failure of the tendon sample indicating that there was no stress raiser at the clamp tendon junction. This is often not possible to achieve in practice and there has been some argument that clamp junction failure results are as valid as those of specimens that fail in their mid-substance [54, 72]. This will be examined in more detail later in this chapter.

The FDS specimens are relatively small in dimensions and the length of specimen that is available for clamping is short. This leads to increased margins of error when calculating displacements during testing, as the percentage error is increased in small samples. It is therefore essential to minimise slipping of the specimen by using the correct type of clamp.

4.2.2 Clamp Types

Many types of clamp and alterations to the tendon within the jaws have been used. The goal has been to achieve high loads without slipping of the sample or premature failure at the clamp tendon junction.

Clamp types used include manual [34], pneumatic [54] and cryo-clamps [60]. Alterations to the surface of the clamp interface such as sinusoidal grips, to increase surface area and dissipate stress raisers, were used by Butler et al [13] in an investigation of tendons and fascia. Alterations to the tendon within the grips have included air drying, wrapping with masking tape [34] as well as freezing [60].

Meaningful comparison of results between different investigators is difficult due to this variation in experimental method as variations in the clamps used can have a significant effect upon the results reported for strain and Young's modulus [54].

Butler et al [13] reported that ten tendons and eleven fascial specimens out of a total of 60 underwent some slippage during tests using a sinusoidal shaped wedge grip and a relatively high strain rate of 100% per sec to failure. The specimens used were much larger in scale than those proposed in the present investigation consisting of samples of fascia lata and quadriceps tendons therefore a greater length of specimen was available for clamping.

Riemersa and Schamhardt [60] and later Sharkey et al [68] described the benefits of a cryo-clamping technique. This relies upon freezing a small section of the specimen within the clamp to make it easier to grip. Riemersa originally described using blocks of dry ice attached to the clamp. The modification by Sharkey et al [68] involved placing the tendon end into a brass clamp with serrated edges. This clamp was not tightened excessively but just sufficient for the teeth to bite into the tissue. The length of tendon in the clamp was then frozen by pumping either liquid carbon dioxide or nitrogen through the clamp via a hollow chamber within it. This method was used successfully to apply loads of up to 3500N through the quadriceps tendon with a 95 % success rate. Clamp

failures, in these experiments, were attributed to either over tightening of the clamp, resulting in fracture of brittle frozen fibres, or allowing the tissue to thaw.
It is necessary for the flow of the freezing agent to be carefully controlled to ensure that the sample is adequately frozen in the clamp and approximately 1cm beyond. However, cryo-clamping was ruled out as the best method for the FDS samples as the specimens were relatively short and the freezing of even a small area of tissue beyond the clamp may have caused a significant alteration in the results.

Ng et al [54] provided a review of different clamping techniques in a study of chicken FDP tendons. These are anatomically similar to human flexor tendons [25, 49]. The effect of different gripping techniques upon slipping, results for strain and ultimate tensile modulus were examined. The validity of results from samples that failed in their mid-substance compared with clamp junction failures was also tested. Pneumatic clamps with either a cardboard or sandpaper lining were used. The effect of treating the portion of the sample in the clamp by freeze-drying or air-drying then wrapping the air-dried ends with masking tape was also examined. Ng concluded that pneumatic clamps with a cardboard lining were the most effective technique, as they provided the highest values for strain and ultimate tensile modulus in the tests.

There are many options to consider. The dimensions of the sample, as well as the range of loads that are to be applied in the experiments dictate the choice of clamp. For experiments involving very high loads and strain rates on large samples then the use of a cryo-clamp is the most suitable. The needs of these experiments were different however, small samples with relatively low loads and strain rates that were modest. Since it was not necessary to investigate the results to failure the strongest clamp was not required but it was necessary to be certain that within the testing range, the samples would not slip and give rise to a significant experimental error. The use of pneumatic clamps and a cardboard lining after the method of Ng was chosen for the experiments. The pneumatic clamps allow a constant grip pressure to be maintained as a sample thins and the cardboard allows even distribution of the force.

4.2.3 Clamp-tendon junction failure

It is common in tensile tests to failure for the sample to fail at the junction with the clamp. This raises the possibility of a stress raiser at this point leading to a premature failure of the specimen. It could be that a sample would take a higher load if the clamping technique was better.

Ng et al [54] investigated this problem. Results from samples that had failed in the mid-substance were compared with those that had failed at the junction with the clamp and found to show no significant difference. This was in agreement with a previous investigation by Smith et al [72] performed on porcine toe extensor tendons.

It is not altogether relevant to the present investigation as the tendons were not tested to failure but it is important when considering the validity of results using a clamping technique that may give rise to such a stress raiser in the sample. The results from Ng and Smith's groups suggest that the results can be accepted as valid from samples that may fail at the clamp tendon junction.

4.3 Testing Protocol

4.3.1 Strain rate and preload and its effect on tendon testing

There are different parameters that can be changed when testing the tendons and these can affect the results. Strain rate and the effect of preloading are two parameters considered here.

Wren et al [84] found that modulus was unaffected but failure stress and failure strain were increased by 15% at higher strain rates when testing human achilles samples. Blevins et al [8] reported that modulus, tensile strength and failure mode were unaffected when comparing results of tests performed at either 10% or 100% elongation per second. Herrick [38] also stated that over their rates of testing there was no significant difference in modulus.

However Lewis and Shaw [48] stated that strain rate did have a statistically significant effect on modulus and Stiffness but not on ultimate tensile strength in his study on

human Achilles. Ng et al [55] also reported a positive correlation between the modulus, strain rate and the ultimate tensile strength of avian flexor tendons tested at 15 different strain rates ranging from 0.05% to 150% per sec. The evidence is therefore not conclusive regarding the effect on modulus. However, the alterations in modulus reported are generally small and only just statistically significant. The author has adopted a constant strain rate for all tests to enable meaningful comparisons to be made between samples.

4.3.2 Pre-loading

Opinions differ regarding preloading. Devkota and Weinhold [20] investigated the effects of preloading on avian flexor tendons to assess any change in the values of tensile failure strength, elastic modulus strain at failure or strain energy density of tendons. It was reported that the values of ultimate tensile failure strength, elastic modulus, strain at failure and strain energy density were unchanged for preloads between 1 and 14%. Other authors such as Haraldsson et al [32] preferred to perform eight pre-conditioning cycles prior to testing patella tendon fibres to failure in the ninth cycle.

The author regards pre-conditioning to be an important procedure in the present experiments as the pre failure visco-elastic properties of the tendon are specifically being examined and these may potentially be affected by preloading protocols. The author could see little disadvantage in adopting a protocol of preloading in order to establish a reproducible response from the samples under test.

4.3.3 Temperature.

In order to duplicate the conditions found in vivo it would be ideal to test all tendons at 37 degrees Celsius. There are investigators who have examined the effects of altered temperature on the results of tensile testing. Rigby et al [61] reported no change in the properties of RTT when tested at different temperatures. Hasberry and Pearcy [33] found no difference in the mechanical characteristics of interspinous sheep ligaments at different temperatures. Lam et al [46] tested the effects on the properties of medial collateral rabbit knee ligaments at temperatures between 25 and 55 degrees Celsius and

reported no alteration in biomechanical properties on varying the temperature. These reports would suggest that testing the FDS samples at room temperature should not invalidate the results.

4.3.4 Hydration

Specimen hydration has been shown to have a significant effect upon the tensile properties of tendons Haut and Haut [35]. Differing experimental protocols have been employed to reproduce in vivo type conditions. Testing with samples immersed in saline [15, 35, 67] or simple spray irrigation [20] have been described. Haut [35] specifically investigated the effect of altering tissue hydration on samples of patella tendon. It was found that the better-hydrated specimens were stiffer especially at higher strain rates.

The specimens in these experiments are small and therefore have a high surface area to volume ratio. Careful attention has been paid to ensure that specimens were wrapped in saline soaked swabs when not being tested to avoid the effects of drying.

4.3.5 Measurement of specimen dimensions.

In order to calculate strain in each of the terminal tendons it was necessary to accurately determine the dimensions of the radial and ulnar slips. A number of differing methods have been reported for accurate quantification of sample cross sectional area (CSA). This is a crucial value for calculations of Young's modulus and stress. It is difficult to report an accurate overall cross sectional area for a specimen, as not all specimens are uniform in their dimensions along their length. The techniques used vary from the use of laser micrometer [15], area micrometer [13], calibrated eye piece [34], volume in bag method [55].

With any method, it is necessary to accept an average value for the CSA. The value obtained therefore results in average stress for the sample but in areas of the tendon with smaller dimensions, the stress will be higher. This effect is increased as a specimen narrows during testing.

A method employing the analysis of images captured from a video camera just prior to testing was used in the present investigation. It allowed accurate measurement of a complex sample. The methods reported above were not devised with the unique problem of measuring a bifurcating sample. This 'video capture and analysis' method

had the advantage of allowing measurement of the precise region of interest as investigated by the texture analysis software.

4.3.6 Length of specimen

The FDS tendon was to be examined along only the last portion of its length i.e. clamped across the chiasma therefore the sample length was relatively small when compared with testing the whole tendon. The question of whether sample length affects results has been investigated by Haut [34] who found that it was a significant factor.

Haut reported that the modulus of rat-tail specimens varied with the length of the sample. An increase of modulus from 960 MPa for a 10 mm specimen compared with 1570 MPa for a specimen 100 mm long was recorded. There were also significant differences in strain at failure depending on sample length. Specimens 50 and 100 mm long failed at a strain of 8.1 and 8.5 % whereas specimens 10 mm long failed at a strain of 17.6%. Haut argued that this difference might be due to tendon deformation being localised to certain regions along its length. It was suggested that for a short specimen the percentage over which this change occurs would represent nearly the length of the specimen.

Haut's theory regarding the strain being isolated to a particular area of the tendon was supported by Wren et al [84], who, in an experiment on human Achilles, found the strain to be at its greatest in the region of the tendon adjacent to the bony insertion. Wren et al argued this might be due to the dimensions of the specimen, as this was also the narrowest part of the achilles tendon.

This effect of specimen length is something that will have to be considered in the interpretation of the author's results, as the specimens used were approximately 3 cm long. The results may therefore not be comparable with authors who have tested the whole of the FDS tendon.

4.4 Surface v grip to grip

The experiments in this chapter will compare the results of grip-to-grip strain readings with those obtained from surface markings for the whole tendon specimens. Reports in

the literature have consistently demonstrated that the values for these two methods differ significantly.

All previous authors have demonstrated consistently higher values for Young's modulus and hence lower values for strain when mid-substance or surface measurement marker techniques are used. The results of three of the authors for strain at failure and Young's modulus are summarised in the table below.

	Grip to Grip		Mid-Substance	
	Modulus (MPa)	Strain (%)	Modulus (MPa)	Strain (%)
Butler et al [13] (Gracilis)	642	32.5	1734	7.8
Wren et al [84]	Not reported	12.8	Not reported	7.5
Haraldsson et al [32]	520	12.4	1232	6.8

Butler et al [13] reported that expressed as ratios surface strains were only 25.2 to 29.9% of the grip-to-grip strains. The surface strain measurement therefore returned a much higher value for the Young's modulus.

Wren et al [84] used a set of bead markers applied to the surface of human Achilles tendons. The bone tendon complex was tested by embedding the calcaneal attachment of the Achilles in PMMA blocks, the tendon was held with a cryo-clamp. Wren et al also reported significantly different values for the strain at failure for the bone tendon complex compared with the mid-substance strain. For a strain rate of 1mm sec the respective strains at failure were 12.8% and 7.5% and at a strain rate of 10 mm sec they were 16.1% and 9.9%. Wren et al attributed the differences to a region of high strain between the insertion of the tendon and the first of the bead markers.

Haraldsson [32] reported significant differences for modulus and strain at failure in a study comparing the mechanical properties of collagen fibres from the anterior and posterior parts of the patella tendon and a summary of these results are presented in the table.

In summary, the use of surface marker techniques provides values of strain that are only 25% to 55% of the magnitude that are measured when using grip-to-grip measures. It is not clear why there should be such a large difference in the readings. Some authors have argued it may be due to inaccuracies in measuring sample length if a sample is not gripped firmly within the clamp jaws or that it may be due to slipping of the sample in the clamp.

Sanghavi et al [63] reported on the use of speckle correlation to measure full field strain in bones and samples of a bone and ligament complex. They used a method very similar to that adopted by the author. They reported on a number of problems that made accurate measurement difficult. First, they talk of the need to avoid glare from moist specimens by using low incident lighting. They utilised a two coat application of speckle pattern by using first a white matt background on top of which a black random pattern was painted to allow for high contrast but the author did not wish to use a complete coating on the small specimens as it was feared that this may alter the characteristics of the tissue. During the test on the ligament specimens they reported problems with the pattern matching algorithm as the ligament complex unravelled prior to failure this caused new surfaces to be revealed which did not have the speckle pattern applied and a consequent breakdown of the pattern matching algorithm. The paper argues strongly in favour of using full field measurement of strain due to the inhomogeneous nature of biological tissues and the effects that strain gauges can have on compressible specimens by changing the response of the material to loading. The author therefore adopted a more cautious testing protocol by not aiming to test the FDS specimens to failure. It was hoped that this would lead to less problems with breakdown of the pattern-matching algorithm.

4.4.1 Reasoning for proposed experimental methodology

The index and ring fingers from each of the hand specimens were tested and compared. These digits were chosen as the author's hypothesis suggested that any differential loading would be most apparent in these digits given that they rotate in opposite directions during full flexion. The middle finger was expected to have little difference in

loading in its terminal tendons and so it was therefore not tested. The little finger was not tested as the varied anatomy, and the essentially vestigial nature of the FDS in this digit made it unsuitable for lengthy data analysis. It was anticipated that any differential in strain would be most apparent from a comparison of the ring and index fingers.

4.5 Methods

4.5.1 Specimen Details

The samples, in their pots, were immersed in warm water for 2 hours to defrost them on the day of testing. Samples were prepared by dissecting the FDS tendon from the flexor sheath while maintaining the attachment to the middle phalanx. The middle phalanx was dissected free from the finger. This resulted in a specimen consisting of the FDS tendon and middle phalanx only.

4.5.2 Cross sectional area measurement

The terminal tendon dimensions were measured by means of image analysis. Each sample was imaged, in the clamp, using a digital camera just prior to being tested. The images were acquired with a millimetre scale adjacent to the tendon. All image files were then processed in Image-J. The scale was used to calibrate the measurements performed in the software. Front and side views were taken to determine the cross sectional area of each terminal tendon. Sample images from this process are shown in Figure 36 and Figure 37.

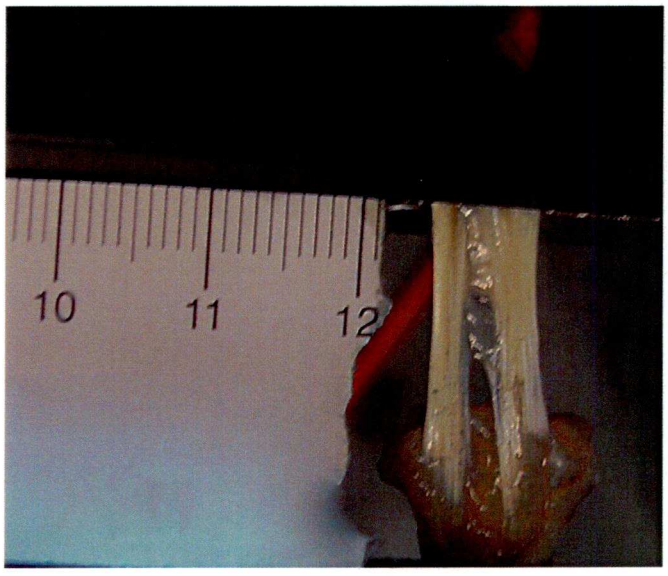

Figure 36 Video capture of specimen and scale front view

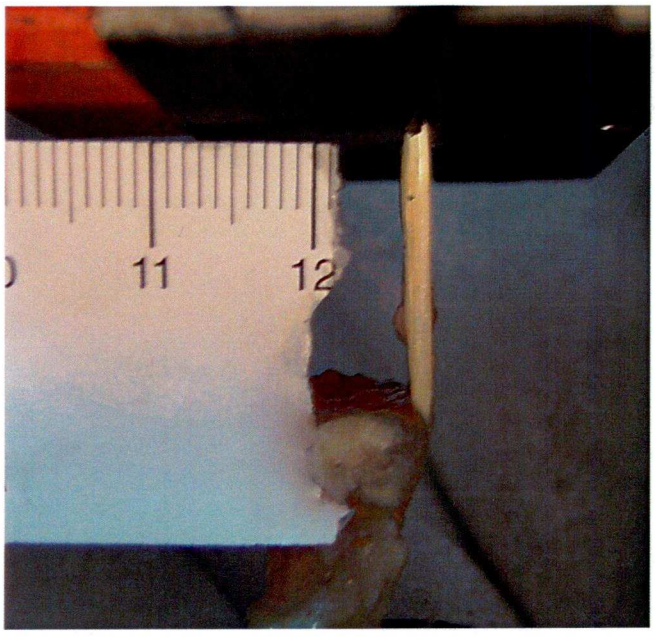

Figure 37 Video capture speciman and scale side-view

Three measurements were made at different points along the length of each terminal tendon and the readings averaged. This value was then expressed in metres squared for strain calculations. Initial sample length was obtained in the same manner, measuring from the border of the clamp to the insertion of the terminal tendon.

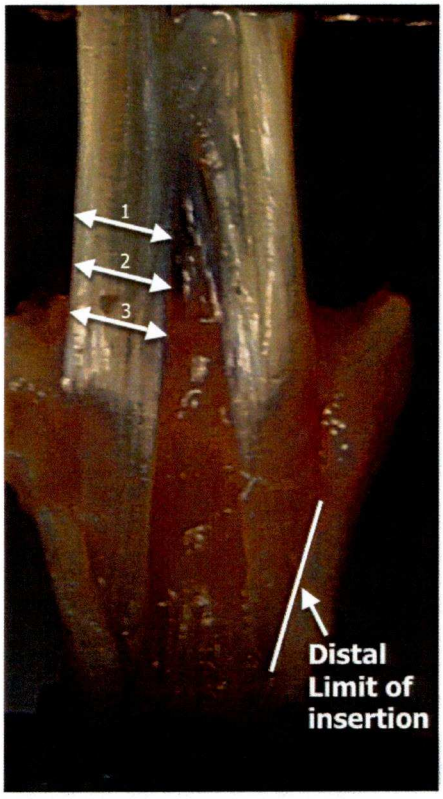

Figure 38 Measurement of width of terminal tendons

4.5.3 Machine specification

An ESH (Electro-Servo-Hydr) tensiometer with capacity between +/- 5kN was used for the experiments. The load cell was located on the top clamp and the lower clamp was used to house the specimen.

4.5.4 Clamps

The tendon end of the sample was held in a pneumatic clamp supplied by Testometric UK. The clamp was lined with cardboard after the method of Ng et al [54]. Care was taken to ensure that the cardboard lining was carefully aligned with the edge of the grip. This was to ensure that no area of the tendon was not gripped by the cardboard within the clamp jaws. This could have resulted in an effective alteration in the sample length. The clamp was closed using a compressed air supply canister running at 8 BAR pressure. This ensured that a constant pressure was maintained on the specimen even if it thinned out while under test.

The middle phalanx was secured by placing its distal half in a 'dumbbell' style clamp. The clamp had a central aperture which allowed the shaft of the phalanx to project through but prevented any slipping of the specimen by being too small for the condyles of the phalanx to pass through.

4.5.5 Texture Application

A random speckle pattern was applied to the terminal tendons just prior to their testing using a spray can of matt black enamel paint. The aperture of the nozzle and optimum spraying distance, to obtain a suitably density and size of dots, was determined by prior experimentation. The paint was rapid drying and easily wiped from the surface of the tendon if the first application was sub-optimal.

4.5.6 Preconditioning Protocol

All tendons underwent preconditioning for 5 cycles before acquiring video analysis data on the last cycle. The preconditioning cycles were analysed for reproducibility using Friedman's test.

4.5.7 Strain Rate

A maximum load of 100N was applied to the tendon specimens over a period of 2secs (from unloaded to loaded and back to fully unloaded again).

4.5.8 Lighting

Optimal lighting of the specimens was necessary to ensure accurate results from the texture analysis. To reduce glare on the reflective surface of the tendons two photographic lamps were used to light the specimens.

These were reflected off a matt white projector screen to provide a soft diffused light source. This reduced glare and harsh shadows, which would have given rise to errors with the pattern-matching algorithm.

4.5.9 Image Capture

Video data was captured on a Panasonic GS120, 3CCD camera. This footage was transferred to a power Mac G5 and an image sequence exported from QuickTime. The Images were converted to 8-bit Greyscale for analysis in the texture correlation software VIC 2D (Correlated Solutions, USA). The working distance, camera to specimen distance, was set at one metre. This represented a compromise between image resolution and minimising error from out of plane motion.

Small working distances provide high-resolution images but any small movement out of plane results in a greater percentage error in the strain analysis. As it was not possible to eliminate all out of plane motion, a one metre distance was used.

4.5.10 Processing

The video data was processed in VIC 2D texture analysis software. The software analysed the sequence of images based on the changes in the texture applied to the tendon. The displacement of discrete regions of the tendon, relative to each other was calculated using a correlation algorithm. The size of each region is known as the subset. The software computes the strain using a Langrangian approach. This could then be displayed as a colour map or interrogated further to define overall values for a marked region and plotted as a graph. The strain was calculated separately for the ulnar and radial terminal tendons. A plot was produced of strain against image sequence number. The image sequence number was then synchronised with the output from the tensiometer to enable load to be plotted against strain for comparison of the two terminal tendons.

4.6 Results

The result of the texture analysis for the terminal tendons is presented in the graphs on pages 113-121. The data from one experimental run are shown for each specimen. The results of strain from the radial and ulnar terminal tendons for a specimen are from the same experimental run i.e. one cycle of loading and unloading of a specimen was filmed and then the optical analysis algorithm was used to equate strain separately in the radial and ulnar terminal tendons. For consistency, the data from the radial terminal tendons is plotted in black and from the ulnar terminal tendons in red.

It can be seen that the three-phase response of the tendon is replicated in the texture analysis data i.e. the toe, heel and linear phase of loading. It is also apparent from looking at the graphs that there is great similarity in the strain plots for the radial and ulnar terminals for all of the specimens examined. Further evidence for any statistical difference in strain between the two terminal tendons in any of the specimens was sought by performing a two sample Wilcoxon test. This demonstrated no statistically significant difference in strain for the radial and ulnar terminal tendons for any of the specimens examined.

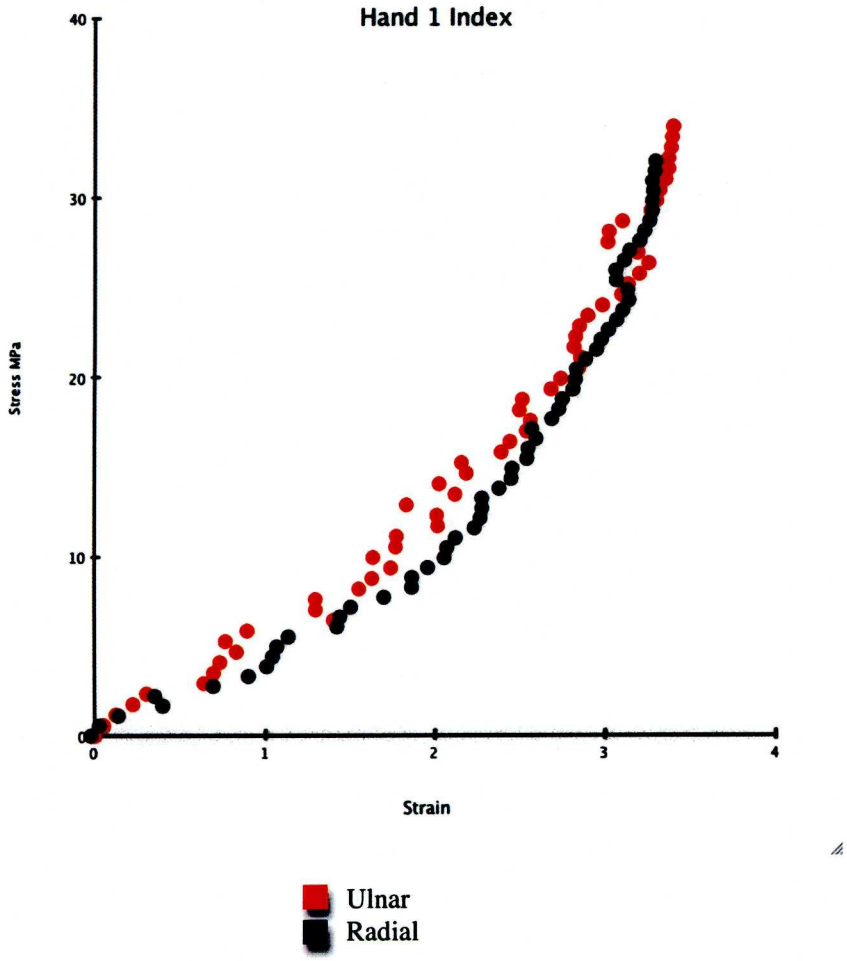
Hand 1 Index
Stress MPa
40
30
20
10
0
0
1
2
3
4
Strain
Ulnar
Radial

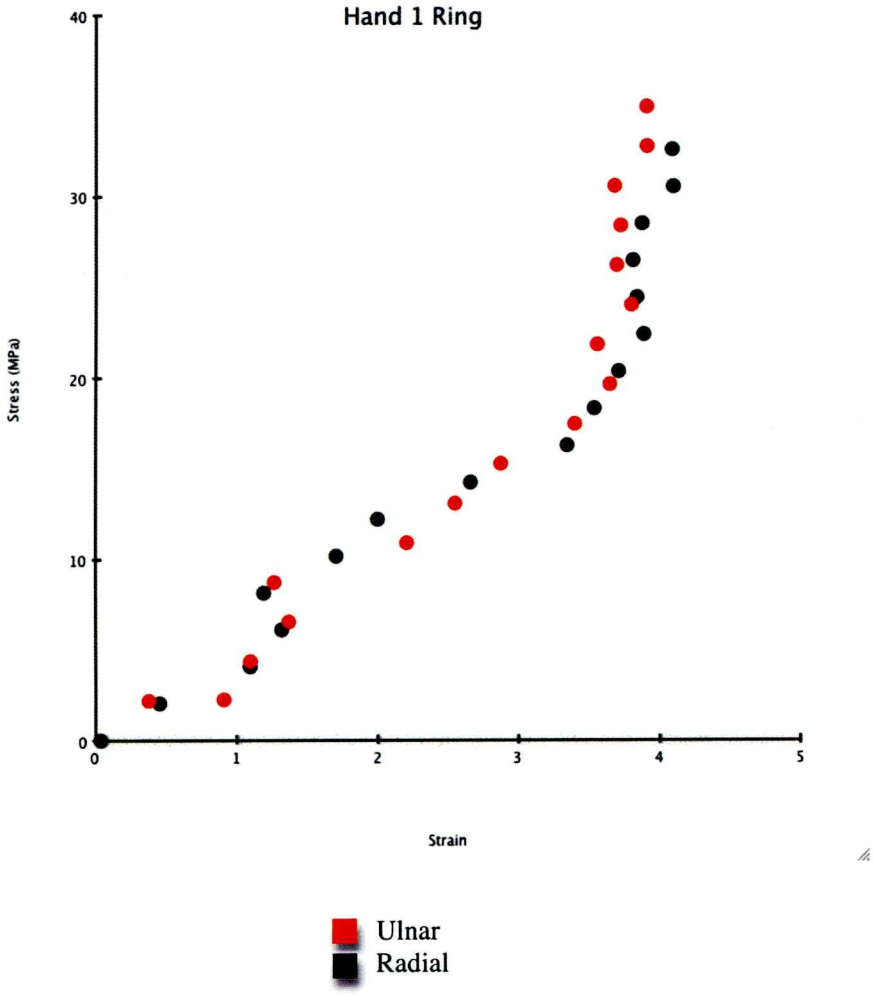
Hand 1 Ring
Stress (MPa)
40
30
20
10
0
0
1
2
3
4
5
Strain
Ulnar
Radial

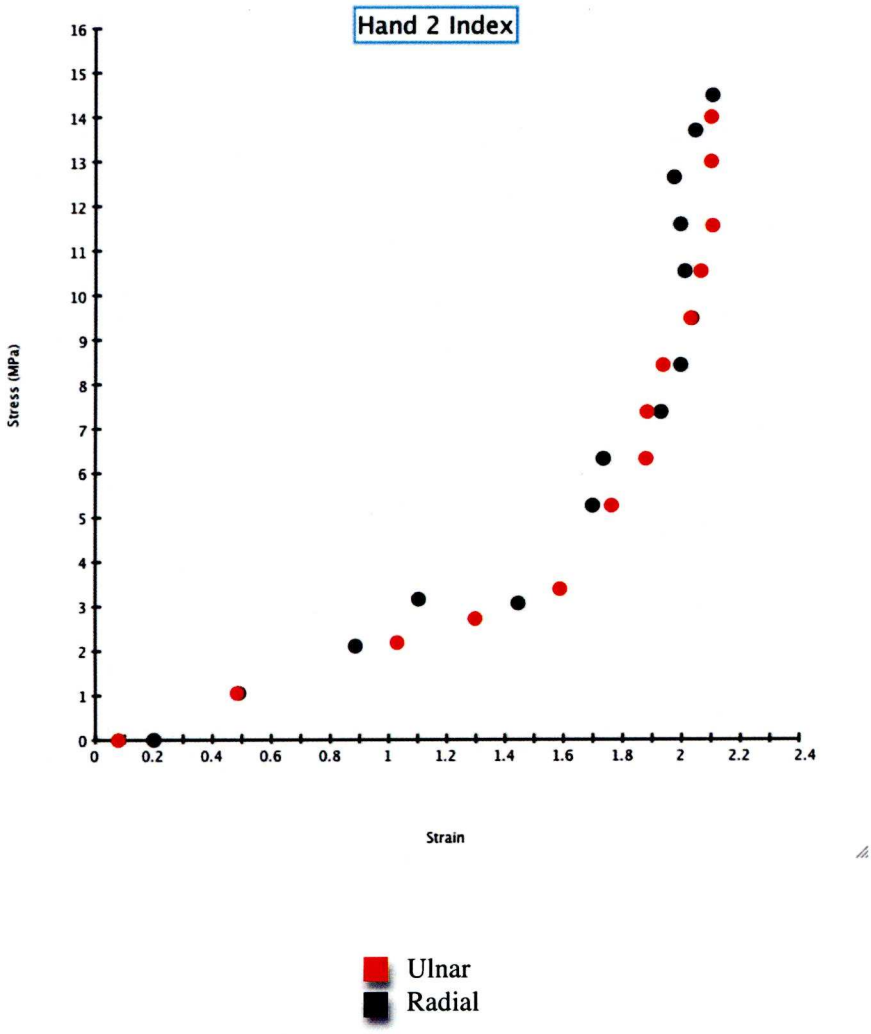
Hand 2 Index
Stress (MPa)
Strain
0
1
2
3
4
5
6
7
8
9
10
11
12
13
14
15
16
0
0.2
0.4
0.6
0.8
1
1.2
1.4
1.6
1.8
2
2.2
2.4
Ulnar
Radial

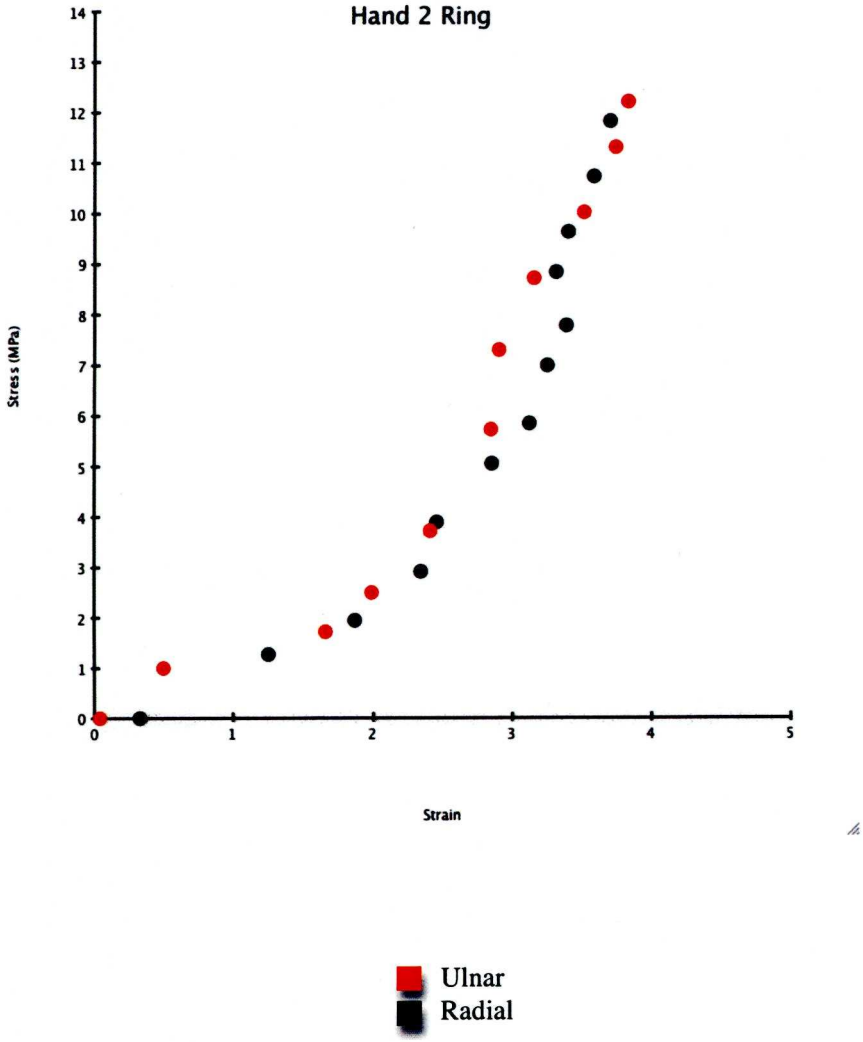
Hand 2 Ring
Stress (MPa)
Strain
0
1
2
3
4
5
6
7
8
9
10
11
12
13
14
Ulnar
Radial

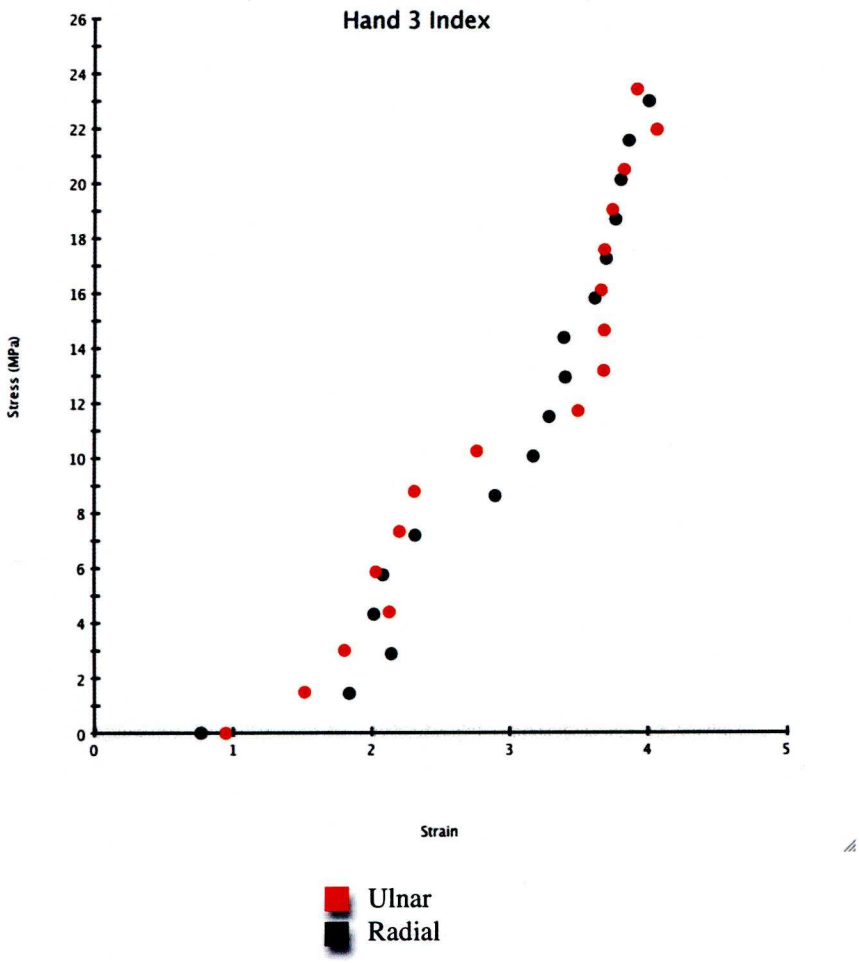
Hand 3 Index
Stress (MPa)
26
24
22
20
18
16
14
12
10
8
6
4
2
0
0
1
2
3
4
5
Strain
Ulnar
Radial

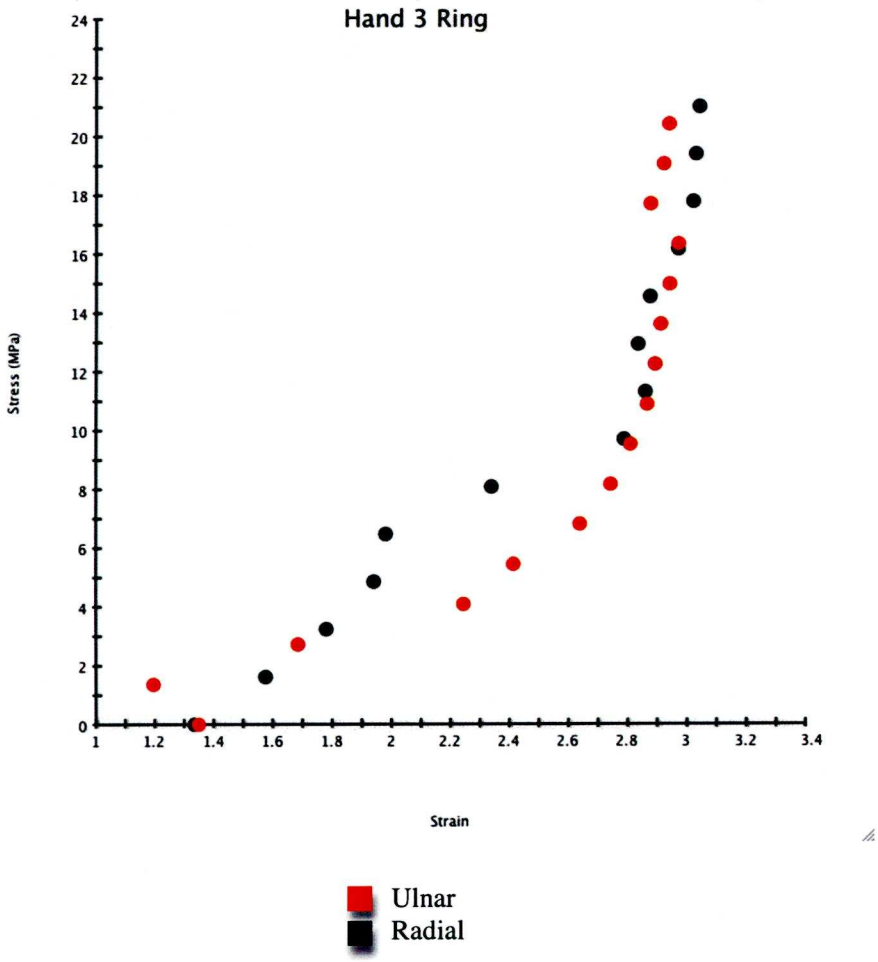
Hand 3 Ring
Stress (MPa)
24
22
20
18
16
14
12
10
8
6
4
2
0
1
1.2
1.4
1.6
1.8
2
2.2
2.4
2.6
2.8
3
3.2
3.4
Strain
Ulnar
Radial

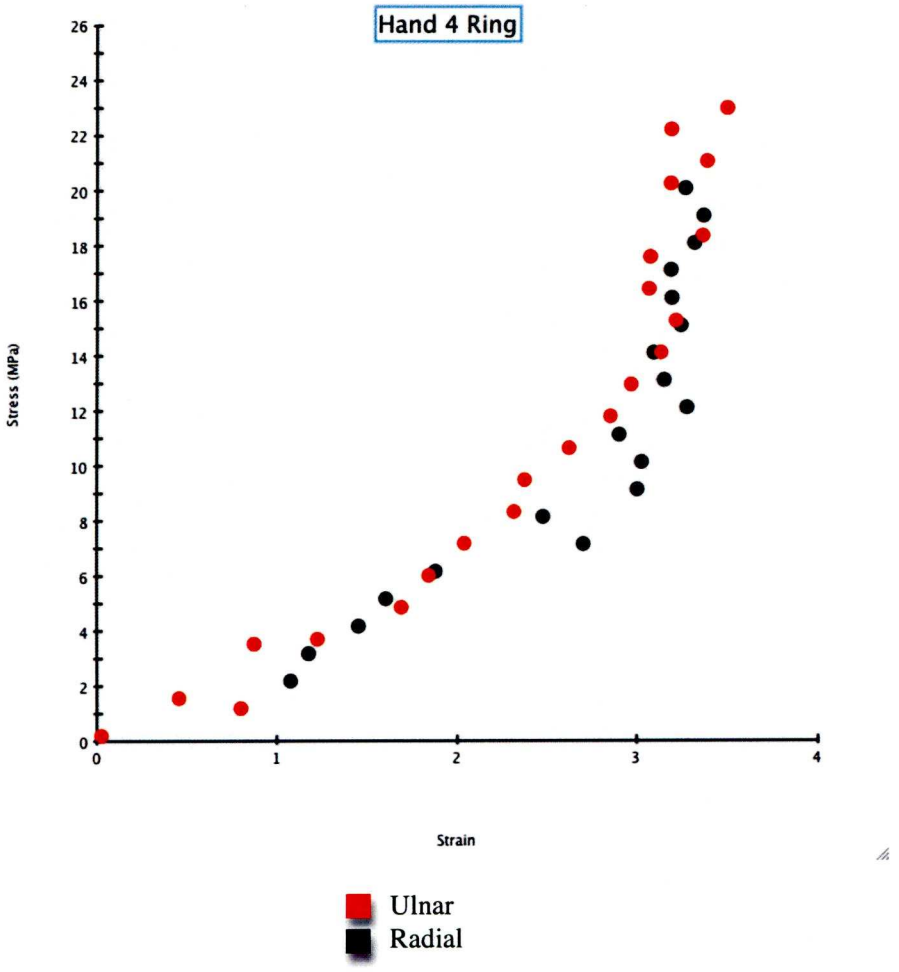
Hand 4 Ring
Stress (MPa)
26
24
22
20
18
16
14
12
10
8
6
4
2
0
0
1
2
3
4
Strain
Ulnar
Radial

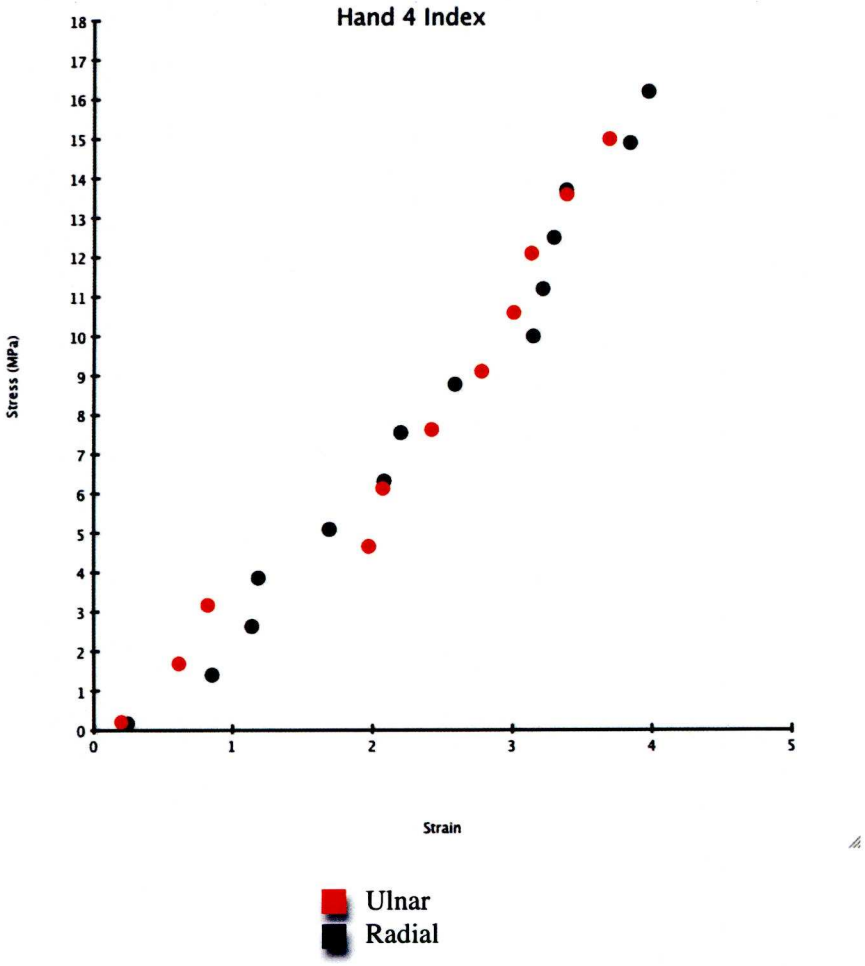
Hand 4 Index
Stress (MPa)
Strain
0
1
2
3
4
5
6
7
8
9
10
11
12
13
14
15
16
17
18
Ulnar
Radial

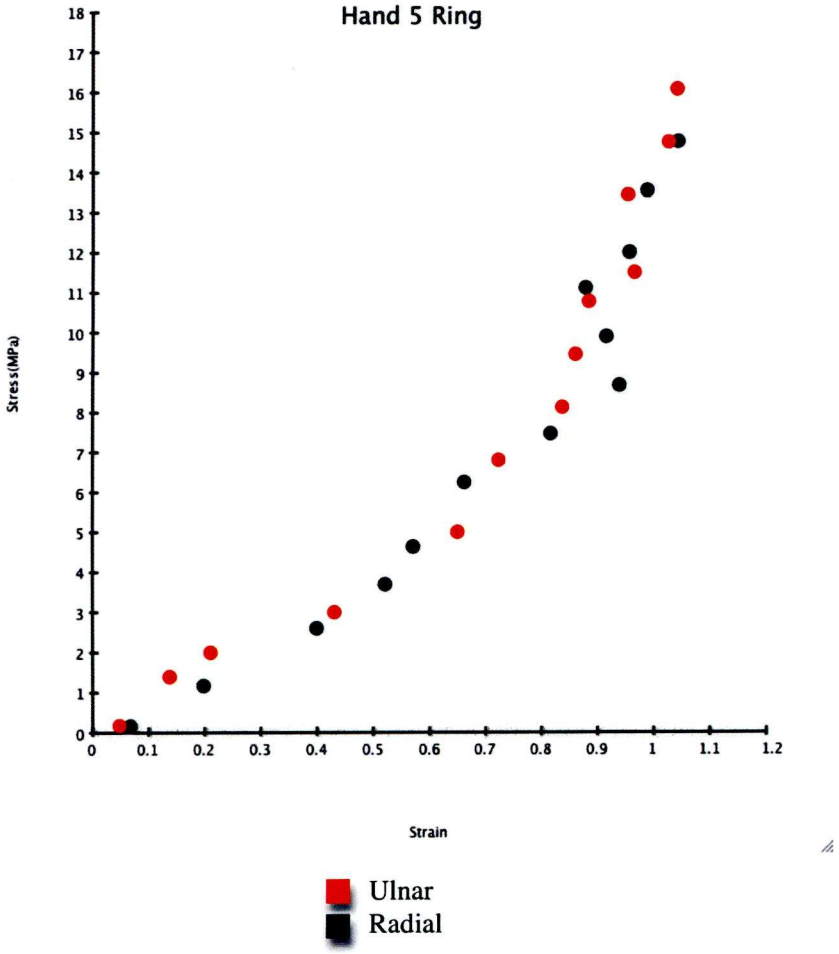
Hand 5 Ring
Stress(MPa)
Strain
0
1
2
3
4
5
6
7
8
9
10
11
12
13
14
15
16
17
18
0
0.1
0.2
0.3
0.4
0.5
0.6
0.7
0.8
0.9
1
1.1
1.2
Ulnar
Radial

4.7 Whole Tendon Results

The table shows the summarised data obtained from the output of the tensiometer and the calculation for Young's modulus based on the gradient of the linear region of the stress/strain plot. This is the data for the whole of the specimen as it was loaded in the tensiometer and is not based on the image analysis data that was used to break down the separate strain components in each of the terminal tendons.

All specimens had a similar Young's modulus with the exception of H4 Index. It may be that the reason for this is that due to the specimen being shorter giving rise to an error in calculating specimen length.

SUMMARY OF TENSIOMETER DATA FOR ALL SPECIMENS

SPECIMEN	PEAK STRESS	PEAK STRAIN	YOUNGS	CSA
H1 RING	1.60E+07	8.76	3.000E+08	6.600E-06
H2 INDEX	1.11E+07	5.71	3.000E+08	9.400E-06
H2 RING	1.17E+07	7.38	3.000E+08	9.200E-06
H3 INDEX	1.24E+07	11.60	2.019E+08	8.720E-06
H3 RING	1.20E+07	11.50	2.146E+08	8.750E-06
H4 INDEX	1.01E+07	10.36	1.000E+08	1.070E-05
H4 RING	1.12E+07	6.56	2.633E+08	9.480E-06
H5 RING	9.03E+06	6.27	2.579E+08	1.180E-05

Figure 39 Summary of data output from the tensiometer

Figure 40 displays the data for age. gender and side (left or right) for each of the specimens used in the experiments.

Specimen No.	Age (yrs)	Sex	Left / Right
1	71	M	L
2	59	M	R
3	65	F	L
4	76	M	R
5	70	F	R

Figure 40 Specimen data

4.8 Discussion

The reader may recall from the introduction the discussion of the equation for calculation of Young's modulus which was rearranged to show that the force in the terminal tendons was directly proportional to Young's modulus, strain and cross sectional area of the terminal tendons.

$$F = E \times CSA \times (\Delta L/L)$$

The data from the texture analysis experiments as presented in the graphs in section 4.6 did not demonstrate any statistically significant difference in strain between the terminal tendons for any of the specimens tested. The Young's modulus of the two terminal tendons can be assumed to be the same and this is confirmed by analysis of the terminal tendon texture analysis data. The graphs for each of the terminal tendons display the same gradient over the linear phase of loading. This gradient is equal to the Young's modulus of the specimen.

The value remaining is the CSA area of the specimens. The results support the hypothesis that the force in the terminal tendons of the FDS is directly proportional to their width. As suggested by Shrewsbury and Tucker [71], this can lead to a significant difference in loading as the joint is flexed. Shrewsbury and Tucker stated that parallel collagen fibres are able to transmit loads of between 15-30 Kgs per mm^2. This asymmetrical loading would provide an active driver to the motion identified in McArthur'swork demonstrating torsional motion of the PIPJ during flexion and extension [51].

Table 2 below shows the measurements for the width of the terminal tendons in the digits used in the experiments in this chapter.

Table 2 Dimensions of Terminal Tendons

	Index Fingers			Ring Fingers	
Specimen	Radial (mm)	Ulnar (mm)	Specimen	Radial (mm)	Ulnar (mm)
H1	4.2	3.9	H1	3.6	4.0
H2	5.0	3.9	H2	3.5	4.1
H3	3.2	3.0	H3	3.6	4.0
H4	4.6	4.2	H4	3.4	3.7
H5			H5	4.5	5.2

The findings agree with Shrewsbury's anatomical study which showed that the radial digits consistently have a wider radial terminal tendon and the ulnar digits have a wider ulnar terminal tendon.

These results would strongly suggest that there is differential loading within the terminal tendons of the FDS. This asymmetrical loading would drive a complex motion of the PIPJ as described by McArthur [51].

Chapter 5

5 Discussion

The purpose of this thesis was to determine if there was differential loading in the terminal tendons of the FDS which would explain the motion of the joint as described previously by Mc Arthur [51] and Uchiyama et al [77] .The author could not identify a suitable methodology to prove the hypothesis and so sought to develop an experimental methodology to answer the question.

Two different methods were trialled, SAXS and MRI texture correlation prior to successful set up using texture correlation with tendons loaded on a tensiometer. The two previous experiments yielded interesting data. To the author's knowledge, the structure of the FDS terminal tendons insertion has not specifically been investigated before or described as differing significantly from the standard description of the enthesis. The majority of work on tendon insertions has been performed on Achilles tendons. It may be wrong to extrapolate this to the rest of the body. The author's findings suggest that in the terminal tendons there is a change in the structure of the terminal tendons far more proximal than would be expected. This merits further investigation with an investigation of the collagen, mineral and proteoglycan content along the length of the terminal tendons. The SAXS data was unable to distinguish whether the molecular disorder in this region was due to a change in packing or types of collagen or due to expression of greater concentrations of high molecular weight proteoglycans.

The MRI experiments yielded high resolution images of the anatomy of the specimens by utilising the magic angle technique to maximise signal from the tendon. This technique is of great value in diagnosing hand pathology as no other imaging modality is able to resolve this level of anatomical detail. Further work on the methods of texture correlation and outline analysis is needed but the author would suggest that this be applied to areas of anatomy with much larger volumes of tissue so that the limitations encountered in the present investigation can be avoided. The previous publication which

successfully employed texture analysis of MRI images had investigated the supraspinatus tendon which is many times larger in cross-sectional area than the terminal tendons of the FDS [6]. Further work on applying magic angle imaging in investigation of hand disorders would also be of merit especially in the field of congenital hand surgery in which the anatomy is often abnormal and the level of resolution required is very high to allow pre operative planning.

Ultimately it was employing software and testing techniques from the industrial sector that yielded the most significant results. This required some compromise on trying to reproduce in-vivo conditions. Even using techniques that are readily used in industry required meticulous set up as there are difficulties when imaging moist biological specimens that are not encountered in materials testing. Further work here could employ a 3D analysis to allow shorter working distances and therefore higher resolution with less error from out of plane motion. This method could also be used to investigate different biological tissues such as ligaments and muscle.

The results from these experiments strongly suggest that the forces in the terminal tendons are directly proportional to their width and therefore the balance of forces in the terminal tendons mirrors the motion of the joint with supination of the ulnar digits due to the ulnar terminal tendon force being greater then the radial terminal tendon and pronation of the radial digits secondary to force in the radial terminal tendon exceeding that in the ulnar terminal tendon..

These results must be interpreted with caution, as there are limitations to the present study. Firstly, the number of specimens examined is relatively small numbering only four and a half and from an elderly population. However the main drawback in this study as that it was not possible to conduct force measurement in the FDS with the soft tissues and FDP intact due to experimental limitations. It is likely there is a change in the force distribution when the FDS courses around and grips the FDP tendon. In the last experiment though the tendon was clamped across the chiasma and from the chiasma onwards the course of the FDS is relatively flat. It would be ideal if the measurements could be performed with the FDP intact and better yet if accurate

assessment could be done in live volunteers. This may be possible with greater resolution scanning and the application of ever more refined software analyses packages but for the present time is not possible.

The implications of this asymmetrical loading in the PIPJ are predominantly in the design and manufacture of prostheses to replace the joint. The lifetime of any prosthesis is limited and as has been seen with the development of knee arthroplasty torsional movements and forces that are not accounted for can have a devastating effect on survival of the implant [78]. We have seen in the development of arthroplasty in the hip and knee that design can have a massive impact on the success of such procedures. If rotational forces are not accounted for in the design over many thousands of cycles of flexion and extension they can lead to loosening, excessive wear and therefore failure of the implant reconstruction.. The author anticipates that the findings presented in this thesis will help to inform those engaged in the development of such prostheses and may have a positive impact on the lifetime success of them.

PRESTON, CHORLEY AND SOUTH RIBBLE LOCAL RESEARCH ETHICS COMMITTEE

Tel/Fax/Answerphone: 01257 247140
E-Mail: Mary.Sykes@[redacted].nhs.uk

Trust Headquarters
Chorley & South Ribble
District General Hospital
Preston Road
CHORLEY PR7 1PP

LREC ref: 2003.3.vii

Mr G Lambe
SHO
Plastic Surgery Directorate
ROYAL PRESTON HOSPITAL

1 October 2003

Dear Mr Lambe

Research Protocol: ***A pilot study investigating the strains within the Flexor Digitorum Superficialis Chiasma using synchrotron X-Ray diffraction data***

The Chairman of the Preston, Chorley & South Ribble Local Research Ethics Committee has considered your response to the issues raised by the Committee at the earlier review of your application on 3 March 2003 as set out in our letter dated 12 March 2003. The documents considered were as follows:

- your letter dated 29 09 03
- patient information sheet and consent form version 1.1 (hand)
- patient information sheet version 1.1 (fingers)

The Chairman, acting under delegated authority, is satisfied that your response has fulfilled the requirements of the Committee and you are therefore given approval for your research on ethical grounds providing you comply with the conditions of approval set out below.

Conditions of approval:

- You do not undertake the research in a NHS organisation until the relevant NHS management approval has been received

- You do not deviate from, or make changes to, the protocol without prior written approval of the REC, except where this is necessary to eliminate immediate hazards to research participants or when the change involves only logistical or administrative aspects of the research. In such cases the REC should be informed within seven days of the implementation of the change.

- You complete and return the standard progress report form to the REC one year from the date on this letter and thereafter on an annual basis, or if sooner, when your research is completed and in this case it should be sent to this REC within three months of completion.

- If you decide to terminate this research prematurely, you send a report to this REC within fifteen days, indicating the reason for the early termination.

- You advise the REC of any unusual or unexpected results that raise questions about the safety of the research.

- The project must be started within three years of the date on this letter.

NHS RECs are compliant with the International Conference on Harmonisation/Good Clinical Practice (ICH GCP) Guidelines for the conduct of trials involving participation of human subjects.

Yours sincerely

E. Mary Sykes
(Administrator)
p.p. I M DRAKE, BMedSci, BMBS, FRCP
Chairman

This application has been given a unique reference number. Please include this on all correspondence with the REC

appriett.Mar 2003

References

1. Derwin KA, Soslowsky LJ, Green WD, Elder SH. A new optical system for the determination of deformations and strains: calibration characteristics and experimental results. J Biomech. 1994;27:1277-1285.
2. Ash HA, Joyce TJ, Unsworth A. Biomechanics of the distal upper limb. Current Orthopaedics. 1996;10:25-36.
3. Bay BK. Texture correlation: a method for the measurement of detailed strain distributions within trabecular bone. J Orthop Res. 1995;13:258-267.
4. Bay BK, Yerby SA, McLain RF, Toh E. Measurement of strain distributions within vertebral body sections by texture correlation. Spine. 1999;24:10-17.
5. Berendsen HJC. Nuclear magnetic resonance study of collagen hydration. J Chem Phys. 1962;36:3297.
6. Bey MJ, Ramsey ML, Soslowsky LJ. Intratendinous strain fields of the supraspinatus tendon: effect of a surgically created articular-surface rotator cuff tear. J Shoulder Elbow Surg. 2002;11:562-569.
7. Bey MJ, Song HK, Wehrli FW, Soslowsky LJ. A noncontact, nondestructive method for quantifying intratissue deformations and strains. J Biomech Eng. 2002;124:253-258.
8. Blevins FT, Hecker AT, Bigler GT, Boland AL, Hayes WC. The effects of donor age and strain rate on the biomechanical properties of bone-patellar tendon-bone allografts. Am J Sports Med. 1994;22:328.

9. Bowers W. The anatomy of the interphalangeal joints. Edinburgh: Churchill Livingston; 1987

10. Bragg WL. The diffraction of short electromagnetic waves by a crystal. Proc Camb Philol Soc. 1913;17:43-57.

11. Brunner JM. Surgical exposure of flexor tendons in the hand. Br J Plast Surg 1951;4:48.

12. Bunnell S. Gig pull-out suture for tendons. J Bone Joint Surg Am. 1954;36-A:850-851.

13. Butler DL, Grood ES, Noyes FR, Zernicke RF, Brackett K. Effects of structure and strain measurement technique on the material properties of young human tendons and fascia. J Biomech. 1984;17:579-596.

14. Bydder GM. New approaches to magnetic resonance imaging of intervertebral discs, tendons, ligaments, and menisci. Spine. 2002;27:1264-1268.

15. Carlson GD, Botte MJ, Josephs MS, Newton PO, Davis JL, Woo SL. Morphologic and biomechanical comparison of tendons used as free grafts. J Hand Surg [Am]. 1993;18:76-82.

16. Clavert P, Kempf JF, Bonnomet F, Boutemy P, Marcelin L, Kahn JL. Effects of freezing/thawing on the biomechanical properties of human tendons. Surg Radiol Anat. 2001;23:259-262.

17. Cooke R, Wien R. The state of water in muscle tissue as determined by proton nuclear magnetic resonance. Biophys Journal. 1971;11:1002.

18. Cowan PM, North ACT, Randall JT. X-ray diffraction studies of collagen fibres. Fibrous Proteins and their Biological Significance. 1955;115–126.

19. Davison PF. The contribution of labile crosslinks to the tensile behavior of tendons. Connect Tissue Res. 1989;18:293-305.

20. Devkota AC, Weinhold PS. Mechanical response of tendon subsequent to ramp loading to varying strain limits. Clin Biomech. 2003;18:969-974.

21. Diamant J, Keller A, Baer E, Litt M, Arridge RG. Collagen; ultrastructure and its relation to mechanical properties as a function of ageing. Proc R Soc Lond B Biol Sci. 1972;180:293-315.

22. Dolgo-Saburoff B. Uber Ursprung und Insertion der Skelettmuskeln. Anat Anz. 1929;68:30-87.

23. Erickson SJ, Cox IH, Hyde JS, Carrera GF, Strandt JA, Estkowski LD. Effect of tendon orientation on MR imaging signal intensity: a manifestation of the magic angle phenomenon. Radiology. 1991;181:389-392.

24. Erickson SJ, Prost RW, Timins ME. The" magic angle" effect: background physics and clinical relevance. Radiology. 1993;188:23-25.

25. Farkas LG, Thomson HG, Martin R. Some practical notes on the anatomy of the chicken toe for surgeon investigators. Plast Reconstr Surg. 1974;54:452-458.

26. W. Folkhard, E. Mosler, W. Geercken, E. Knorzer, H. Nemetschek-Gansler, Th. Nemetschek, M.H.J. Koch Quantitative analysis of the molecular sliding mechanism in native tendon collagen-time resolved dynamic studies using synchrotron radiation. Int J Biol Macromol. 1986;9:169-175.

27. Fratzl P, Bordas J. Structure and mechanics of muscle and tendon. Synchrotron Radiation News. 2002;15:18-26.

28. Fratzl P, Misof K, Zizak I, Rapp G, Amenitsch H, Bernstorff S. Fibrillar structure and mechanical properties of collagen. J Structural Biol. 1998;122:119-122.

29. Fullerton GD, Cameron IL, Ord VA. Orientation of tendons in the magnetic field and its effect on T2 relaxation times. Radiology. 1985;155:433-435.

30. Fung BM. Correlation of relaxation time with water content in muscle and brain tissues. Biochim Biophys Acta. 1977;497:317-322.

31. Gathercole LJ, Keller A. Crimp morphology in the fibre-forming collagens. Matrix. 1991;11:214-234.

32. Haraldsson BT, Aagaard P, Krogsgaard M, Alkjaer T, Kjaer M, Magnusson SP. Region-specific mechanical properties of the human patella tendon. J Appl Physiol. 2005;98:1006-1012.

33. Hasberry S, Pearcy MJ. Temperature dependence of the tensile properties of interspinous ligaments of sheep. J Biomed Eng. 1986;8:62-66.

34. Haut RC. The influence of specimen length on the tensile failure properties of tendon collagen. J Biomech. 1986;19:951-955.

35. Haut TL, Haut RC. The state of tissue hydration determines the strain-rate-sensitive stiffness of human patellar tendon. J Biomech. 1997;30:79-81.

36. Hazlewood CF, Chang DC, Nichols BL, Woessner DE. Nuclear magnetic resonance transverse relaxation times of water protons in skeletal muscle. Biophys Journal. 1974;14:583.

37. Helmer KG, Nair G, Cannella M, Grigg P. Water movement in tendon in response to a repeated static tensile load using one-dimensional magnetic resonance imaging. J Biomech Eng. 2006;128:733-741.

38. Herrick WC, Kingsbury HB, Lou DYS. A study of the normal range of strain, strain rate, and stiffness of tendon. J Biomed Materials Res. 1978;12:877-894.

39. Hirsch EF, Morgan RH. Causal significance to traumatic ossification of the fibrocartilage in tendon insertions. Arch Surg. 1939;39:824-837.

40. Hodge AJ, Petruska J.A. Aspects of Protein Structure. New York: Academic Press; 1963

41. Hoffman AH, Grigg P. A method for measuring strains in soft tissue. J Biomech. 1984;17:795-800.

42. Tyson J and Schmidt T. Advanced photogrammetry for robust deformation and strain measurement. SEM Annual Conference proceedings. 2002

43. Kobayashi A. Handbook on experimental mechanics. New York: 1987

44. Krasnosselskaia LV, Fullerton GD, Dodd SJ, Cameron IL. Water in tendon: orientational analysis of the free induction decay.
Magn Reson Med. 2005;54:280-288.

45. Kuczynski K. Less-known aspects of the proximal interphalangeal joints of the human hand. J Hand Surg (European Volume). 1975;7:31.

46. Lam TC, Thomas CG, Shrive NG, Frank CB, Sabiston CP. The effects of temperature on the viscoelastic properties of the rabbit medial collateral ligament. J Biomech Eng. 1990;112:147-152.

47. Leitschuh PH, Doherty TJ, Taylor DC, Brooks DE, Ryan JB. Effects of postmortem freezing on tensile failure properties of rabbit extensor digitorum longus muscle tendon complex. J Orth Res. 1996;14:830-833.

48. Lewis G, Shaw KM. Tensile properties of human tendo achillis: Effect of donor age and strain rate. J Foot Ankle Surg. 1997;36:435-445.

49. Lindsay WK, Thomson HG, Walker FG. Digital flexor tendons: an experimental study. Part II. The significance of a gap occurring at the line of suture. Br J Plast Surg. 1960;3:1-9.

50. Mathes SJ. Plastic Surgery, Vol. 8: The Hand and Upper Limb, Part 2 (Hardcover). New York: Saunder; 2005

51. Mc Arthur P. Kinematics of the proximal interphalangeal joint [PhD Thesis]. Sheffield University; 2001.

52. Misof K, Rapp G, Fratzl P. A new molecular model for collagen elasticity based on synchrotron X- ray scattering evidence. Biophys journal. 1997;72:1376-1381.

53. Mosler E, Folkhard W, Knorzer E, Nemetschek-Gansler H, Nemetschek T, Koch MH. Stress-induced molecular rearrangement in tendon collagen. J Mol Biol. 1985;182:589-596.

54. Ng BH, Chou SM, Krishna V. The influence of gripping techniques on the tensile properties of tendons. Proc Inst Mech Eng [H]. 2005;219:349-354.

55. Ng BH, Chou SM, Lim BH, Chong A. Strain rate effect on the failure properties of tendons. Proc Inst Mech Eng [H]. 2004;218:203-206.

56. Nisenoff M, Fan HY. Electron spin resonance in neutron-irradiated silicon. Physical Review. 1962;128:1605-1613.

57. Peterfy CG, Janzen DL, Tirman PF, van Dijke CF, Pollack M, Genant HK. "Magic-angle" phenomenon: a cause of increased signal in the normal lateral meniscus on short-TE MR images of the knee. AJR Am J Roentgenol. 1994;163:149-154.

58. Puxkandl R, Zizak I, Paris O, Keckes J, Tesch W, Bernstorff S, Purslow P, Fratzl P.. Viscoelastic properties of collagen: synchrotron radiation investigations and structural model. Philos Trans Royal Soc B. 2002;357:191-197.

59. Rechenmacher AL, Finno RJ. Digital image correlation to evaluate shear banding in dilative sands. Geotechnical Testing Journal. 2004;27:13-22.

60. Riemersa DJ, Schamhardt HC. The cryo-jaw, a clamp designed for in vitro rheology studies of horse digital flexor tendons. J Biomech. 1982;15:619-620.

61. Rigby BJ, Hirai N, Spikes JD, Eyring H. The mechanical properties of rat tail tendon. J Gen Physiol. 1959;43:265-283.

62. Sakurada I, Nukushina Y, Ito T. Experimental determination of the elastic modulus of crystalline regions in oriented polymers.
J Polymer Sci. 1962;57:651-660.

63. Sanghavi P, Bose D, Kerrigan J, Madeley NJ, Crandall J. Non-contact strain measurement of biological tissue. Biomed Sci Instrum. 2004;40:51-56.

64. Sasaki N, Odajima S. Elongation mechanism of collagen fibrils and force-strain relations of tendon at each level of structural hierarchy.
J Biomech. 1996;29:1131-1136.

65. Sasaki N, Odajima S. Stress-strain curve and Young's modulus of a collagen molecule as determined by the X-ray diffraction technique.
J Biomech. 1996;29:655-658.

66. Sasaki N, Shukunami N, Matsushima N, Izumi Y. Time-resolved X-ray diffraction from tendon collagen during creep using synchrotron radiation.
J Biomech. 1999;32:285-292.

67. Screen HR, Lee DA, Bader DL, Shelton JC. An investigation into the effects of the hierarchical structure of tendon fascicles on micromechanical properties. Proc Inst Mech Eng [H]. 2004;218:109-119.

68. Sharkey NA, Smith TS, Lundmark DC. Freeze clamping musculo-tendinous junctions for in vitro simulation of joint mechanics. J Biomech. 1995;28:631-635.

69. Sharpey W. Elements of Anatomy. London: Longmans; 1856

70. Shrewsbury MM, Kuczynski K. Flexor digitorum superficialis tendon in the fingers of the human hand. J Hand Surg (European Vol). 1974;6:121-133.

71. Shrewsbury MM, Tucker AB. A study of the flexor digitorum superficialis tendon in flexion and extension at the proximal interphalangeal joint. Bull Hosp Joint Dis 1975;36:40-47.

72. Smith CW, Young IS, Kearney JN. Mechanical properties of tendons: changes with sterilization and preservation. J Biomech Eng. 1996;118:56-61.

73. Sobel M, Bohne WH, Markisz JA. Cadaver correlation of peroneal tendon changes with magnetic resonance imaging. Foot Ankle. 1991;11:384-388.

74. Stack HG. Muscle function in the fingers. J Bone Joint Surg, British Vol. 1962;44:899-909.

75. Thomopoulos S, Williams GR, Gimbel JA, Favata M, Soslowsky LJ. Variation of biomechanical, structural, and compositional properties along the tendon to bone insertion site. J Orthop Res. 2003;21:413-419.

76. Timins ME, Erickson SJ, Estkowski LD, Carrera GF, Komorowski RA. Increased signal in the normal supraspinatus tendon on MR imaging: diagnostic pitfall caused by the magic-angle effect. AJR Am J Roentgenol. 1995;165:109-114.

77. Uchiyama S, Cooney 3rd WP, Linscheid RL, Niebur G, An KN. Kinematics of the proximal interphalangeal joint of the finger after surface replacement. J Hand Surg [Am]. 2000;25:305-312.

78. Vanhegan JA, Dabrowski W, Arden GP. A review of 100 Attenborough stabilised gliding knee prostheses. J Bone Joint Surg, British Vol. 1979;61:445-450.

79. Viidik A. A rheological model for uncalcified parallel-fibred collagenous tissue. J Biomech. 1968;1:3-11.

80. Viidik A. On the correlation between structure and mechanical function of soft connective tissues. Verh Anat Ges. 1978;75-89.

81. Waggett AD, Ralphs JR, Kwan AP, Woodnutt D, Benjamin M. Characterization of collagens and proteoglycans at the insertion of the human Achilles tendon. Matrix Biol. 1998;16:457-470.

82. Walbeehm ET, McGrouther DA. An anatomical study of the mechanical interactions of flexor digitorum superficialis and profundus and the flexor tendon sheath in zone 2. J Hand Surg (European Vol). 1995;20:269-280.

83. Warren BE. X-ray Diffraction. London: Dover Pubns; 1990

84. Wren TA, Yerby SA, Beaupre GS, Carter DR. Mechanical properties of the human achilles tendon. Clin Biomech (Bristol, Avon). 2001;16:245-251.